Design and Implementation of a Dual Polarised L-Band Parabolic Dish Antenna for NeXtRAD

Presented by:

Stephen Thomas Paine

Prepared for:

Prof. Daniel O'Hagan

and

Prof. Barry Downing

Dept. of Electrical Engineering

University of Cape Town

A dissertation submitted to the Department of Electrical Engineering,
University of Cape Town,
in partial fulfilment of the requirements for the
degree of Master of Science in Engineering specialising in
Radar and Electronic Defence.

April 28, 2016

Declaration

I declare that this dissertation is my own, unaided work. I have used the IEEE style of referencing. This dissertation is being submitted for the degree of Master of Science in Engineering in the University of Cape Town. It has not been submitted before for any degree or examination in any other university.

Signature of Author .....

Cape Town
April 28, 2016

Abstract

Research into multi-static, multi-band networked radar has led to the development of the NeXtRAD radar system. This dissertation will investigate the design and implementation of a dual polarised L-Band prime focus dish antenna with a centre frequency of 1.3 GHz and a HPBW of 10° in the azimuth plane. The antenna is required to handle a peak power of 1.5 kW over a 50 MHz bandwidth and be able to withstand environmental factors such as wind while mounted on a tripod. This dissertation forms part of the larger NeXtRAD project and as such, the antenna design requirements have been set based on the wider system specifications.

Previous investigations into the feasibility of various antenna designs have concluded that a prime focus parabolic dish antenna would be the most appropriate to meet the design requirements. The dissertation details the design and manufacturing process followed. All antenna parameters have been simulated using a combination of FEKO v7 and CST 2014 to compare and verify the designs and simulations.

Due to manufacturing limitations, the optimal antenna design could not be manufactured and, as a result, compromises had to be made in order for an antenna prototype to be manufactured and tested. These tests include, amongst others, characterisation of the return loss, cross polarisation, gain, beamwidth and beam pattern of the antenna in both planes of polarisation. These results have been recorded, analysed and compared to those found through simulations.

It has been shown that the measured results correspond well with the simulated results, therefore illustrating that with adequate manufacturing facilities, the optimally designed and manufactured antenna will meet the system specifications. The built antenna prototype has been found to have an azimuth HPBW of 13.9° and 12.4° when horizontally and vertically polarised respectively. The prototype antenna meets all bandwidth and power requirements while maintaining a relatively compact size. The results have shown that using a prime focus parabolic dish antenna to meet the strict requirements is both feasible and practical.

Acknowledgements

First and foremost I would like to thank my supervisors, Professor Daniel O'Hagan and Professor Barry Downing for their continual support and guidance thoughout the course of this project. I would also like to make a special note of thanks to my good friend and colleague, Po-Kai 'Randy' Cheng for the many hours spent assisting me in the lab and with measurements.

I would like to thank the UCT Radar Remote Sensing Group (RRSG) and everyone involved for all the (many) ups and downs throughout this project and I wish you all great success in the future. A big thank you the CSIR and Ledger for giving me the opportunity to pursue my MSc by providing me with the funds required.

Lastly I would like to thank my parents, Craig and Sharon as well as my girlfriend, Michaela, for all their support and patience over the course of this project and all the years leading to it. I could not have gotten this far without the love and encouragement they have given me.

Contents

List of Figures

List of Tables

List of Symbols

B	—	Transmitted RF bandwidth (Hz)
c	—	Speed of light in a vacuum ($3 \times 10^8 m/s$)
f_0	—	Centre frequency of system (Hz)
λ_0	—	Free-space wavelength (m)
λ_g	—	Waveguide wavelength (m)
θ	—	3 dB azimuth beamwidth (°)
φ	—	3 dB elevation beamwidth (°)
f/D	—	Ratio of focal length to aperture diameter
F/B	—	Front to back ratio
f	—	Focal point
D	—	Antenna diameter
D_w	—	Waveguide diameter
D_0	—	Antenna directivity
G	—	Antenna gain (dBi)
η	—	Antenna efficiency (%)
S_{11}	—	Return loss of horizontally polarised feed
S_{22}	—	Return loss of vertically polarised feed
S_{21}	—	Polarisation isolation
Tx	—	Transmit
Rx	—	Receive
HH	—	Horizontal transmit, horizontal receive
HV	—	Horizontal transmit, vertical receive

Nomenclature

GPSDO — GPS Disciplined Oscillator used for timing synchronisation between nodes.

FEKO — Electromagnetic simulation software.

CST — Computer Simulation Technology, a software package used for electromagnetic simulations.

CAD — Computer-aided design.

HPBW — Half power beamwidth, the same as the 3 dB beamwidth.

Azimuth — A polar angle measured as the variation from a centre point parallel to the horizon.

Elevation — A Polar angle measured as the variation from a centre point perpendicular to the horizon.

dB — Logarithmic unit of measurement in decibels.

dBi — Decibels with respect to an isotropic radiator.

dBm — Decibels with respect to a milliwatt.

dBc — Decibels with respect to a carrier.

Beamwidth — The angular width of a slice through the mainlobe of the radiation pattern of an antenna in the horizontal, vertical or other plane.

EM wave — Electromagnetic wave.

RF — Radio Frequency.

TE — Transverse Electric.

TM — Transverse Magnetic.

Polarisation — Polarisation of an electromagnetic wave is defined as the orientation

of the electric field with respect to the surface of the earth.

Dual Polarisation — An antenna is said to be dual polarised when it can operate in both horizontal and vertical polarisation without any physical modification or rotation of the antenna.

3 dB Beamwidth — The angular width of the mainlobe whereby the power levels remain above half the mainlobes maximum power.

SLL — Side lobe level.

SFDR — Spurious free dynamic range.

RTBW — Real time bandwidth.

Cross-polarisation — The polarisation orthogonal to the reference plane of polarisation.

Co-polarisation — The polarisation in the reference plane of polarisation.

Characteristic impedance — The instantaneous impedance of a transmission line or junction as seen by an electromagnetic wave.

DUT — Device under test.

AUT — Antenna under test.

MATLAB — Mathematical equation simulation software.

Chapter 1

Introduction

1.1 Background to Project

The University of Cape Town (UCT) together with University College London (UCL) are in the process of building a multistatic networked radar system that aims to improve on a previous radar system known as NetRAD. NetRAD was originally developed by UCL [2].

NetRAD works by networking multiple S-Band ($f_0 = 2.45$ GHz) receivers and a single transmitter together. This allows the radar to transmit pulses from a single node (the Tx node) and be able to receive return echoes from multiple angles using the multiple Rx nodes. In its current form, NetRAD operates using off-the-shelf singularly polarised Wi-Fi ($f_0 = 2.45$ GHz) dish antennas that come with a predefined 10° beamwidth in both azimuth and elevation planes.

One of the objectives set by the designers of NetRAD was to be able to measure and compare target reflections for pulses in different planes of polarisation. An example of this type of measurement would be to transmit in vertical polarisation and receive in vertical polarisation (VV) or to transmit in vertical polarisation and receive in horizontal polarisation (VH).

In its current form, NetRAD operates by having three nodes, one active Tx/Rx node in the centre and two passive Rx only nodes on each side of the central, active, node as shown in Figure 1.1. The radar then transmits pulses with a centre frequency of 2.45 GHz (bandwidth of 50 MHz) from the central node and receives the target return on all three nodes. This allows the target echo to be observed from multiple aspect angles.

One of the main limitations of the NetRAD system is that to network each node together, a wired network connection (limited to 50 m) is required to achieve accurate node synchronisation. While the system has subsequently been fitted with GPSDO's, allowing for multi-kilometre baselines to be achieved, various reliability issues resulted in a fall-back to the wired connections. This severely limits the distance between each node and as a result, limits the aspect angles achievable between target and each node. Another limitation is that the system has not been dual polarised and therefore to perform polarimetric measurements, the antennas need to be manually rotated between each measurement and therefore cannot operate in VH or HV mode.

To overcome the various limitations of NetRAD, a new system was commissioned. The new system, named NeXtRAD, improved on NetRAD by removing the wired limitation on each node and will also be fully polarimetric. That is, NeXtRAD can operate in VV, HH, HV or VH planes of polarisation.

To further improve upon NetRAD, NeXtRAD has been designed to utilise two frequency bands as opposed to one, namely L-Band ($f_0 = 1.3$ GHz) and X-Band ($f_0 = 8.5$ GHz). To allow direct comparison between NetRAD and NeXtRAD data, it was necessary for some technical features of NeXtRAD, such as azimuth beamwidth, to remain the same or close to NetRAD. As a result of some NetRAD and NeXtRAD similarity requirements, the half power beamwidth (HPBW) and bandwidth of the antennas in this dissertation have attempted to achieve an azimuth beamwidth of 10°.

Figure 1.1 shows the basic node geometry of the NeXtRAD system.

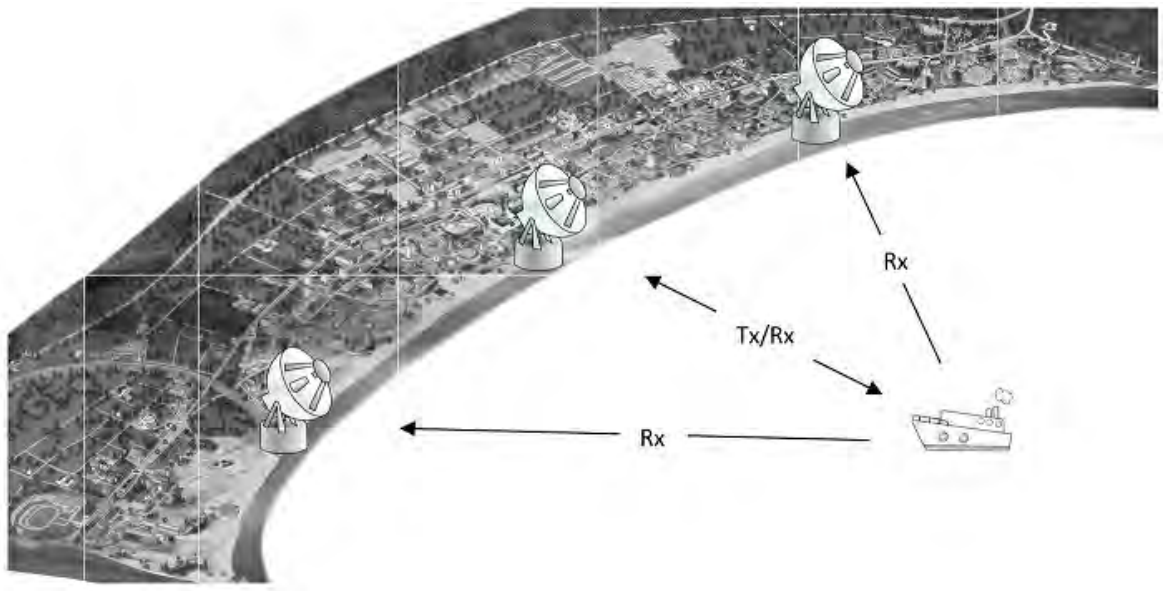

Figure 1.1: Basic NeXtRAD antenna layout with central active Tx/Rx node and two passive Rx-only flanking nodes.

One of the key features of the NeXtRAD system is that it is able to operate in both X- and L-Band, switching between both planes of polarisation as required. The central active node will transmit a horizontally or vertically polarised pulse in either X- or L-Band, while the target echo can be received by all three nodes in either horizontal or vertical polarisation.

1.2 User Requirements

While this project forms part of the larger NeXtRAD project, this dissertation focuses specifically on the design and implementation of an L-Band dish antenna that is required to meet the following design criteria:

- Dual polarised (Horizontal and Vertical)
- L-Band with centre frequency of $f_0 = 1.3$ GHz ($\lambda_0 = c/f_0 = 230$ mm)
- Minimum 50 MHz (4%) bandwidth (1.275 GHz to 1.325 GHz)
- 10° 3 dB azimuth beamwidth (regardless of the plane of polarisation)
- Be able to be mounted on a tripod and withstand harsh environmental conditions such as high winds
- 1.5 kW peak power handling capabilities

1.3 Objectives of Study

As mentioned in Section 1.2, the objective of this dissertation is to investigate the design and implementation of a suitable L-Band dish antenna that would meet all the given design criteria.

In addition to the requirements set in Section 1.2, the system as a whole is further constrained by budget limitations in that a high power L-Band switch (to switch between transmit and receive as well as to switch between planes of polarisation) is un-feasible at the time of writing. As a result, to achieve the necessary isolation between the Tx and Rx channels, the Tx/Rx active node requires two separate, co-located, dual polarised L-Band antennas, one for Tx and one for Rx. This adds to the engineering challenge as co-locating antennas requires the antennas to be as small as practically possible.

In a previous report by the author titled: "Design and Implementation of a Dual Polarised L-Band Antenna with 10 Degree Azimuth Beamwidth" [1], an in-depth investigation was carried out to determine the feasibility of various antenna designs for meeting the project requirements as outlined in Section 1.2. Various designs, including patch, dish, horn and pillbox antenna designs were investigated and the results of these findings are discussed in Chapter 2.

Due to the strict system design requirements, an antenna of this nature poses many engineering challenges that are to be overcome throughout this dissertation. One of the major challenges to be overcome has been the once off manufacturing of a parabolic antenna, all of which has been investigated in detail throughout this dissertation. All technical information required for the design and manufacture of the final optimised antenna has been provided in this dissertation.

1.3.1 Purpose of Study

This dissertation forms part of a larger ongoing study on multi-frequency, multistatic, networked radar systems. The NeXtRAD system, which is ultimately designed to be a land-to-sea radar, forms an advanced continuation of the work carried out by UCL on the NetRAD system.

The principle of operation for NeXtRAD is as follows: there are three nodes, comprising of one central active node which allows both Tx and Rx at either L- ($f_0 = 1.3$ GHz) or X- ($f_0 = 8.5$ GHz) Band and two passive Rx flanking nodes either side of the active central node. Each node has antennas for both frequency bands that are dual polarised, meaning that it can transmit (in the case of the active node) and receive (on all three nodes) in both planes of polarisation, at either frequency.

In order for the system to be fully polarimetric, each antenna is required to be dual polarised where the polarisation is controlled by the radar operator. The purpose of this study is to investigate, design, manufacture and test a prototype L-Band antenna that meets the requirements set in Section 1.2.

1.4 Scope and Limitations

The scope of this project is to design, manufacture and test a dual polarised L-Band parabolic dish antenna with 10° azimuth beamwidth that is small enough to be mounted on a tripod and placed on the side of a mountain in windy conditions.

One of the major limitations is the manufacturing facilities available to this project. Due to the fact that a prototype needs to be manufactured and tested, the standard procedure of producing a mould from which the antennas could be made is not within budget. As a result, various other manufacturing techniques have needed to be explored.

Another limitation is the lack of a reflection free environment, such as an anechoic chamber, to perform accurate antenna measurements. Local measurement facilities would have required minor modifications to accomodate the L-Band antenna. Dissertation time limits have excluded anechoic chamber measurements and therefore chamber measurements do not feature in this dissertation. The measurements will, nevertheless, be undertaken soon prior to project completion.

This dissertation focuses exclusively on the design and implementation of the L-Band dish antenna. The full operational description of NeXtRAD is not within the scope of this dissertation but details can be found in [2][3].

1.5 Plan of Development

Chapter 1 begins by providing a complete overview of the dissertation, describing the basic operation of the NeXtRAD radar system. The user requirements and objectives are outlined before summarising the scope and limitations of the dissertation.

Chapter 2 reviews the relevant literature and explores the feasibility of various antenna designs. This chapter covers the design characteristics of patch antenna arrays, Yagi antennas, sectoral horn antennas, pillbox antennas and reflector dish antennas before determining the most appropriate design to be a parabolic reflector antenna.

Chapter 3 discusses the application specific design of a parabolic dish antenna. Relevant theory on parabolic dish antennas is discussed, providing an overview of the critical aspects involved in the design of parabolic dish antennas.

Chapter 4 explores the design methodology, simulations and prototype antenna construction, outlining the key aspects involved in the design of an antenna that meets the requirements set in Section 1.2. The manufacturing process is described in detail along with the various manufacturing compromises that have needed to be made.

Chapter 5 details the testing procedure followed to fully characterise the manufactured prototype antenna. The measured prototype antenna results are compared to the simulated results obtained in Chapter 4 and conclusions are drawn.

Chapter 6 summarises the design procedure, simulations, manufacturing process and measured results before concluding with recommendations for future research. It is shown that the prototype antenna performs as designed, with the measured results closely correlating with the simulated results.

Relevant theory not covered in Chapters 1 to 6 has been included in Appendix A. Appendix B to I contain measured and simulated results that are referenced throughout the dissertation.

Chapter 2

Literature Review

The aim of this chapter is to review relevant literature in order to develop an in-depth understanding of the fundamental aspects pertaining to antenna design. This chapter provides a broad overview of previous research into the feasibility of various antenna designs to meet the project requirements as outlined in Section 1.2.

2.1 Antenna Designs Considered

This section outlines the various antenna designs that were considered for meeting the design specifications set in Section 1.2. Each antenna design is discussed, giving both the advantages and disadvantages for each as well as a brief overview of the feasibility of the particular design. The antenna designs that have been considered include:

- Patch Antenna Array
- Yagi-Uda Antenna
- Sectoral Horn Antenna
- Pillbox Antenna
- Reflector Dish Antenna

2.1.1 Patch Antenna Array

The first antenna design that has been investigated is a patch antenna array. A patch antenna is a resonant structure that is made from a thin conducting surface, separated from the ground plane by a dielectric material.

Figure 2.1 illustrates the basic structure of a patch antenna.

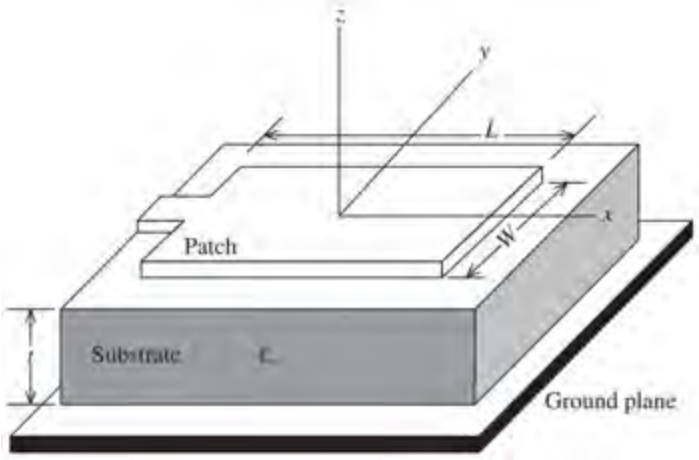

Figure 2.1: Basic layout for a square patch antenna showing the substrate sandwiched between the patch antenna element and the ground plane.[4].

The main advantage with using a patch antenna is their simple and light weight manufacture. Their low-profile allows easy mounting of the antenna to a tripod while maintaining very low overall antenna volume.

The disadvantage of using patch antennas is that they are inherently low bandwidth. It is common for a patch antenna to have a fractional bandwidth of between 1% and 2% and while it has been shown that a bandwidth of 50% is achievable, this has only been achieved in a low power, single plane of polarisation patch antenna [1]. The bandwidth of a patch antenna is dependant on the relative permittivity (η_r) and the thickness (t) of the substrate as well as the ratio of the width (W) to the length (L) of the patch. Equation (2.1) can be used to determine the approximate bandwidth of a patch antenna [4].

$$B = 3.77 \left(\frac{\epsilon_r - 1}{\epsilon_r^2} \right) \left(\frac{W}{L} \right) \left(\frac{t}{\lambda_0} \right) \tag{2.1}$$

To ensure that the patch array is cable of being dual polarised, it is essential that the patch be symmetric and therefore a square patch is chosen (where $W = L$). Choosing a substrate that will maximise the bandwidth of the patch means it must have a very low relative permittivity and be as thick as possible. The RT/Duriod 5880 [5] substrate was chosen as it best fits the requirements with a relative permittivity of 2.2 F/m and a thickness of 3.175 mm. The bandwidth of the patch to be is therefore:

$$B = 3.77 \left(\frac{2.2 - 1}{2.2^2} \right) \left(\frac{3.175}{230} \right) \approx 1.2\% \tag{2.2}$$

It can be seen that the bandwidth of the patch antenna using an off-the-shelf substrate is not sufficient for the application, where a 4% fractional bandwidth is required. This

limitation can be overcome by using a thick (10 mm) air substrate such as expanded polystyrene (EPS), however, this introduces further mechanical and manufacturing limitations.

Another limitation to using a patch array is the power handling capabilities. A patch antenna can typically handle up to 100 W depending on the size of the patch as well as the substrate used [4]. This limitation can be overcome through the use of multiple patch elements, however this greatly complicates the feed network.

A previous investigation into the feasibility of patch antennas resulted in the following conclusions being drawn by the author [1]:

- The power requirements could be met by using an array of patches, however, it was found that the required 10° azimuth beamwidth could only be achieved through the use of a minimum of 10 to 12 square patches in any single plane. Feeding an array with a number of elements not equal to 2^n is extremely difficult and impractical at high power levels.
- Manufacturing a patch antenna that is 1510 mm long, the length required to accommodate 12 patches, regardless of the substrate used is a challenging engineering task.
- The azimuth SLL for an array of 12 patches in a single plane was found to be at 13.5 dB, shown in Figure B.3 in Appendix B. This can be improved by stacking patches in the vertical plane of the array however, this results in a solid aperture area of well over half a square meter and as a result, even though the physical volume is low, the wind resistance is more than what would be experienced if an equivalent meshed dish antenna were to be used.
- The bandwidth of a square patch used in the patch antenna array when using a standard RT/Duroid 5880 [5] substrate was found to be half the required bandwidth at only 23 MHz or 2%. The bandwidth was shown to improve to 92 MHz or 7% when using a 10 mm thick air substrate such as EPS in place of the RT/Duroid 5880 [5]. However, the use of EPS as a substrate would result in mechanical issues affecting the structural integrity of the antenna. The results of the simulations can be seen in Figures B.1 and B.2 in Appendix B.
- The feed network required to feed 12 dual polarised patch antennas in an array from a single input port would be extremely complex.

It has therefore been decided that the use of a patch antenna array would not be feasible due to the various problems mentioned.

2.1.2 Yagi-Uda Antenna

The second antenna design to be investigated was a Yagi-Uda antenna, commonly called a Yagi antenna, consists of a number of straight elements positioned along a boom. The driven element is normally a folded-dipole with a reflector $\lambda_0/4$ to its rear along the boom. To the fore of the driven element are the parasitic directors.

Figure 2.2 illustrates the basic configuration for a Yagi antenna.

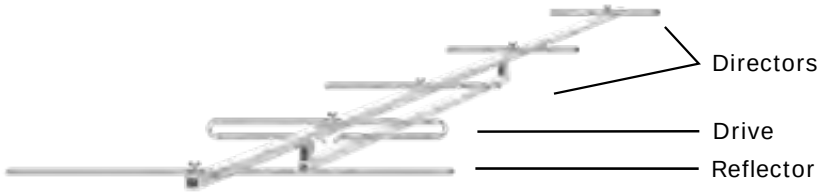

Figure 2.2: Typical Yagi configuration. The largest element to the rear of the boom represents the reflector (±5% larger than the driven element). The dipole acts as the active driven element (folded-dipole) while the directors are placed in front of the driven element (±5% shorter than the driven element) [6].

The driven element of a Yagi antenna, which is situated between the reflector and director elements, is the equivalent of a centre-fed half-wave dipole antenna. Parallel to the driven element, and approximately 0.2 to 0.5 wavelengths on either side of it, are straight rods called reflectors and directors [6]. A reflector, which is slightly longer than half a wavelength, is placed a quarter wavelength behind the driven element which focuses the beam along the boom of the Yagi. Directors are placed in front of the driven element and are slightly shorter than half a wavelength.

A typical Yagi antenna has one reflector and multiple directors parallel to a single radiating element. The more directors, the higher the gain and the longer the antenna. However, it must be noted that adding more directors does not increase the gain linearly. A Yagi antenna is an endfire structure and therefore the EM energy is concentrated in the direction of the directors. Both the reflector and the directors are passive elements used for focusing the EM wave [6].

Yagi antennas are primarily used for line-of-sight communications applications where a gain of 10 dBi to 15 dBi is required and are generally found to have a beamwidth in the plane of polarisation of 30° to 50° [6][7]. Due to the fact that a Yagi antenna uses a half wavelength dipole antenna as its driven element, Yagi antennas typically have a very low bandwidth, approximately 2% to 3% [8]. A well designed Yagi antenna can be seen to exhibit a bandwidth of up to 5% when using a folded dipole feed. It has been shown that this can be even further increased to 20% however, the increase in bandwidth corresponds with an increase in element spacing and an elongation of

the antenna [8][9]. Generally, the more director elements, the higher the gain and the narrower the bandwidth of the antenna [10].

The input impedance to a Yagi antenna is generally found to be between 10 and 40 ohms. This results in a mismatch between the feed and the antenna, a serious problem in high powered systems due to the large amounts of reflected power. This problem can be solved by properly matching the input to the Yagi through the use of a 'T' match fed by a 1:1 balun at the centre of the two gamma matches [10]. The downside to this is often found to be a loss in bandwidth and can be expensive to implement at high power levels [10].

The main limitation of a Yagi antenna is that the HPBW is too wide to meet the system requirements. To achieve a HPBW of 10°, the required length would be in excess of 4 m and the SLL in the plane of polarisation would be significant [7]. Using a Yagi antenna in the form of a Yagi array will result in high side lobe levels as well as present feed difficulties while barely reducing the overall length of the antenna due to the non-linear properties of the directors and therefore is not considered. As a result of these limitations, it has been decided that a Yagi antenna would not meet the system requirements as detailed in Section 1.2, as maintaining a bandwidth greater than 4% with a HPBW of less than 20 degrees is not realistically achievable [4][10].

2.1.3 Sectoral Horn Antenna

A horn antenna is a simple aperture antenna, commonly used at high frequencies due to their high gain and simple design. The most common type of horn antenna is a pyramidal or sectoral horn as shown in Figure 2.3. A full pyramidal horn antenna would result in an aperture size that too large (1500 mm × 1500 mm). A sectoral horn antenna would allow for a smaller aperture than a pyramidal horn and could potentially be used to meet the project requirements.

Figure 2.3 illustrates the basic differences between a pyramidal and a sectoral horn antenna.

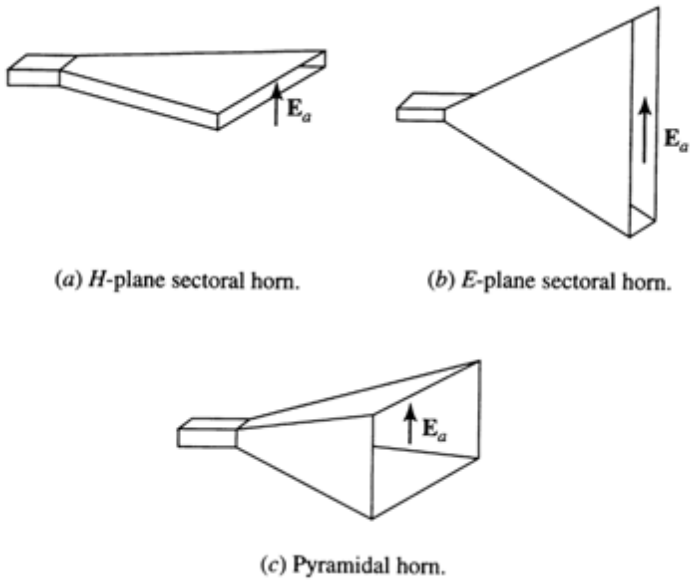

Figure 2.3: Basic geometry of pyramidal and sectoral horn antennas. (a) H-plane sectoral horn antenna used for a fan-beam radiation pattern in the elevation plane. (b) E-plane sectoral horn antenna used for a fan-beam radiation pattern in the azimuth plane. (c) Pyramidal horn antenna for a narrow beam in both azimuth and elevation planes [11].

Sectoral horn antennas were investigated by the author [1] as to whether they would meet the project requirements. This investigation resulted in the following conclusions:

- Dual polarisation and power handling are easily achieved with a sectoral horn antenna.
- Due to the aperture illumination of a sectoral horn antenna, the azimuth beamwidth was shown to vary by almost 4 degrees when switching between horizontal and vertical polarisation as can be seen in Figure B.4 in Appendix B.
- Also as a result of the non-uniform aperture illumination when horizontally polarised, the SLL in the azimuth plane are found to be 15.3 dB. The azimuth SLL when vertically polarised is found to be 20.5 dB.
- While a sectoral horn antenna meets almost all the requirements, it is too large to use at L-Band. Table 2.1 outlines the approximate dimensions required to achieve a 10° azimuth beamwidth from a sectoral horn with a centre frequency of 1.3 GHz.

Table 2.1: The required dimensions for achieving a 10° azimuth beamwidth using a sectoral horn antenna [1].

Dimension	**Approximate Value**
Length	3000 mm
Width	1500 mm
Height	176 mm

From Table 2.1 it can be seen that the required antenna is physically large and would not be able to be used on a standard tripod. An array of horn antennas was investigated and it was found that due to the cosinusoidal aperture illumination when vertically polarised, the SLL was as high as 7 dB and as a result, it was decided that no further research into the use of horn antennas to meet these requirements would be conducted. The results of these simulations can be seen in Figure B.5 in Appendix B.

2.1.4 Pillbox Antenna

A pillbox or cheese antenna, is a parallel plate structure whereby a reflector is sandwiched between two conducting parallel plates as shown in Figure 2.4.

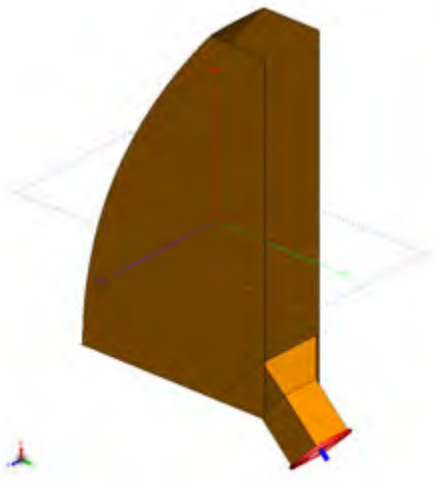

Figure 2.4: Basic structure of a pillbox or cheese antenna fed by a square pyramidal horn waveguide antenna [1].

A pillbox has the advantage that it can be used as a high power, dual polarised antenna while producing an accurate and narrow beam pattern. A disadvantage to the pillbox antenna is that they are generally large in volume due to the parallel plates. This makes them difficult to mount unless mounting to large flat surfaces such as the roof or underside of a vehicle.

A previous investigation into the feasibility of a pillbox antenna to meet the project requirements resulted in the following conclusions [1]:

- Dual polarisation and power handling were easily achieved.
- In order to achieve the required 10° azimuth beamwidth, the antenna diameter had to be 1500 mm, resulting in a large and heavy structure.
- Mounting the pillbox antenna to a tripod was found to be very mechanically challenging due to its large volume and weight.
- It has been found that while the volume of the antenna was significantly larger than that of an equivalent patch antenna array, a meshed reflector between the parallel plates would allow for significantly reduced wind resistance.
- According to both simulated and measured results, the pillbox antenna appears to suffer from feed defocusing when switching between planes of polarisation. This can be seen in Figure B.6 in Appendix B.

It has therefore been decided that the pillbox antenna would not be suitable to meet the project requirements.

2.1.5 Parabolic Reflector Antenna

Parabolic reflectors come in many forms, however, the basic mode of operation remains the same. Parallel EM waves are received by the parabolic reflector and focused to a point known as the focal point. The feed of the antenna is placed at the focal point and receives the focused EM waves [12]. The reciprocal is also true in that the feed emits EM waves which get reflected off the parabolic reflector as parallel waves as shown in Figure 2.5.

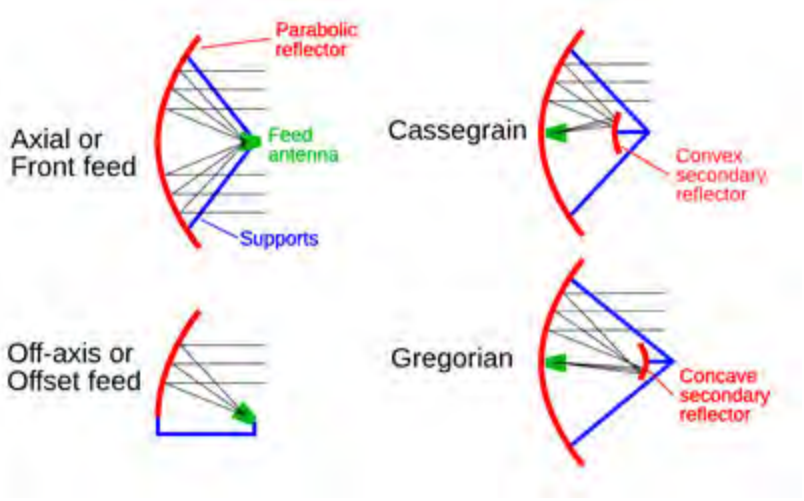

Figure 2.5: Different parabolic reflector feed designs. (Top left) Front fed prime focus parabolic dish antenna. (Top right) Dual reflector Cassegrain fed parabolic dish antenna. (Bottom left) Offset fed parabolic dish antenna. (Bottom right) Dual reflector Gregorian fed parabolic dish antenna. [13].

Figure 2.5 illustrates the various different parabolic antenna feed designs that are commonly used. Parabolic reflector antennas have been investigated by the author [1] as to whether or not they meet the project requirements set in Section 1.2. The investigation resulted in the following conclusions [1]:

- A dish antenna can be dual polarised and can handle high power levels.
- In order to maintain a relatively small structure, a truncated parabolic dish antenna is required. Due to the dual polarisation requirement, the feed must remain symmetrical and as a result, spillover and side lobe levels will need to be carefully considered.
- While the aperture of a parabolic dish antenna is larger than any of the other antenna designs, the wind resistance can be greatly reduced through meshing of the parabolic surface.
- The volume of a dish is considerably smaller than an equivalent horn or pillbox antenna.
- Feed blockage and efficiency for a small dish antenna remains an engineering challenge and various design trade-offs need to be considered.

Considering the advantages and disadvantages of using a parabolic dish antenna to meet the requirements set in Section 1.2, it has been decided that the most feasible antenna design to pursue would be a parabolic reflector antenna.

2.2 Summary

This section has discussed the various theoretical concepts required to design an antenna that meets the requirements set in Section 1.2. Various antenna design trade-offs have been discussed along with the basic antenna properties required when characterising an antenna.

The feasibility of various antenna designs has been discussed. A parabolic dish antenna was found to be smaller in volume than all other designs apart from a patch antenna. The ability to mesh a dish antenna allows for lower wind resistance than any of the other antenna designs considered. While the Yagi, horn and pillbox antenna designs all allow for high power, dual polarised operation, the parabolic reflector allows for higher bandwidth and narrower beamwidth in a more compact design.

It has therefore been concluded that the most appropriate design would be to use a parabolic reflector antenna.

Chapter 3

Reflector Antenna Theory

In Chapter 2, various antenna designs have been investigated and their feasibility for NeXtRAD have been discussed. Due to the nature of the system requirements, it has been decided that the most feasible antenna would be a reflector antenna.

3.1 Types of Reflector Antennas

A reflector antenna falls within the aperture class of antennas, whereby a feed structure radiates EM energy towards a reflector where it gets reflected forward as a focused beam.

Reflector antennas are generally used in situations that require:

- High gain
- Moderate bandwidth
- High power handling

Reflector antennas come in many different geometric configurations, with the most common being the plane, corner and curved reflectors. The four most common configurations of reflector antennas are shown in the Figure 3.1.

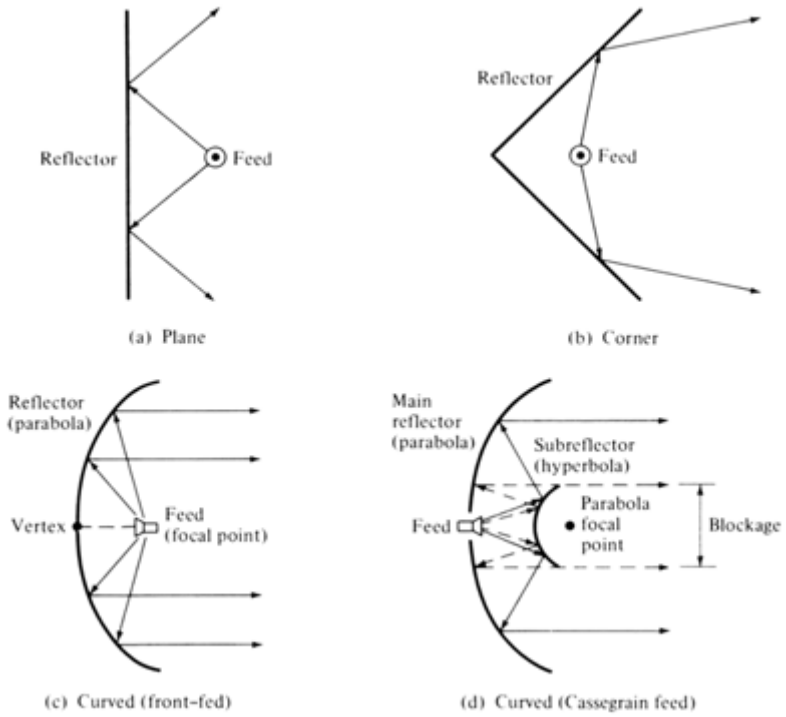

Figure 3.1: Four most common reflector antenna and feed configurations are shown. (a) Plane reflector (b) Corner reflector (c) Curved reflector with front mounted feed (d) Curved reflector with cassegrain feed [12].

3.1.1 Plane Reflector

The most basic reflector antenna is the plane reflector. A plane reflector can be used to direct radiation in a particular direction as seen in Figure 3.1(a). The polarisation, beamwidth and position of the feed can be used to control the radiation pattern of the plane reflector [12]. Geometric optics can be used to determine the superposition of the EM waves and the overall radiation characteristics can therefore be determined.

A plane reflector simply ensures that the radiation from the feed radiated in a single 180 degree direction. The major drawback to plane reflectors is reduced gain and directivity as a result of its inefficient beam focusing.

3.1.2 Corner Reflector

To achieve maximum radiation in any particular direction, the geometric shape of the plane reflector must be altered such that radiation in the backwards and sidewards directions is limited. One way of achieving this is through the use of a corner reflector. The simplest form of a corner reflector can be observed in Figure 3.1(a) whereby the corner reflector is created by combining two plane reflectors together [14].

Corner reflectors have a very unique property in that they will reflect any received signal directly back in the direction of the received signal provided the corner angle is 90 degrees. This phenomenon can be observed in Figure 3.2(b). This unique feature makes corner reflectors especially useful in system calibration, while radar and platform system designers use this idea to reduce the number of reflecting angles on vehicles in an attempt to reduce radar detection [12].

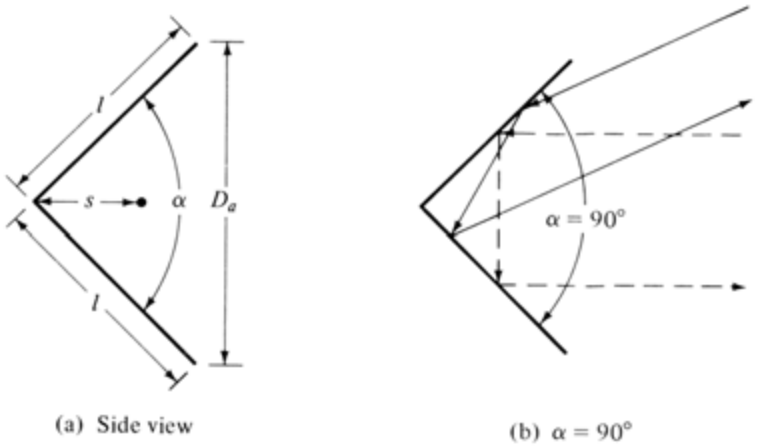

Figure 3.2: Corner reflectors are constructed by joining two plates together at a vertex. Corner reflectors with 90 degree included angles reflect received signals directly back to the receiver as can be seen in (b) [12].

When designing a corner reflector, it is important to maintain the system efficiency. Maintaining system efficiency is done by ensuring that the spacing between the vertex and the feed element increases as the angle between the two plates decreases and vice versa. Most corner reflectors are fed using a dipole element and are therefore generally linearly polarised structures [12][14].

3.1.3 Parabolic Reflector

One means of further improving on the radiation properties (radiation pattern, gain, antenna efficiency, polarisation purity, etc.) is by using a parabolic shaped reflector. It can be shown by using geometric optics that if a beam of parallel rays is incident upon a parabolic reflector, then those waves will converge to a point known as the focal point [4]. The reciprocal of this is that if a source is placed at the focal point, the rays reflected off the parabolic reflector will emerge as a parallel beam [12].

There are many different ways to feed a parabolic reflector, however two of the more compact designs utilise a prime focus feed or a cassegrain feed, both of which can be seen in Figure 3.1(c) and 3.1(d) respectively. Each has its advantages and disadvantages which will be discussed in the following section.

3.1.4 Feeding a Parabolic Reflector

Correctly feeding a parabolic reflector is of utmost importance to the performance of the antenna and as a result requires careful design. A challenge that needs to be overcome when designing a parabolic reflector is the positioning and design of the feed. It is of critical importance that the feed does not result in blockage as this will degrade the antenna performance [4][12].

While placing the feed of the antenna at the focal point, referred to as a prime focus antenna, simplifies the design and manufacture of the antenna, it does have drawbacks. One of the main disadvantages of prime focus parabolic reflectors is that the transmission line to the feed must be long enough to reach the transmitting or receiving equipment (usually situated behind or below the reflector).

Figure 3.3 illustrates the geometric differences between placing the feed at the focal point of a reflector and using a secondary reflector such as in a cassegrain design.

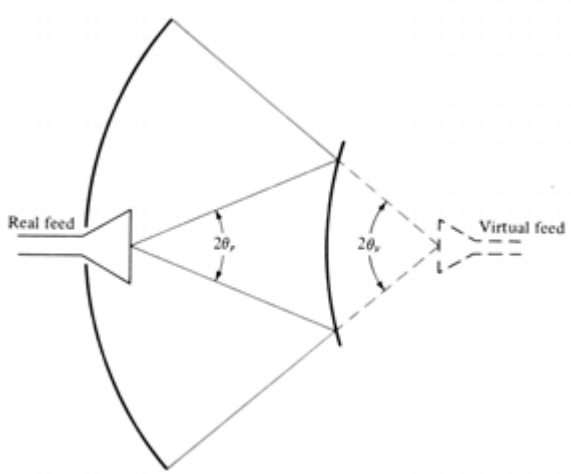

Figure 3.3: Feed comparison between prime focus and cassegrain whereby the hyperbolic reflector acts as a secondary source at the focal point [12].

In some applications, this can be overcome by placing the receiver on or behind the feed itself. However, this approach is not without its own difficulties, especially in cases where large, high power amplifiers or low noise receivers are required. Due to the physical size and weight of the feed for high power systems, the feed cannot be adequately supported or the resultant blockage would be too high [12].

To overcome this limitation, a feed design known as a cassegrain feed can be used. The cassegrain feed uses the fact that any wave emanating from the focal point of the antenna will reflect off the reflector as a parallel beam. The feed can then be moved to behind the main reflector and using a secondary hyperbolic reflector, the beam can be focused as if the feed were placed at the focal point. This therefore eliminates the need

for long transmission lines and allows for easier mechanical placement of transmitter and receiver equipment [12].

A further advantage to using a cassegrain feed design on large antenna systems is that it allows for easier beam forming. Beam forming using a cassegrain feed is done by manipulating the second hyperbolic reflector and can be used to achieve a more uniform illumination of the main reflector as well as reduce spillover.

It has however, been shown that for a cassegrain feed antenna to have a higher efficiency than a prime focus fed antenna, the minimum dish diameter must be greater than $50\lambda_0$ with a minimum sub-reflector diameter of $20\lambda_0$. This equates to a fairly large dish and is therefore often not considered at lower L-Band frequencies due to size constraints [13].

It is clear that regardless of the feed design, feed blockage is of major concern for symmetric parabolic reflectors as it leads to an increase in side lobe levels as well as a reduction in overall gain. A further side effect as a result of feed blockage is a reduction in cross-polarisation discrimination [12].

The most common technique used for overcoming feed blockage is through the use of an offset feed arrangement. Offset parabolic reflector systems have been developed for both single and dual reflector systems [12].

Figure 3.4 illustrates the basic geometry of an offset feed reflector antenna.

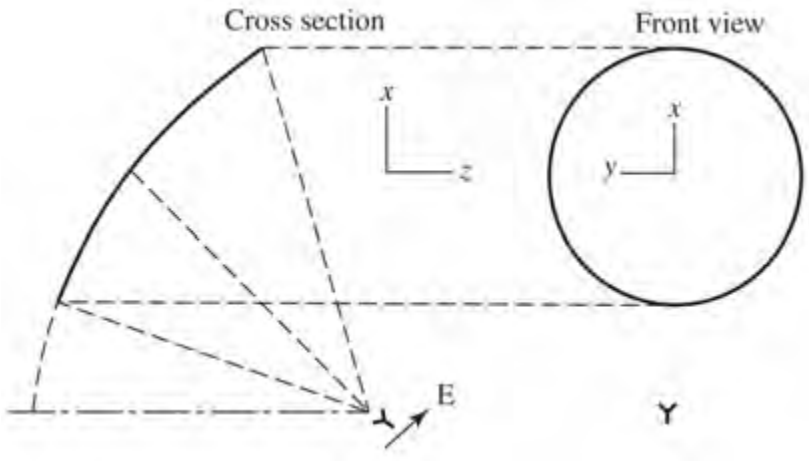

Figure 3.4: Offset feed reflector geometry showing the cross section as well as the front view as seen by the antenna feed. It can be seen from the side view that the feed no longer blocks or interferes the radiation path [4].

Due to the asymmetry of the system, design and analysis becomes more complicated however, the focal point of an offset feed dish is less critical than that of a prime focus dish [15]. Other than reducing the feed blockage found in prime focus designs, the

offset feed also allows for the use of larger f/D ratios. This allows for improved pattern manipulation as well as better suppression of cross-polarised radiation emanating from the feed [12].

One major problem encountered when designing an offset feed is the cross-polarisation caused by a linearly polarised wave reflecting off the parabolic reflector. This causes a polarisation mismatch that can be overcome through the use of circularly polarised feeds. However, the use of circularly polarised feeds leads to squinting of the main beam which must be taken into account when designing the system [12].

3.2 Properties of Electrically Small Parabolic Antennas

Although all antennas are characterised by common antenna parameters such as beam pattern, gain and bandwidth, reflector antennas have additional parameters that need to be carefully considered when designing and characterising the antennas.

3.2.1 Focal Length and f/D Ratio

A dish antenna works much the same way as an optical lens in that parallel EM waves arrive from a distant source, strike the reflecting surface and get focused to a point known as the focal point of the antenna. This phenomenon occurs if the reflecting surface is parabolic in shape ($y = ax^2$) [16].

It is therefore clear that one of the most important parameters to be considered when designing a reflector antenna is the f/D ratio. The f/D ratio defines the ratio of the focal (f) point to the dish diameter (D). This is a critical parameter in that it defines the depth and curvature of the dish. f/D ratios between 0.3 to 1 are most common.

As the f/D ratio approaches infinity, the dish becomes a plane structure while becoming deeper as f/D becomes smaller. The deeper the dish, i.e. the smaller the f/D ratio, the more critical the focal point [17].

Figure 3.5 illustrates the effect of the f/D ratio on the curvature of the dish [4].

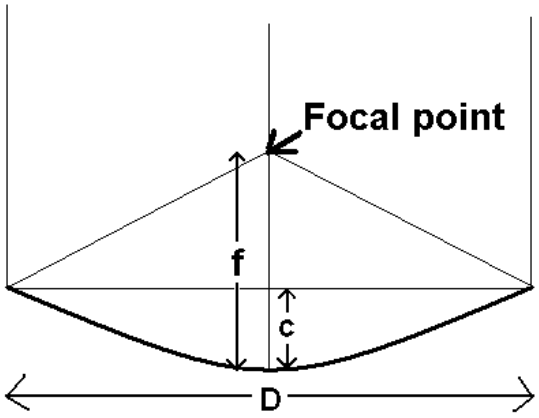

Figure 3.5: f/D ratio of a parabolic reflector where f is the distance from the origin of the parabola to the focal point. D is defined as the largest diameter, usually a constant, of the dish.

One way to determine the f/D ratio of a parabolic dish is to measure the diameter and depth of the dish and use the mathematical expression [16][18]:

$$f = \frac{D^2}{16H} \tag{3.1}$$

where H is the depth of the dish. This way one can determine the focal point, f, and subsequently the f/D ratio of any dish antenna [16].

3.2.2 Factors Affecting Efficiency

The efficiency of an antenna depends on its design as well as its electric size. There are two main types of efficiency, aperture efficiency and radiation efficiency. The radiation efficiency of a dish antenna is generally close to 100% [19]. For electrically large antennas, an aperture efficiency greater than 90% is common. However, for electrically small dish antennas, that is a dish antenna with a diameter less than $10\lambda_0$ [13], the aperture efficiency is generally between 45% and 50% [4][12][17].

The efficiency of small dish antennas is quickly degraded by various size-specific factors. One of the main contributors to the decrease in efficiency of small dish antennas is the large size of the feed in comparison to the relatively small reflector. It is generally not possible to reduce the size of the feed, especially in the case of waveguide feeds (see Appendix A on waveguide theory) [19].

The dominant factors affecting efficiency include [19]:

- Spillover and blockage caused by prime focus feed
- Properties of the EM wave emanating from the feed

– Diffraction originating from the feed and its supporting struts

– Main beam interference due to the back and side lobes of the feed itself

– Impedance matching

Feed Spillover

Spillover is a measure of how much radiation from the feed is not reflected as a result of the reflector being of finite size. Spillover causes a decrease in the front-to-back, F/B, ratio and therefore results in high back lobes [18]. Spillover is the result of over illumination of the reflector surface.

Figure 3.6 demonstrates the three different variations of dish illumination.

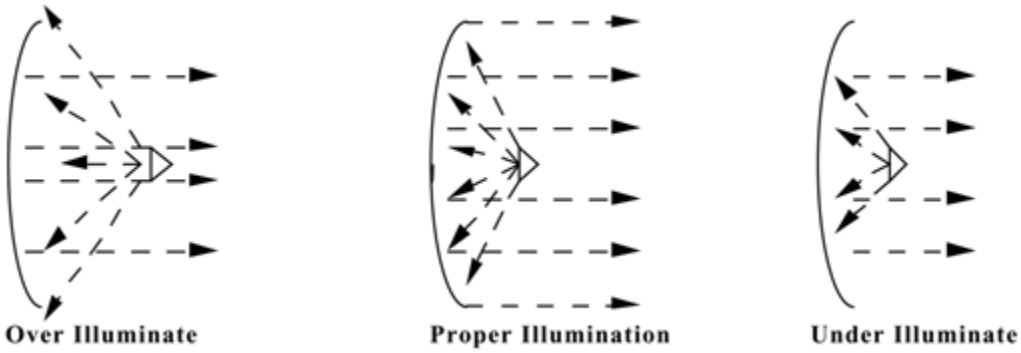

Figure 3.6: (Left) Over illumination results in an increase in spillover, (Centre) correct illumination allows for the highest efficiency while (Right) under illumination results in an underutilisation of dish area therefore lowering aperture efficiency [13].

To combat the effect of spillover, the f/D ratio can be decreased or the feed can be moved closer to the dish. The downside to this is that the efficiency of the system tends to decrease as the f/D ratio goes below 0.4 due to the fact that the dish becomes deep and as a result the feed is required to illuminate over a very large angle. An f/D ratio of 0.25 results in the focal point of the feed being level with the rim of the dish, therefore requiring a feed that provides illumination across an angle of 180 degrees [13].

While the radiation pattern of the feed does not affect the beamwidth of the dish antenna system, it has a significant effect on the side lobe levels and the aperture efficiency [4]. To maximise the performance of the antenna, the side lobe levels need to be kept to a minimum.

To achieve the best compromise between low spillover and high aperture efficiency, the feed should radiate towards the reflector such that the ratio of power at the reflector

edge to the power at the centre is −10 dB [4][12][18]. This effect of edge taper, also known as illumination taper, is illustrated in Figure 3.7.

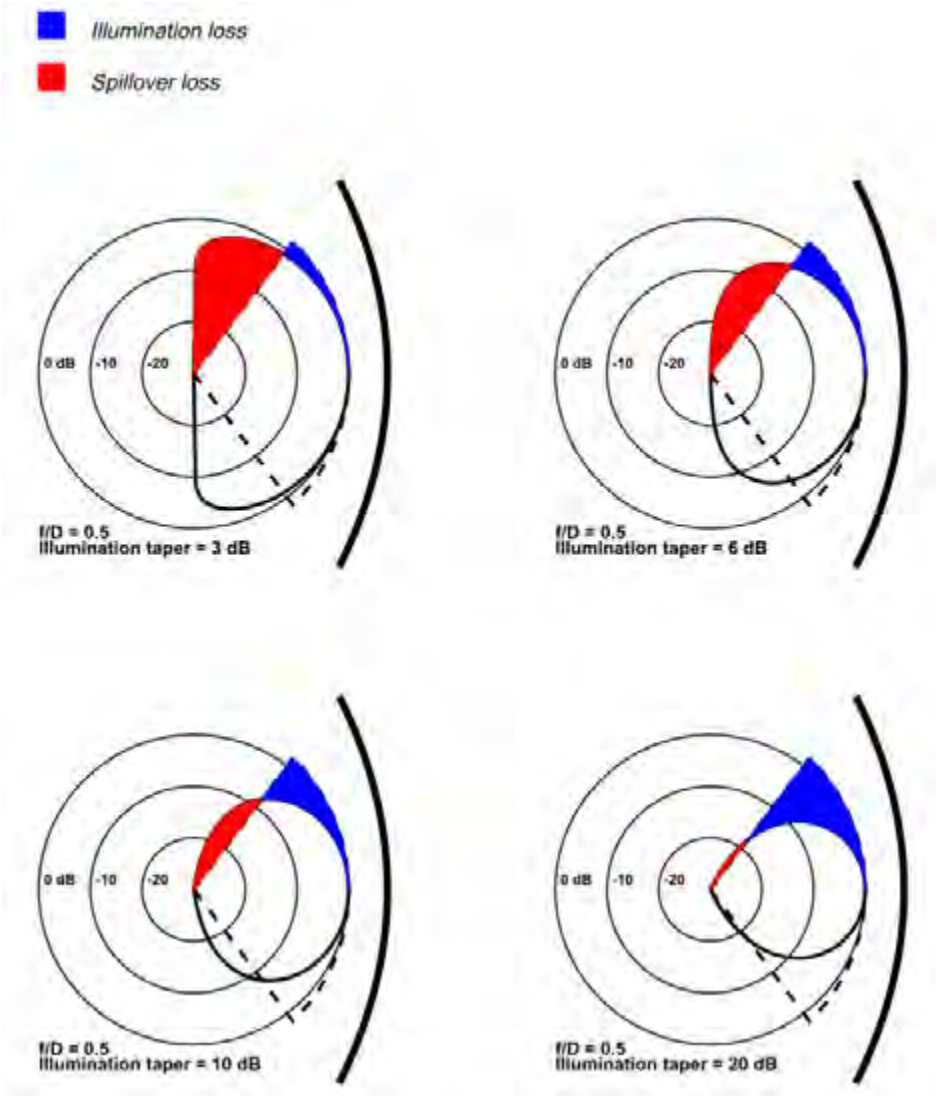

Figure 3.7: Different feed illumination patterns for a given f/D ratio showing the effect on aperture efficiency and spillover for different illumination tapers. (Top left) Illumination taper of 3 dB leads to large spillover losses due to over illumination. (Top right) Illumination taper of 6 dB results a large spillover loss and a small illumination loss. (Bottom left) Illumination taper of 10 dB. This will offer the best compromise between spillover loss and illumination loss. (Bottom right) Illumination taper of 20 dB is as a result of a very narrow feed beamwidth. This configuration leads to high illumination loss and low aperture efficiency [16].

Expanding on the idea that the edge taper should be at the −10 dB point of the feed, the focal length can be related to the illumination pattern of the feed. This is expressed as follows [16]:

$$f/D = \frac{1}{4 \times \tan(\theta/2)} \tag{3.2}$$

where θ is the 10 dB beamwidth of the feed. The feed could either optimised to fit a given f/D ratio (in the case of a pre-fabricated dish) by rearranging (3.2), or the

appropriate f/D ratio for a given feed could be determined depending on what is required [12][16]. Ideally, the feed of the antenna is designed such that the -10 dB point lies on the edge of the reflector. This results in the best compromise between aperture efficiency and spillover loss. This is further explored in Chapter 4.

Feed Blockage

Blockage is caused as a result of having a feed or feed support structures placed in the radiation path of the reflector, see Figure 3.1(d). Blockage plays a large role in decreasing the aperture efficiency of the antenna and results in large unwanted side lobe levels [4][13].

Feed blockage loss becomes significant on electrically small dishes. A dish is considered electrically small when the diameter of the dish is less than $10\lambda_0$ [13]. The gain of a parabolic dish antenna with a prime focus feed is given by [16]:

$$G = \eta_{total} \frac{\pi^2 (D^2 - d^2)}{\lambda^2} \tag{3.3}$$

where D is the reflector diameter, d is the feed diameter and η_{total} is the total combined efficiency of the antenna.

To minimise the effects of feed blockage, it is important to ensure that the feed diameter is no more than 10% of the dish diameter [20]. It can be seen from (3.3) that the efficiency of the dish drastically decreases as the ratio of D to d decreases. The effect of decreasing this ratio is shown graphically in Figure C.1 in Appendix C where it can be seen that the efficiency for small dishes depends heavily on the size of the dish with respect to the size of the feed.

Performance Degradation due to Feed Supports

Diffraction effects are seen when a propagating EM wave interacts with an object in its path such as feed supporting structures or the feed itself. Diffraction introduces additional losses due to the disturbance of the field homogeneity and the field distribution across the aperture of the reflector [19].

The feed supports therefore need to be carefully designed to ensure minimal impact on antenna performance. This is further explored in Chapter 4.

F/B ratio

The F/B ratio of an antenna represents the front (F) to back (B) ratio of the antenna radiation and is a measure of the directivity of a directional antenna [18]. The F/B ratio is the ratio of the gain in the maximum direction to the gain in the backwards direction (180 degrees off the main beam).

This parameter is usually provided in dB and for properly designed dish antennas is generally greater than 30 dB [4][18]. The F/B ratio can be affected by various parameters such as, amongst others, build material, build accuracy and mesh structure.

Prime Focus Dish Feed Matching

In reflector antennas that utilise prime focus feeds, issues with impedance mismatch may arise due to reflections from the centre of the reflector. These issues, positive or negative depending on the design, are due to the position of the feed in a prime focus antenna system, the centre of the reflector reflects energy back into the feed.

Depending on the size of the dish, the f/D ratio and the type of feed design used, the effects of the reflected energy back into the feed can vary from minimal to significant influence on the port match or port-to-port isolation in the case of a dual polarised system [15].

The effects of these reflections increases with small parabolic antennas as the feed is usually located very close to the reflector and as such needs to be carefully considered. The basic geometrical parameters of a prime focus dish antenna can be seen in Figure 3.8.

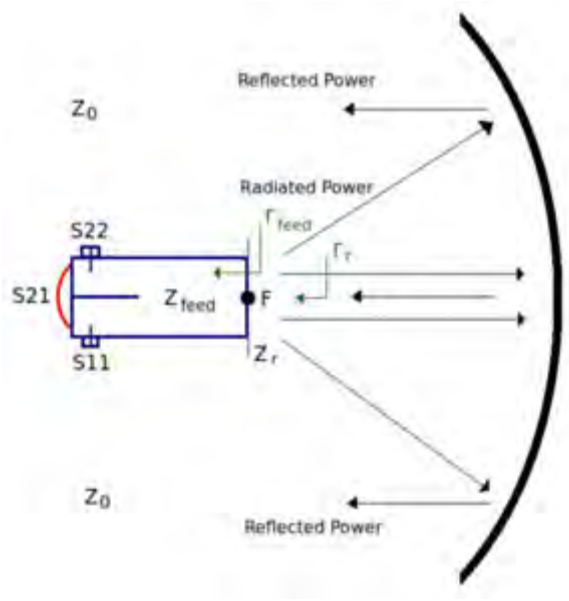

Figure 3.8: Basic prime focus geometric configuration where an open-ended waveguide feed is placed at the focal point of the antenna. The reflections off the central area of the parabolic dish reflect directly back into the path of the feed. This causes interference which results in feed mismatch and a change in port-to-port isolation. [15].

From Figure 3.8 it can be seen that the system becomes a transmission line problem in that the feed needs to be re-matched once configured with the reflector. As the phase centre of the feed must remain at the focal point of the antenna, the only way to achieve this is by adjusting either the probe length or their positions within the waveguide feed [15][21]. The adjustments required to optimise the feed transition can only be completed after the design of the dish is complete as the distance to the focal point of the dish is critical to the performance of the feed. This is further explored in Section 4.2.4.

J. Pawlan et al. [15] have shown that using a larger dish (especially for dishes with a low f/D ratio) will reduce the effect of reflections back into the feed. It has also been noted that the use of RF absorptive material or a shaped reflector at the apex of the dish would decrease the antenna performance by raising the noise temperature of the antenna [15].

3.2.3 Wind-loading and Meshing

This is a critical design parameter that needs to be carefully considered as often wind-loading results in trade-offs needing to be made, such as sacrificing antenna gain in an attempt to make the antenna smaller. These design trade-offs are due to the fact that for wind gusting at 36 m/s, the antenna structure will experience a force of 80 kg/m^2 [22]. This means that a dish antenna with a diameter of 900 mm will experience a

wind-load of approximately 50 kg. While not being a particularly large dish, this is a substantial force [22].

One way of overcoming the effects of wind-loading is to use a mesh structure as the surface of the dish. This way the cross sectional area of the dish remains the same while the actual amount of wind-loading decreases drastically. Mesh dishes have the added benefit that they are also lighter than solid dishes.

To ensure that the mesh dish will perform like a solid dish, it is of utmost importance that the holes in the mesh are smaller than 1/10 of a wavelength in diameter [22].

3.3 Summary

This section has provided a in depth overview of the required theory and design considerations that must be taken into account when designing a truncated parabolic dish antenna. Different types of parabolic dish antenna designs have been investigated, illustrating the advantages and disadvantages of each dish and feed combination. The most common parabolic dish antenna designs that are used today are prime focus fed, Cassegrain fed and offset fed parabolic dish antennas. After reviewing the various advantages and disadvantages of each, it has been decided that the most appropriate feed design to meet the requirements set in Section 1.2 would be a prime focus feed.

In an attempt to reduce wind loading, meshing of the antenna is required. It has been shown that feed blockage plays a major role in overall antenna performance and it is therefore of utmost importance that the feed blockage be kept to a minimum. The feed position at the focal point of the dish is critical to the performance of the antenna and therefore requires careful design.

Literature emphasises the importance of ensuring the correct illumination of the reflecting dish in order to achieve desired performance. Having an edge taper of -10 dB is generally considered an appropriate compromise between over- and under-illuminating the main reflector.

Chapter 4

Design Procedure

The following Chapter focuses on the design and simulation of the L-Band antenna, including the antenna feed and mounting system. Theory not covered in this Chapter can be found in Chapter 2, 3 and Appendix A.

FEKO v7 [23] has been used for simulating and optimising antenna performance, while CST 2014 [24] has been used for simulating and optimising the waveguide feed performance.

The reason for using use CST for the feed simulations and FEKO for the antenna simulations is due to the fact that CST is more proficient in simulating port parameters, while FEKO is more suitable for simulating large structures such as antennas. In some instances, simulations were done using both FEKO and CST and where appropriate, the simulation results have been compared in an attempt to improve overall simulation confidence.

4.1 Application Requirements

As stated in Section 1.2, the following requirements are to be met by the final antenna design:

- Dual polarised (Horizontal and Vertical)
- L-Band with centre frequency of $f_0 = 1.3$ GHz ($\lambda_0 = c/f_0 = 230$ mm)
- Minimum 50 MHz (4%) bandwidth (1.275 GHz to 1.325 GHz)
- 10° 3 dB azimuth beamwidth (regardless of the plane of polarisation)

- Be able to be mounted on a tripod and withstand harsh environmental conditions such as high winds
- 1.5 kW peak power handling capabilities

4.2 Antenna Design

As stated in Chapter 2, various antenna designs have been explored and it has been concluded that the most appropriate approach to fulfil the user requirements would be to utilise a parabolic dish antenna.

To properly design the parabolic dish as well as the feed, it is important that a rough approximation of the required dish size be determined. For a uniformly illuminated parabolic dish, the following formula is used to determine the approximate diameter, D, required to produce a desired beamwidth, θ, [4][18][21]:

$$D = \frac{70\lambda_0}{\theta} \tag{4.1}$$

It can therefore be seen that to achieve a 10° azimuth beamwidth, the approximate diameter of the dish is required to be:

$$D = \frac{70 \times \lambda_0}{10} = 7\lambda_0 \tag{4.2}$$

with the free-space wavelength, $\lambda_0 = c/f_0$ =230 mm, the diameter is:

$$D = 7 \times 230 = 1615.4 \text{ mm} \tag{4.3}$$

Immediately it can be seen from (4.3) that the required diameter, D, is physically quite large and will require various optimisations to make it small enough to be able to be mounted on a tripod as required. It must be noted that while the required diameter is relatively large, the antenna is still considered an electrically small dish antenna as the diameter is less than the $10\lambda_0$. It also falls short of the $50\lambda_0$ diameter requirement for the efficient use of a cassegrain feed design and hence it has been decided that the best approach would be to design the antenna with a prime focus feed.

4.2.1 Feed Design

Ordinarily, when designing a parabolic reflector, the dish is designed first, followed by the design of an appropriate feed. This design sequence will achieve the desired beam

pattern and have more flexibility over the design of the dish itself. However, as stated in Section 1.4, the manufacturing capabilities available to this project were severely limited and as a result, the feed had to be the first design step.

A waveguide feed has been chosen as it has been shown in Chapter 3 to be the most appropriate feed design for this application [1]. Due to the dual polarised requirement, a symmetric feed such as a square or circular waveguide feed is required. To achieve the best performance as a dual polarised antenna, it has been decided that a circular waveguide feed would be used. It has been shown in previous research and experiments by the Author [1], that using a circular waveguide over an equivalent rectangular waveguide can improve port-to-port isolation by as much as 8 dB [1].

Aside from the performance advantages achieved through the use of a circular feed, they also have the advantage of being simpler to manufacture. Unlike at higher frequencies such as X-Band, L-Band waveguides are not readily available commercially and often need to be specifically manufactured. The manufacture of L-Band waveguides can be difficult and expensive due to their large size, however certain tin cans can be used to make a circular waveguide. There are many examples where high performance waveguides have been manufactured from tin cans, a prime example of this being MIT's "Coffee Can Radar" [25][26].

Figure 4.1 shows the schematic of a circular waveguide.

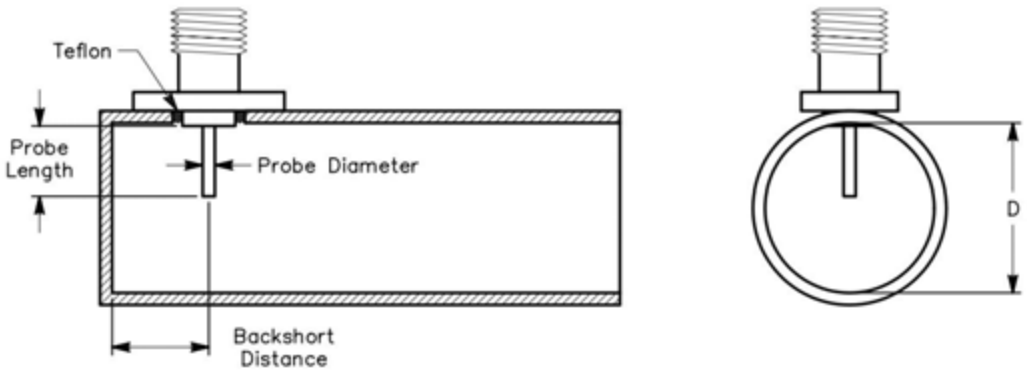

Figure 4.1: (Left) Side view and (Right) front view of a circular waveguide illustrating the basic probe placement parameters [27].

As discussed in Chapter 3, feed blockage plays a major role in determining the overall performance of an antenna, especially in the case of a small dish antenna (where $D < 10\lambda_0$). As a result of the required antenna being relatively large but electrically small ($D = 7\lambda_0$), it has been decided that an open ended waveguide feed with no flair would be used as this will keep feed blockage to a minimum. This will also allow for simpler manufacture as symmetry will be easier to achieve.

The main requirement for selecting a suitable waveguide is that the inner diameter is large enough to support the fundamental mode across the entire bandwidth of operation without introducing higher order modes. To determine the appropriate diameter of the waveguide, the cut-off frequency is determined:

$$\lambda_c = \frac{C}{f_c} \tag{4.4}$$

where λ_c is the lower cut-off wavelength and f_c is the lower cut-off frequency, below which the fundamental TE_{11} mode will not propagate. The cut-off wavelength, λ_c, can be related to the diameter, D_w, of the waveguide as [25][27]:

$$\lambda_c = 1.705 D_w \tag{4.5}$$

$$\therefore D_w = \frac{C}{1.705 \times f_c} \tag{4.6}$$

Equation (4.6) shows that the diameter of the waveguide is inversely proportional to the frequency. As the frequency approaches the cut-off frequency, the input impedance increases dramatically and as a result, it is important to design the waveguide such that the lowest operating frequency is well above the absolute cut-off frequency.

The waveguide in question is required to operate at L-Band ($f_0 = 1.3$ GHz) which has a lower cut-off frequency of 1 GHz. This results in a diameter size of:

$$D_{L-Band} = \frac{3 \times 10^8}{1.705 \times 1 \times 10^9} = 176 \text{ mm} \tag{4.7}$$

It is of utmost importance that higher order modes do not propagate within the waveguide. The next higher order mode of concern in a circular waveguide is the TM_{01} mode [12][28]. The cut-off frequency for the TM_{01} mode is [12]:

$$f_c = \frac{2.4049 \times c}{\pi D_w} \tag{4.8}$$

$$f_c = \frac{2.4049 \times 3 \times 10^8}{\pi \times 0.176} = 1.312 \text{ GHz} \tag{4.9}$$

It can be seen from (4.9) that the unwanted higher order mode cut-off frequency is at

1.312 GHz, which falls within the band of interest (1.275 GHz to 1.325 GHz). For a mode to propagate through a waveguide, an appropriate launcher is required to excite the mode. Due to the launcher design and the use of a single monopole probe to launch the fundamental TE_{11} mode, the TM_{01} mode will not be able to propagate through the waveguide [29]. This is due to the fact that the monopole launcher will not facilitate the launching of the TM_{01} mode [12]. To launch the TM_{01} mode, the boundary conditions need to be satisfied as discussed in Appendix A [29]. As can be seen by the field distribution shown in Figure A.1, to satisfy the boundary conditions, it would require either the monopole launcher to be inserted through the centre of the back-wall of the waveguide or the use of a magnetic field spiral launcher [12]. It has been confirmed through simulations, see Figures 4.3 and 4.5, that the TM_{01} mode has little to no effect on the fundamental TE_{11} mode when using the waveguide configuration as designed.

The cut-off frequency at which the next higher order TE mode is excited needs to be observed. The next higher order TE mode is the TE_{21} mode. The TE_{21} mode can be launched into the waveguide from the monopole probe if the diameter is too large. To ensure that this does not occur, the cut-off frequency for the next higher order mode must be determined using the calculated diameter [12][28]:

$$f_c = \frac{3.0542 \times c}{\pi D_w} \tag{4.10}$$

using the waveguide diameter as calculated in (4.7), the cut-off frequency for the next higher order TE mode is [28]:

$$f_c = \frac{3.0542 \times 3 \times 10^8}{\pi \times 0.176} = 1.67 \text{ GHz} \tag{4.11}$$

Equation (4.11) shows that the cut-off frequency for the next higher order TE mode is 1.67 GHz. This is ideal as the centre frequency of NeXtRAD is 1.3 GHz, which lies exactly in the centre of our waveguide band of operation. The operating band of the waveguide is therefore set as 1 GHz to 1.6 GHz to ensure only the fundamental TE_{11} mode propagates.

After searching for an appropriate cylinder, it has been found that a 5 litre paint can has an inner diameter 175 mm and a length of 230 mm (almost exactly $1\lambda_0$) and is adequate for use as a waveguide at the desired L-Band frequencies.

Another important consideration when designing a waveguide is the coaxial to waveguide transition. The design of this transition is critical because it affects the performance of the entire system. The impedance of this transition is defined by the length, position and thickness of the inset probe. Looking at Figure 4.1, it can be seen that

the inset probe is a simple quarter wavelength monopole radiator [21][27]. The length of the probe required for a centre frequency of 1.3 GHz is therefore:

$$L_{probe} = \frac{\lambda_0}{4} = \frac{C}{4 \times f_0} = 57.7 \text{ mm} \tag{4.12}$$

The backshort distance is defined as the distance from the probe to the back-wall of the waveguide. By using a quarter wavelength spacing between the back-wall and the probe, the reflected wave will constructively interfere with the transmitted wave and propagate forward. Unlike the probe length, which is defined by a quarter free-space wavelength, the backshort distance is defined using the waveguide wavelength. As shown in Appendix A, the waveguide wavelength is given by (A.3) as:

$$\lambda_g = \frac{230}{\sqrt{1 - (\frac{230}{1.705 \times 175})^2}} \approx 360 \text{ mm} \tag{4.13}$$

$$\therefore L_{backshort} = \frac{\lambda_g}{4} \approx 90 \text{ mm} \tag{4.14}$$

CST has been used to simulate and optimise the circular waveguide across the calculated 600 MHz frequency band from 1 GHz to 1.6 GHz. Initially a singularly polarised waveguide is simulated in an attempt to optimise the launcher probe position before attempting to optimise the feed as a dual polarised feed.

Figure 4.2 shows the CST render of the single polarised waveguide with the coaxial to waveguide transition.

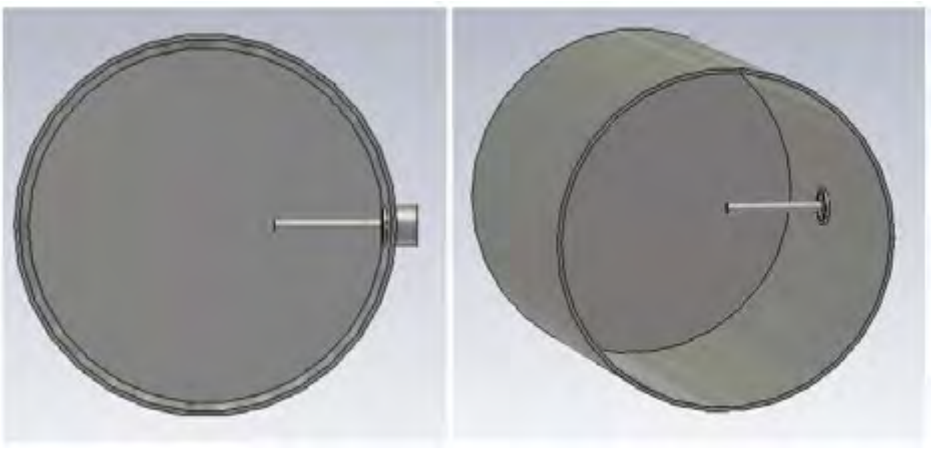

Figure 4.2: CST render of a single polarised waveguide with the coaxial to waveguide transition.(Left) Front view. (Right) Side view.

Figure 4.3 illustrates the simulated S_{11} results of the CST optimised feed structure.

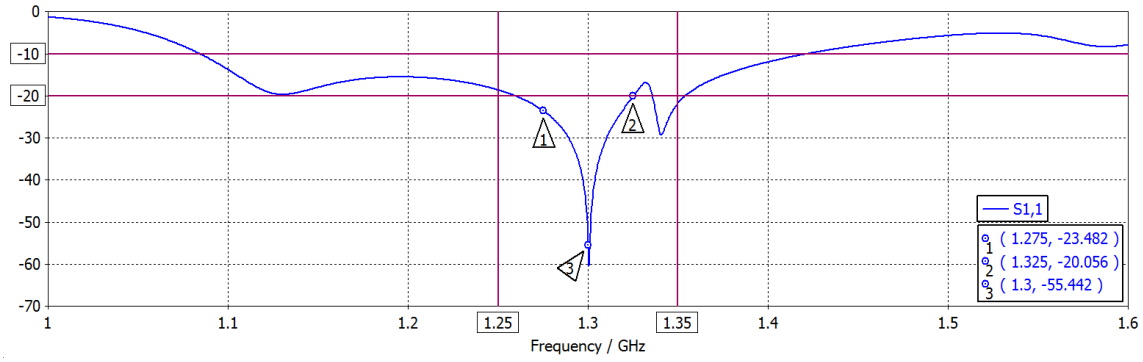

Figure 4.3: S_{11} magnitude [dB] of a singularly polarised standalone waveguide simulation from 1 GHz to 1.6 GHz with a centre frequency of 1.3 GHz. The reflection coefficient is below -20 dB across the entire band of interest.

It can be seen from Figure 4.3 that the feed design works as expected and importantly, meets the bandwidth requirements of 50 MHz. Once the optimal feed design for a standalone singularly polarised waveguide has been determined, a second probe is inserted orthogonally to the first probe to achieve dual polarisation.

Figure 4.4 shows the CST render of the dual polarised waveguide with two orthogonal coaxial to waveguide transitions.

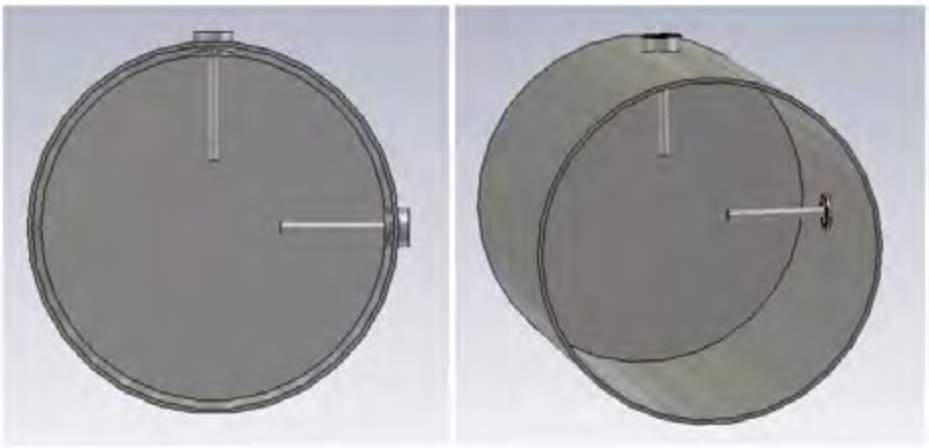

Figure 4.4: CST render of a dual polarised waveguide with two coaxial to waveguide transition.(Left) Front view. (Right) Side view.

The dual polarised waveguide has been simulated and optimised using CST and the optimised S-parameter results are shown in Figure 4.5.

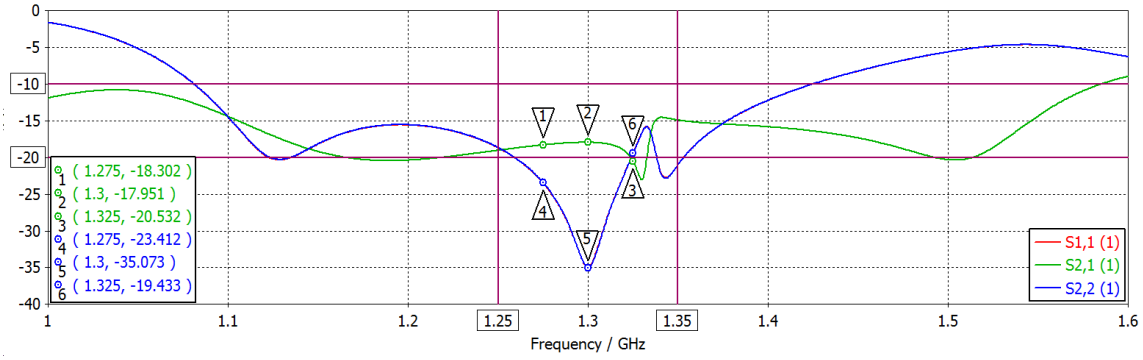

Figure 4.5: S_{11}, S_{22} and S_{21} magnitude [dB] of a dual polarised standalone waveguide simulation. The blue and red plots represent the S_{11} and S_{22} reflection coefficients while the green plot represents the S_{21} port-to-port isolation, all of which are greater than -15 dB across the band of interest.

It can be seen from Figure 4.5 that the simulated S-parameter results of a dual polarised waveguide feed shows that the feed performs as expected with the return loss (both S_{11}* and S_{22}) being significantly higher than the minimum -10 dB requirement across the entire band of operation. It has also been found that the port-to-port isolation is flat and higher than -15 dB across the entire operating band with the lowest isolation level being approximately -18 dB.

The isolation can be improved by spacing the probes a half wavelength apart as mentioned in Appendix A, however this would require that the feed be doubled in length to accommodate the probe separation. With the feed already being 230 mm long, it would be impractical to extend it further. The feed has been simulated with tuning screws added in an attempt to improve port-to-port isolation, however it has been found that the length of the tuning screw would need to be greater than a quarter wavelength before any beneficial effect is seen and even then, the effect of a tuning screw is minimal (less than 1 dB change across the entire bandwidth). It has therefore been decided that tuning screws would not be used. Table 4.1 summarises the calculated vs CST optimised dimensions for the dual polarised waveguide feed.

Table 4.1: Summary of calculated vs CST optimised dimensions for the dual polarised waveguide feed.

Parameter	Calculated	CST Optimised
Probe Length	57.7 mm	59.9 mm
Backshort Length	90 mm	90.3 mm

Table 4.1 shows that the calculated and CST optimised dimensions are very closely matched. This indicates that the calculated values provide an excellent starting point

*The S_{11} and S_{22} are identical and therefore overlap in Figure 4.5

and only small refinements need to be made during the optimisation process. The optimal diameter of the probes has been found to be 5.6 mm. Making the probes this thick in practice is difficult as the N-type launchers available only allow for a 3 mm diameter probe to be inserted. The diameter of the probe plays a role in the reactance of the probe and therefore in practice, small adjustments in the probe length can be used to compensate for the reduction in probe diameter.

Using N-Type connectors as launchers for the coaxial-to-waveguide transitions allow for power handling in excess of 1.5 kW peak power and 600 W average power [30], therefore ensuring the power specification be met by the design.

Feed Mounting Support Structure

There are two critical mechanical problems that need to be addressed when designing a dish antenna, these include mounting the feed to the antenna and mounting the dish to a tripod. As most small dish antennas have no back support structure, mechanically supporting a feed from the thin surface leads to deformation. While the mounting of the antenna to a tripod can be overcome using various bracing techniques, the mounting of the antenna feed is more complicated as it is in the near-field region of the antenna.

With the feed structure being in the near-field region of the antenna, it is of critical importance that the size of support structure be minimised to reduce blockage and near-field interference. Reduction in near-field interference is done by keeping any supporting struts small in diameter and by utilising insulating materials. Another useful technique used to reduce blockage is to mount the support struts diagonally such that they are not in the plane of polarisation [16].

It has been found through FEKO simulation that the most appropriate feed structure would be a single strut supporting the feed from the centre of the dish. It has also been found that when a metallic feed support strut is used, beam squinting occurs when horizontally polarised. The beam squinting is a result of the EM wave reflecting off the metallic rod when horizontally polarised. This squinting effect is not seen when the feed is vertically polarised. The FEKO simulated results showing the effect of beam squinting can be seen in Figures D.1 and D.2 in Appendix D.

To solve the problem of beam squinting, it has been decided that the feed support strut would be made from wood rather than aluminium. Fibre glass can be wrapped around the strut to increase its strength while nylon ties can be attached between the outer antenna edges and the feed to maintain rigidity as well as decrease the load on the wooden strut.

Another advantage of having a single feed mounting point is that the antenna mounting bracket can be attached at a single point. This allows the tripod mounting bracket to be mounted to the central part of the dish and add rigidity to that section of the antenna where the feed arm attaches. The support arm and mounting structure can be seen in Figure 4.8.

Phase Centre of Feed

The phase centre of a radiating source is the point at which the EM radiation appears to emanate as a single point source [16]. The phase centre of an aperture antenna is often found to be slightly forward or back from the boundary of the aperture. For an open ended circular waveguide or circular horn antenna, the phase centre is said to be $0.1\lambda_0$ forward from the aperture boundary [16].

FEKO has been used to determine the phase centre of the feed and it has been found to be 25.8 mm (approximately $0.11\lambda_0$) in front of the aperture boundary. This implies that for the feed to be focused at the focal point of the dish antenna, the aperture boundary needs to be placed 25.8 mm back from the calculated focal point.

4.2.2 Full Reflector Design

As discussed in Section 3.1.4, it is important to ensure that the edge taper for the dish is at the -10 dB point of the feed. To do this, the beamwidth of the designed feed needs to be determined. As the feed is a circular aperture, the beamwidth can be determined as [4][18]:

$$\theta = \frac{70\lambda_0}{D} \tag{4.15}$$

The problem with this approach however, is that it gives the HPBW (i.e. the -3 dB point) rather than the desired -10 dB point. To accurately determine the -10 dB beamwidth, the feed has been simulated using FEKO and the resultant vertically polarised radiation pattern can be seen in Figure 4.6.

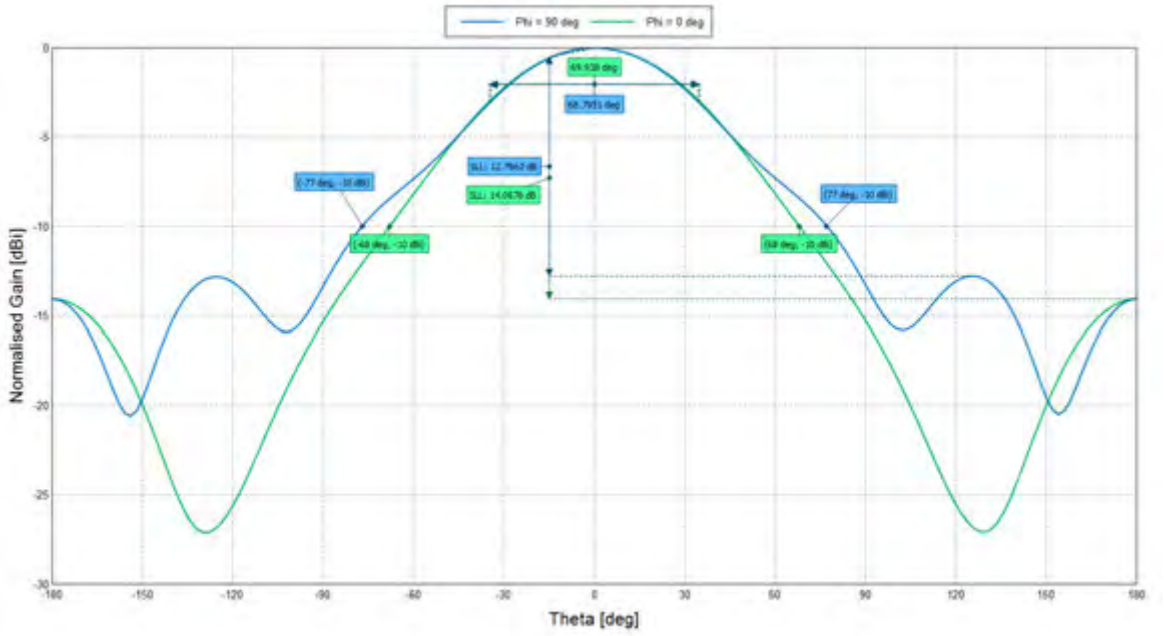

Figure 4.6: Radiation pattern of the designed feed when vertically polarised. (Blue) Azimuth plane where the HPBW is shown to be 69.8°with a -10 dB beamwidth of 154°. (Green) Elevation plane where the HPBW is shown to be 68.8°with a -10 dB beamwidth of 136°.

Due to the symmetrical nature of the feed, the azimuth and elevation beam patterns will interchange when the feed is horizontally polarised. From Figure 4.6, it can therefore be seen that the -10 dB azimuth beamwidth for the feed is:

Horizontal Polarisation - 154°
Vertical Polarisation - 136°

It can be seen that, depending on the plane of polarisation, the azimuth beamwidth varies slightly. This is due to the fact that when vertically polarised, the aperture is uniformly illuminated however, when horizontally polarised, the aperture in the azimuth plane is no longer uniformly illuminated as shown in Figure 4.7 [21].

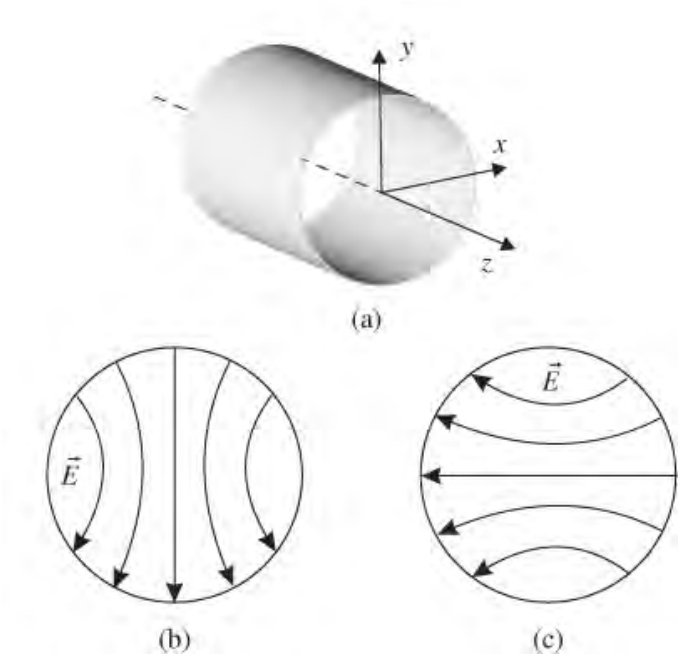

Figure 4.7: Illumination pattern of a dual polarised circular waveguide. (a) Circular waveguide geometry. (b) Vertically polarised illumination pattern for TE_{11} mode. (c) Horizontally polarised illumination pattern for TE_{11} mode [27].

The optimal f/D ratio for the feed is obtained using (3.2) from Section 3.1.4. The minimum f/D ratio that can be used to properly illuminate the dish such that the edge taper is at the desired -10 dB point is:

$$f/D = \frac{1}{4 \times \tan(154/4)} = 0.31 \tag{4.16}$$

The maximum f/D ratio that can be used is:

$$f/D = \frac{1}{4 \times \tan(136/4)} = 0.37 \tag{4.17}$$

It is therefore shown that the f/D ratio must lie between $0.31 \leq f/D \leq 0.37$. To ensure that the spillover remains minimal, the wider beamwidth is to be catered for and therefore an f/D ratio of 0.31 is chosen.

Once the f/D ratio has been determined, the other dish parameters are calculated. The diameter of the dish is calculated using (4.3) to be 1615.4 mm. Using the calculated diameter, the focal point can be determined. The focal point is found to be:

$$f = 0.31 \times D = 0.31 \times 1615.4 = 500.8 \text{ mm} \tag{4.18}$$

The depth of the antenna is therefore [13]:

$$H = \frac{D^2}{16f} = \frac{1615.4^2}{16 \times 500.8} = 325.7 \text{ mm} \tag{4.19}$$

The full parabolic dish antenna has been simulated and further optimised using FEKO, the results of which can be found in Appendix E.1. It can be seen that the antenna performs exactly as expected with a 10° beamwidth in both azimuth and elevation planes for both horizontal and vertical polarisation.

Table 4.2 summarises the performance characteristics of the both the calculated and the FEKO optimised full parabolic dish antenna.

Table 4.2: Simulated antenna performance characteristics for both the designed and the FEKO optimised full parabolic dish antenna.

Parameter	**Calculated**	**FEKO Optimised**
Diameter	1615.4 mm	1500 mm
Focal Point	500.65 mm	495 mm
f/D ratio	0.31	0.33
Parabolic Equation	$y = (4.99 \times 10^{-4})x^2$	$y = (5.05 \times 10^{-4})x^2$
HPBW (Az)	H-Pol - 9.53° V-Pol - 9.53°	H-Pol - 10.04° V-Pol - 10.06°
HPBW (El)	H-Pol - 9.53° V-Pol - 9.53°	H-Pol - 10.06° V-Pol - 10.04°
SLL (V-Pol)	Azimuth - 23.17 dB Elevation - 23.81 dB	Azimuth - 23.12 dB Elevation - 21.61 dB
SLL (H-Pol)	Azimuth - 23.81 dB Elevation - 23.17 dB	Azimuth - 21.61 dB Elevation - 23.12 dB
F/B ratio	-28.5 dB	-25.4 dB

From Table 4.2 it can be seen that while the original empirical design performs almost exactly as designed and expected, the diameter of the antenna can be reduced by up to 7% through optimisation and still maintain the required beamwidth as well as maintaining favourable performance in all of the other performance metrics.

4.2.3 Truncated Reflector Design

While the full dish antenna design performs as expected, with low side lobe levels and a 10° azimuth and elevation beamwidth in both planes of polarisation, it is too large to have two of them co-located on a single tripod. As a result it has been decided that

to reduce the size of the antenna, a truncated dish would be used rather than a full dish.

Designing a dual polarised truncated dish has one major drawback due to the fact that the feed must remain symmetrical (to maintain its radiation pattern in both planes of polarisation). This results in an unavoidable increase in spillover in the plane of the truncation, where the dish diameter is at its smallest.

The requirements state that the beamwidth in the azimuth plane must be 10°. The requirements on the elevation plane beamwidth are slightly more flexible and therefore the antenna diameter can be reduced in the elevation or vertical plane.

The design of the truncated dish follows the same procedure as the full dish, with the exception that the new vertical height needs to be determined. It is important that the dish remain as compact as possible while still maintaining acceptable side lobe levels.

It has therefore been decided that the edge taper for the vertical plane would be at the -3 dB point as opposed to the horizontal edge taper which is designed to be at the -10 dB point. To maintain the smallest possible size, the diameter of the dish will remain 1500 mm, the same as the diameter of the FEKO optimised full dish antenna found in Section 4.2.2.

The HPBW, -3 dB point, of the feed can be approximated using (4.15) as:

$$\theta = \frac{70 \times 230}{175} = 92^\circ \tag{4.20}$$

This has been confirmed through simulation, the results of which can be found in Figure 4.6, where the HPBW in each plane of polarisation has been found to be:

Horizontal Polarisation - 90°
Vertical Polarisation - 107°

An edge taper of -3 dB therefore results in the following f/D ratio:

$$f/D = \frac{1}{4 \times \tan(90/4)} = 0.6 \tag{4.21}$$

and,

$$f/D = \frac{1}{4 \times \tan(107/4)} = 0.5 \tag{4.22}$$

It is shown that the f/D ratio for the vertical cut of the antenna must be between $0.5 \leq f/D \leq 0.6$. Obviously the focal point cannot change between the vertical and

horizontal dimension of the dish and the appropriate height of the antenna that will allow for a minimum edge taper of -3 dB can be determined.

It can be seen from (4.16) and (4.17) that the range of f/D ratios that are appropriate lie between $0.31 \leq f/D \leq 0.37$ and while the FEKO optimised f/D ratio of 0.33 for the full dish falls within this range, it has been decided that the widest possible beamwidth would be designed for, giving an f/D ratio of 0.31. An f/D ratio of 0.31 combined with a diameter of 1500 mm results in the focal point of the antenna being at 465 mm out from the centre of the dish.

While maintaining the same FEKO optimised full dish diameter of 1500 mm, shown in Section 4.2.2, choosing the new f/D ratio to be 0.6 ensures that the dish has the smallest allowable vertical height of:

$$D_{vertical} = \frac{465}{0.6} = 775 \text{ mm} \tag{4.23}$$

Table 4.3 summarises the calculated parameters required by the truncated dish antenna.

Table 4.3: Final calculated truncated dish antenna dimensions.

Parameter	**Dimension**
Diameter	1500 mm
Height	775 mm
Depth	302.4 mm
Focal Point	465 mm
f/D ratio	0.31
Parabolic Equation	$y = (5.38 \times 10^{-4})x^2$

The truncated dish antenna has been simulated and further optimised using FEKO and the results of the simulations can be found in Appendix E.2 where it can be seen that the antenna performs as designed.

Table 4.4 summarises the performance characteristics of both the calculated and FEKO optimised truncated dish antennas.

Table 4.4: Simulated antenna performance characteristics for both the designed and FEKO optimised truncated dish antennas.

Parameter	**Calculated**	**FEKO Optimised**
Diameter	1500 mm	1440 mm
Height	775 mm	744 mm
Depth	302.4 mm	290.3 mm
Focal Point	465 mm	446 mm
f/D ratio	0.31	0.31
Parabolic Equation	$y = (5.38 \times 10^{-4})x^2$	$y = (5.60 \times 10^{-4})x^2$
HPBW (Az)	H-Pol - 9.8° V-Pol - 9.2°	H-Pol - 10.7° V-Pol - 10.0°
HPBW (El)	H-Pol - 15.5° V-Pol - 15.7°	H-Pol - 16.4° V-Pol - 16.6°
SLL (Az)	H-Pol - 20.3 dB V-Pol - 17.1 dB	H-Pol - 20.3 dB V-Pol - 16.9 dB
SLL (El)	H-Pol - 15.0 dB V-Pol - 13.9 dB	H-Pol - 15.1 dB V-Pol - 15.0 dB
F/B ratio	H-Pol - 25.1 dB V-Pol - 27.0 dB	H-Pol - 24.7 dB V-Pol - 30.7 dB

It can be seen in Table 4.4 that while the FEKO optimised and the designed antenna characteristics are very similar, in some cases within a dB of each other, well within the margin for error, the goal has been to design the antenna to be as compact as practically possible and this has been achieved in the optimised design.

4.2.4 Built Prototype Antenna

As stated in Section 1.4, one of the major limitations with this project is that budget has limited the manufacturing scope. To simplify the manufacturing process, a pre-fabricated 2.45 GHz Wi-Fi antenna was purchased with the intention of modifying the antenna to meet the given requirements.

The difficulty with such an approach is that a pre-fabricated dish antenna has a predefined curvature and therefore an associated predefined f/D ratio. This means that the modified antenna is limited to the same parabolic curvature of the pre-fabricated antenna.

The idea was to design a modified version of the pre-fabricated antenna, optimise it through simulations and test it to illustrate that the simulations are accurate enough to

warrant further manufacturing expense. This will allow future builds to be made using the optimised antennas designed previously in sections 4.2.2 and 4.2.3 respectively.

The largest pre-fabricated 2.45 GHz antenna available had the following properties:

Table 4.5: Measured pre-fabricated antenna properties.

Measured Parameter	**Value**
Frequency	2.45 GHz
Polarisation	Single (H or V)
Diameter	1000 mm
Height	600 mm
Depth	155 mm
Focal Point	403 mm
f/D ratio	0.4
HPBW	Azimuth - 8.7° Elevation - 11.8°
F/B ratio	31 dB
Gain	24 dBi
Weight	3.6 kg

The 2.45 GHz antenna was purchased and the beam pattern and resultant HPBW of the antenna has been confirmed through testing. The results of these tests can be found in Appendix F.

To modify the pre-fabricated antenna, the parabolic equation for the pre-fabricated antenna needed to be determined. The generic form of a parabola is given as:

$$y = ax^2 \tag{4.24}$$

By solving (4.24) using the dimensions of the pre-fabricated antenna, shown in Table 4.5, the equation is found to be:

$$y = 8.16 \times 10^{-4} x^2 \tag{4.25}$$

Using the optimised diameter value determined for the truncated dish in Section 4.2.3, it is found that the depth of the modified antenna would be 423 mm.

Considering the focal point for such an antenna would sit 306.4 mm from the centre of the antenna, with an f/D ratio of 0.21, the dish would be too deep as this would require a feed that can radiate over an angle far greater than 180 degrees. Using the same feed that has been designed in Section 4.2.1, it can be seen that the feed would

only be able to effectively illuminate the dish over a limited angle, resulting in greatly reduced aperture efficiency.

The diameter of the antenna therefore needs to be reduced such that the feed efficiently illuminates the entire aperture of the dish. Allowing for a maximum angle between the edge of the dish and the radiating feed of 90 degrees, i.e. such that the focal point is in line with the depth of the dish, the new diameter of the dish can be determined.

Letting $f = H$ gives:

$$H = \frac{D^2}{16H} = \frac{D}{4} \tag{4.26}$$

By equating (4.25) and (4.26):

$$\frac{D}{4} = 8.16 \times 10^{-4} x^2 \tag{4.27}$$

where $x = D/2$,

$$\therefore \frac{x}{2} = 8.16 \times 10^{-4} x^2 \tag{4.28}$$

and subsequently,

$$x = 612.75 \text{ mm} \tag{4.29}$$

This gives us a new diameter of $D = 2x$ =1225.5 mm and a focal point f of $x/2$ =306.4 mm. The result of which gives us an f/D ratio of 0.25.

The height of the pre-fabricated antenna cannot realistically be altered due to mechanical constraints in maintaining a parabolic curvature in both horizontal and vertical planes and is therefore set at the pre-fabricated height of 600 mm.

Table 4.6 shows a summary of the various calculated parameters required by the modified antenna.

Table 4.6: Summary of basic designed parameters for the modified antenna.

Parameter	**Value**
Diameter	1225.5 mm
Height	600 mm
Depth	306.4 mm
Focal Point	306.4 mm
f/D ratio	0.25

The modified design has been simulated and further optimised using FEKO and the results of these simulations can be found in Appendix E.2. Table 4.7 summarises the performance characteristics of both the calculated and the FEKO optimised antenna design.

Table 4.7: Simulated FEKO optimised antenna performance characteristics for the modified pre-fabricated antenna.

Parameter	FEKO Optimised
Diameter	1350 mm
Height	600 mm
Depth	370 mm
Focal Point	307.85 mm
f/D ratio	0.23
Parabolic Equation	$y = (8.16 \times 10^{-4})x^2$
HPBW (Az)	H-Pol - 13.9° V-Pol - 12.1°
HPBW (El)	H-Pol - 19.7° V-Pol - 20.5°
SLL (Az)	H-Pol - 17.4 dB V-Pol - 17.4 dB
SLL (El)	H-Pol - 16.3 dB V-Pol - 15.2 dB

From Table 4.7, it can be seen that while the antenna is very deep, according to simulations it should produce relatively good results. One parameter that needs special mention is the HPBW. The HPBW at 12.1° and 13.9° is wider than the required HPBW of 10°, however this is unavoidable given the manufacturing limitations available to this dissertation.

As a result, building the antenna and illustrating that it performs as designed and simulated, shows that the optimised dish antenna designed in Section 4.2.3 would perform as designed if built using more advanced manufacturing techniques.

4.3 Antenna Manufacturing

As mentioned, one of the major limitations throughout this dissertation has been the manufacturing facilities available. As a result, to develop the antenna prototype designed in Section 4.2.4, a pre-fabricated antenna characterised in Table 4.5 was purchased and modified as required.

This section details the manufacturing process followed while describing the various manufacturing choices that have been made. Once the dimensions of the antenna had been determined, CAD drawings, found in Appendix H, were produced and the

antenna manufactured as described below.

Figure 4.8 shows the completed prototype antenna.

Figure 4.8: Built prototype antenna with dual polarised waveguide feed mounted to a tripod for testing purposes. Note the support ties connected from the upper edge of the antenna to the feed arm.

The purchased antenna consists of two sections that are bolted together in the middle. To extend the dish to the required diameter, 3 mm thick aluminium flat-bar was used to join each side of the antenna together. Each piece of flat-bar was pop-riveted together to form a strong skeletal structure that could support both the feed and the mesh structure. Aluminium has been used in an attempt to reduce the weight of the antenna structure while also preventing any possible oxidation.

Once the skeletal shape had been completed, the mesh structure was then placed over the entire face of the antenna. The mesh that has been used is a diamond shaped "chicken mesh" with a "gap" diameter of 18 mm at its widest point (less than the maximum allowable 23 mm gap).

Figure 4.9 shows the complete meshed dish without the feed arm attached.

Figure 4.9: Complete meshed antenna structure without the feed structure attached.

Once the antenna structure had been manufactured and its new dimensions confirmed, the waveguide feed was built. The feed was built using an unused 5 litre paint tin. To ensure that the opening of the waveguide remains as flush as possible, the flange along the rim of the can was removed. The probe feeds were then measured and cut to be slightly longer than the designed length. This allowed for adjustments to be made by cutting the probe smaller during testing.

The holes were drilled in the waveguide with careful consideration taken to ensure that the holes were orthogonal to each other. The probes were inserted and the waveguide placed onto the wooden support structure such that the waveguide phase centre sits at the dish focal point.

To ensure that the antenna was stable and that the feed did not move around, nylon string was used to connect the outer corners of the antenna to the feed arm, as seen in Figure 4.8. This gave the antenna superior rigidity and therefore allowed the feed to remain perfectly centred regardless of the external factors such as wind.

Figure 4.10 shows a single standalone probe as well as the completed waveguide with two orthogonal probes.

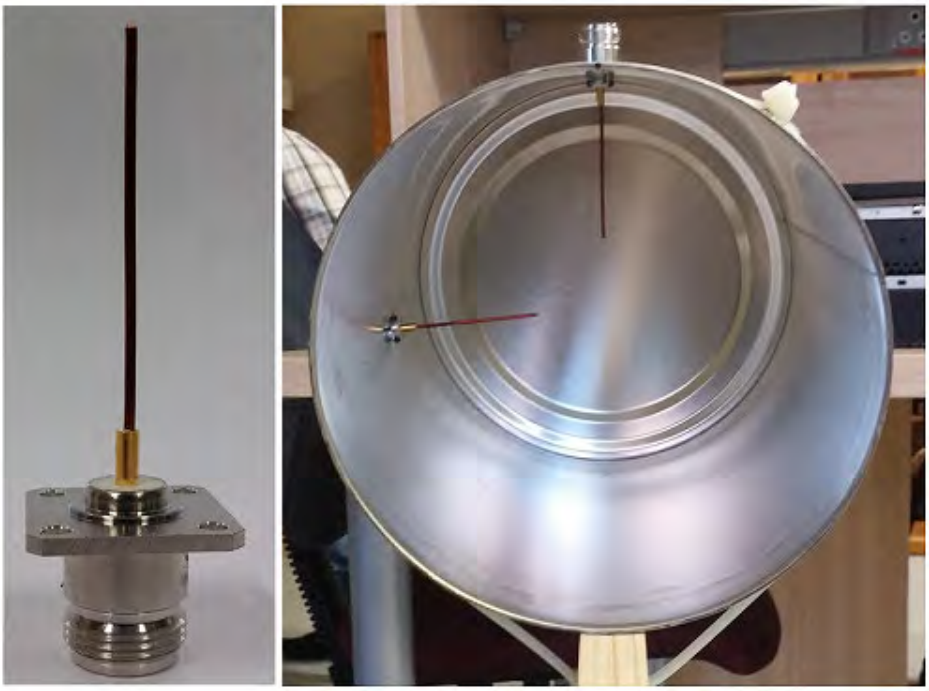

Figure 4.10: Dual Polarised waveguide feed for the antenna. (Left) Single N-Type launcher with probe. (Right) Manufactured dual polarised waveguide with orthogonal probes mounted in place.

Once the antenna prototype had been manufactured and all the dimensions had been confirmed to correspond with those calculated in Section 4.2.4, the antenna was tested and the results compared to the simulated results shown in Section 5.

4.3.1 Manufacturing Considerations

Key aspects to consider during the manufacture of the antenna:

- The parabolic shape of the antenna is of critical importance and due to the hand built nature of the antenna, some uneven surfaces were observed. This has been lessened through the use of mesh as the mesh allowed some flexibility in the curvature of the surface.
- Attaching of the mesh to the skeletal structure has been done with the use of cable ties. Cable ties were chosen because they are insulators and therefore will have no noticeable effect on the surface of the antenna.
- The supporting arm has been fixed to the antenna through the use of small aluminium L-brackets.

- Positioning the phase centre of the feed at the focal point of the antenna is absolutely critical and therefore the feed has been attached to the feed arm using cable ties. Once the exact position was found, the feed was attached using tiny screws.
- Ensuring that the probes are perfectly orthogonal to each other is critical to the performance of the antenna.
- The probe length and backshort distance was within a ± 0.5 mm accuracy. This could lead to variations in the simulated and measured results.

4.4 Summary

This chapter has discussed the design and construction of the dish antenna. Three dish antennas have been designed and simulated. It has been found that due to manufacturing limitations, the optimal design could not be built and therefore a revised design has been completed.

The purpose of the revised design is to be able to manufacture, measure and compare the results with the simulated results in a cost effective and timely manner, to determine the accuracy of the simulations as well as any potential manufacturing issues before attempting to manufacture a final product using more advanced and expensive techniques. The completed prototype antenna can be seen in Appendix I.

The final antenna design chosen for manufacture, while not optimal, has been chosen due to the manufacturing limitations imposed on this project. The optimal antenna design has been discussed and the appropriate CAD drawings and simulations can be found in Appendix H.

Chapter 5

Results

5.1 Introduction

This Chapter details the testing of the manufactured prototype antenna and the results of these tests are discussed in detail. The equipment used and the procedures followed during testing are discussed in depth. All results are compared and analysed with reference to the simulated results obtained in Section 4 before conclusions are drawn.

5.2 S-Parameter Measurements

5.2.1 Equipment Used

The S-parameters of the feed have been tested and compared to the simulated results found in Section 4. The following equipment has been used for the testing of the S-parameters:

- Agilent Technologies E5071B 300 kHz to 8.5 GHz Network Analyser
- 85032E N-Type Calibration kit
- SMA coaxial cables with 50 Ω characteristic impedance

The testing procedure for determining the feed characteristics has been performed as follows*:

*Equipment that requires calibration has been fully calibrated and left to warm up for 30 minutes before each test to ensure accurate and repeatable results.

1. The standalone feed was connected to the network analyser with the feed opening pointing towards the roof as this provided the least number of reflections.

2. The S_{11}, S_{22} and S_{21} parameters were recorded using the network analyser.

3. The probe length was adjusted by cutting a small piece off the end of the probe and step 2 was repeated. This process was repeated multiple times until the optimal feed performance as shown in simulation was achieved.

4. The standalone feed was then attached to the antenna and the new S_{11}, S_{22} and S_{21} parameters were measured.

5.2.2 Standalone Waveguide

The first measurements to be completed were done to confirm the performance of the antenna waveguide feed as it was designed in Section 4.2.1. Figure 5.1 shows the S_{11} return loss as measured for a singularly polarised standalone waveguide and compares the result to that of the simulated result seen in Figure 4.3 in Section 4.2.1.

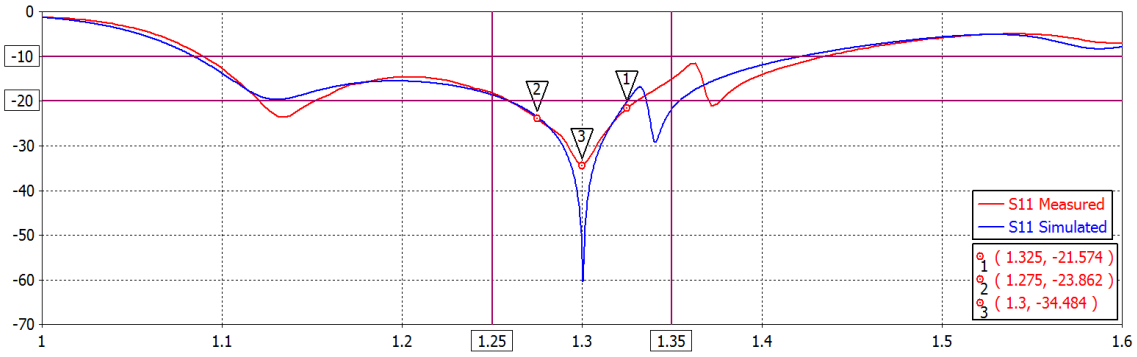

Figure 5.1: Simulated (Blue) versus measured (Red) S_{11} magnitude [dB] for a singularly polarised standalone feed. The measured results compares well with the simulated results with the measured reflection coefficient remaining below -20 dB across the entire band of interest.

It can be seen from Figure 5.1 that the measured result follows the same curve as the simulated result. The two bold horizontal lines represent the -10 dB and -20 dB points while the two bold vertical lines represent a 100 MHz bandwidth from 1.25 GHz to 1.35 GHz. In order for the feed of an antenna to perform adequately, the reflection coefficient across the entire usable bandwidth needs to be below -10 dB [4][12], that is to say that more than 90% of the received power is transmitted. It is clear from Figure 5.1 that the reflection coefficient across the entire 50 MHz bandwidth is below -20 dB and therefore more than 99% of the received power is transmitted.

Once it has been confirmed that the singularly polarised feed works as expected and the measured results align with the simulated results, the dual polarised feed can be tested. The dual polarised feed has been tested in much the same way as the singularly polarised feed however, with the additional S_{21} port-to-port isolation parameter being measured.

Figures 5.2, 5.3 and 5.4 show the S_{11}, S_{21} and S_{22} measurements respectively and compares them to the CST simulated models of the same dual polarised standalone waveguide feed.

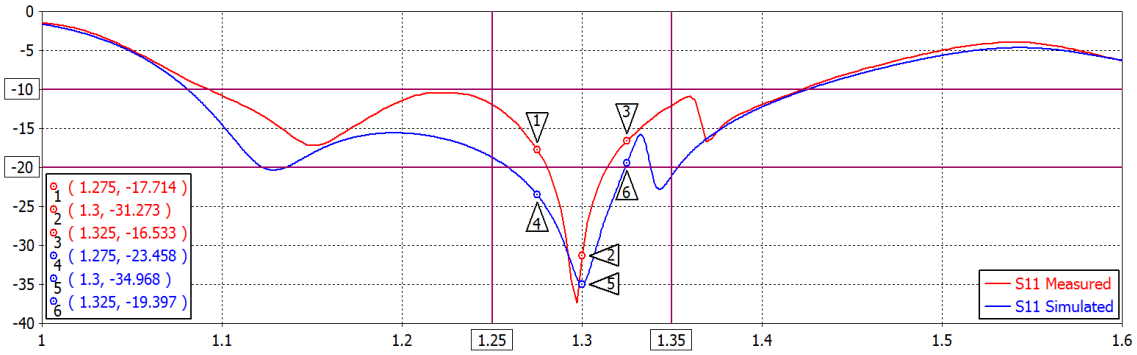

Figure 5.2: Simulated (Blue) versus measured (Red) S_{11} magnitude [dB] for a dual polarised standalone feed. The measured reflection coefficient is found to remain well below -15 dB across the entire band of interest with a centre frequency of roughly 1.3 GHz.

It can be seen in Figure 5.2 that the measured S_{11} result is in close alignment with the simulated result. The measured result shows that the prototype feed has slightly less bandwidth than expected from the simulations, with the difference attributed to manufacturing tolerances and a reduction in required probe thickness. It must be noted that even though the bandwidth is reduced, it is still greater than the required 50 MHz with $f_0 = 1.3$ GHz.

Figure 5.3 illustrates a comparison between the measured and simulated S_{21} port-to-port isolation of the dual polarised standalone waveguide feed.

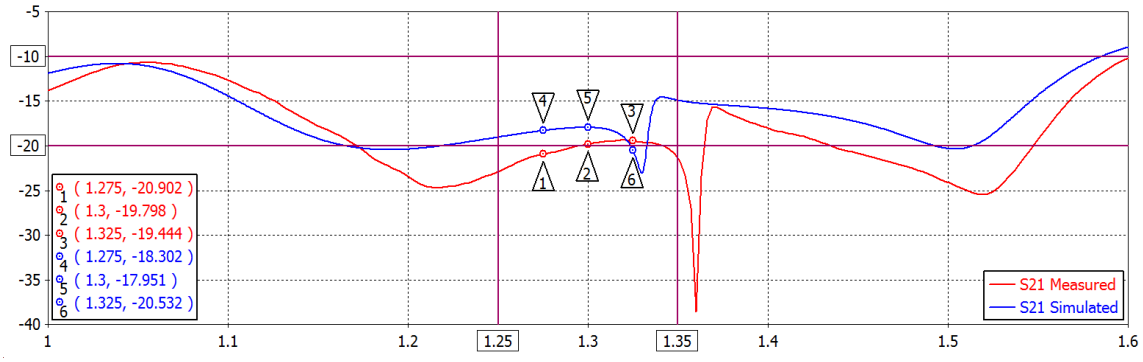

Figure 5.3: Simulated (Blue) versus measured (Red) S_{21} isolation [dB] for a dual polarised standalone feed. The port-to-port isolation for the measured results are better than the simulated results. The measured port-to-port isolation is found to be better than -19 dB across the entire band of operation.

The port-to-port isolation is a critical parameter in the design of a dual polarised antenna system. It can be seen from Figure 5.3 that the measured port-to-port isolation is better than the CST simulated result, with the two graphs closely aligned across the entire measured band.

Figure 5.4 shows the difference between the measured and simulated S_{22} reflection coefficient of the dual polarised standalone waveguide feed.

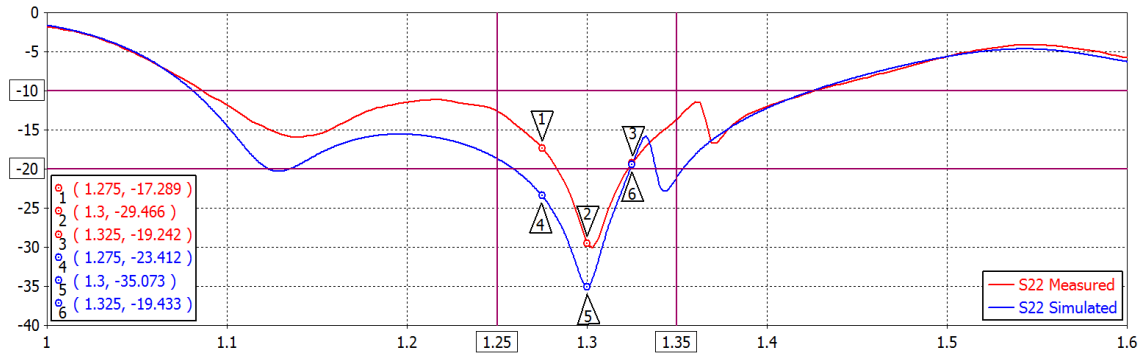

Figure 5.4: Simulated (Blue) versus measured (Red) S_{22} magnitude [dB] for a dual polarised standalone feed. The measured result is found to have a lower bandwidth than the simulated result however the measured reflection coefficient still remains below -17 dB across the entire band of interest.

Much like what can be seen from the S_{11} results, by looking at Figure 5.4, it can be seen that the results of the S_{22} measurements closely align with the simulated results. While the measured bandwidth is once again slightly less than the simulated bandwidth, it

still operates beyond the required 50 MHz bandwidth with the centre frequency being almost exactly 1.3 GHz.

Figure 5.5 shows all the measured S-parameter results overlaid onto a single cartesian plane.

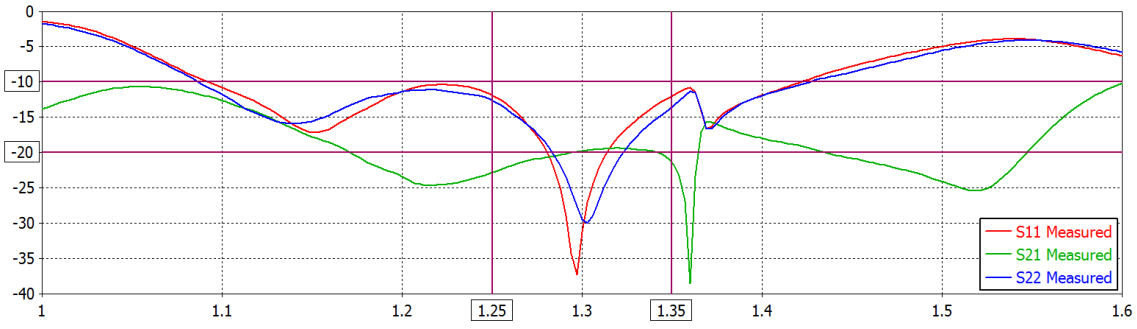

Figure 5.5: Combined S_{11}, S_{22} and S_{21} measurements [dB] for a dual polarised standalone feed. Superimposing all measured results onto a single cartesian plane shows that while each port differs slightly from the other due to manufacturing tolerances, the waveguide performs as expected.

Plotting the S_{11} and S_{22} measurements together illustrate how closely they align to each other with the difference between them being attributed to manufacturing tolerances.

As was found with the singularly polarised standalone waveguide, the measured S-parameters of the dual polarised standalone waveguide closely align with the CST simulated results. It has been shown that both the S_{11} and S_{22} parameters are well below the required -10 dB point across the entire bandwidth of interest with a centre frequency of 1.3 GHz. The S_{21} parameter which, representing the isolation between the probes, is higher than the idealised CST simulated version.

No particular isolation requirement has been given in the dissertation outline. The goal is therefore to achieve as much isolation as realistically possible with a minimum target of -15 dB across the entire band from 1.275 GHz to 1.325 GHz [15].

5.2.3 Antenna with Waveguide Feed

Once it had been shown that the standalone waveguide performs as designed and the measured results closely align with the simulated results, the waveguide was then attached to the prototype dish antenna. The waveguide was attached with its phase centre (see Section 4.2.1) at the focal point of the dish antenna and the S-parameters of the antenna feed system were remeasured.

It was found that when placed on the antenna, the S-parameters of the feed change considerably, as expected from Section 3.2.2. The S-parameters were then simulated

in CST to verify and confirm the measured results. Figures 5.6, 5.7 and 5.8 illustrate a comparison between simulated and measured S-parameters for the full antenna and feed system.

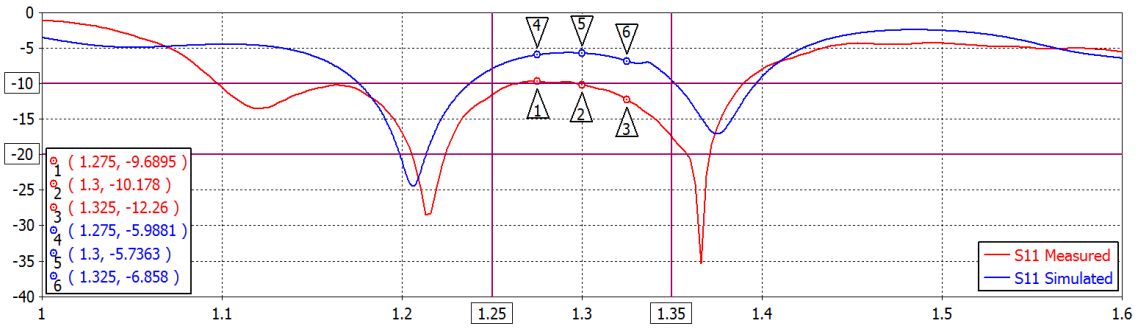

Figure 5.6: Simulated (Blue) vs the measured (Red) S_{11} magnitude [dB] results of the antenna with the phase centre of the feed at the focal point of the antenna. These results illustrate a large amount of interference from reflections, leading to greatly reduced performance.

Figure 5.6 shows a comparison between the measured and simulated S_{11} results for the waveguide feed once it has been attached to the prototype dish. While the measured antenna prototype seems to be of slightly higher performance than the simulated one, the performance of the feed is considerably lower than what was found with the standalone feed. It is noted that although performance is greatly reduced, the results show a close agreement between the simulated and measured values.

Figure 5.7 compares the measured and simulated port-to-port isolation of the dual polarised waveguide feed when attached to the antenna.

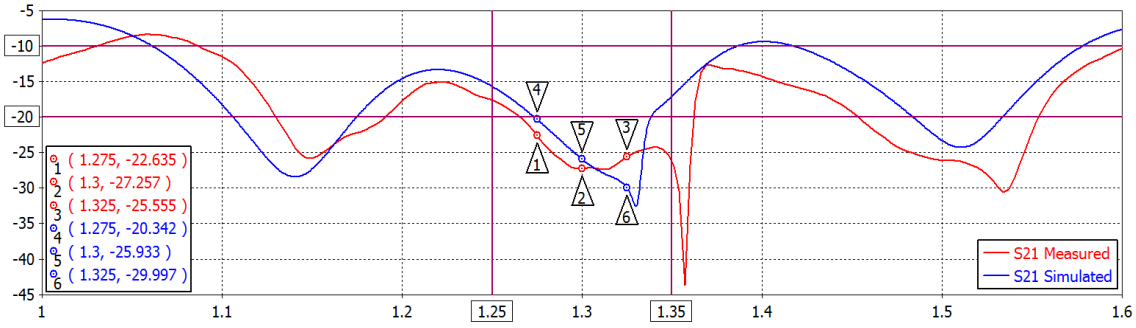

Figure 5.7: Simulated (Blue) vs the measured (Red) S_{21} port-to-port isolation [dB] results of the antenna with the phase centre of the feed at the focal point of the antenna. As a result of the reflections back into the feed from the centre of the dish, the port-to-port isolation has greatly improved from the standalone waveguide results.

Unlike the results of the S_{11} measurement in Figure 5.6 where the performance decreased from the performance found for the standalone waveguide, the S_{21} port-to-port isolation is seen to improve by us much as 3 dB. It can be seen that the simulated

and measured results align closely and that the worst case isolation for the measured antenna across the band of interest is found to be -22.6 dB.

Figure 5.8 compares the measured and simulated S_{22} results of the dual polarised waveguide feed when attached to the antenna.

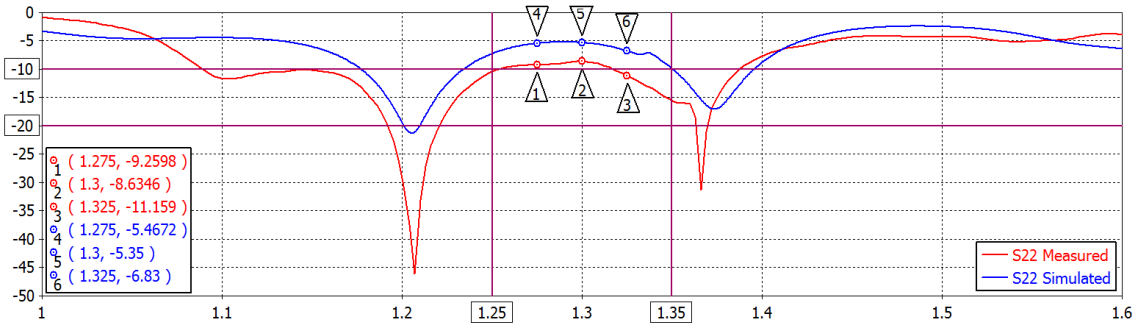

Figure 5.8: Simulated (Blue) vs the measured (Red) S_{22} magnitude [dB] results of the antenna with the phase centre of the feed at the focal point of the antenna. There is a decrease in performance from the standalone waveguide results due to reflections from the dish into the feed.

The results are almost identical to the results seen in Figure 5.6 where a decrease in performance over the standalone results is seen. Once again, the simulated and measured results are closely aligned.

It can be seen from Figures 5.6, 5.7 and 5.8 that the simulated and measured results largely agree, and while the measured results are slightly better than the CST simulated predictions, performance is not satisfactory, especially considering that the antenna is required to handle a peak power of 1.5 kW. The isolation has improved greatly over the standalone feed results, improving from a worst case -19.2 dB to a worst case -22.6 dB across the band of interest. With a worst case S_{11} of -8.6 dB however, roughly only 86%[†] of the received power would be transmitted and therefore the reflected power would be as much as 210 W[‡].

The reason for the dramatic decrease in performance of the antenna system from the performance seen with the standalone waveguide, is attributed to reflected signals that cause interference with the impedance of feed as mentioned in Section 3.2.2. The only way to overcome this phenomenon is to re-optimise the feed such that the interference caused by the reflected waves is mitigated. Re-optimising the feed while attached to the dish has been done by adjusting the probe and backshort lengths, such that the resultant interference pattern from the backshort cancels with the interference pattern caused by the reflected waves.

[†] $P_{transmitted} = (1 - 10^{\frac{-8.6}{10}}) \times 100\% = 86\%$
[‡] $P_{reflected} = 1500\text{ W} \times 14\% = 210\text{ W}$

The optimisation process has been done using CST and Table 5.1 shows the final parameters of the re-optimised feed.

Table 5.1: CST parameter optimisation results: Standalone feed optimisation vs antenna with feed optimisation.

Parameter	Standalone Feed	Antenna with Feed
Probe Length	54.4 mm	56.9 mm
Backshort Length	80.4 mm	133.3 mm

These new feed parameters result in the simulated S-parameters which are shown in Figure 5.9.

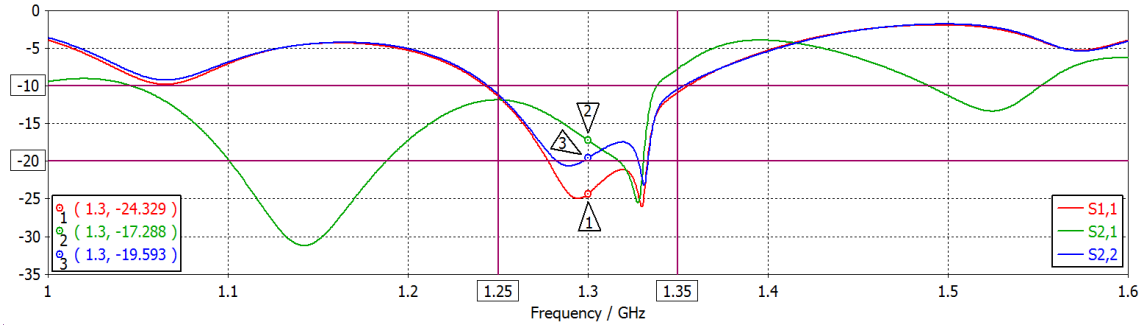

Figure 5.9: Simulated S_{11}, S_{21} and S_{22} magnitudes [dB] showing the re-optimised feed results.

The re-optimised results show greatly improved S_{11} and S_{22} parameters over those found in the unoptimised results of Figures 5.6 and 5.8. The S_{21} port-to-port isolation is found to decrease slightly from the previous results, however it is still found to above the -15 dB point.

It can be seen that to improve the S-parameter results sufficiently, the probe has to be moved forward considerably (roughly a quarter wavelength forward from the backshort). The feed adjustments have been made and the newly optimised feed has been placed with its phase centre at the focal point of the antenna. Figures 5.10, 5.11, 5.12 and 5.13 show the results of the re-optimisation.

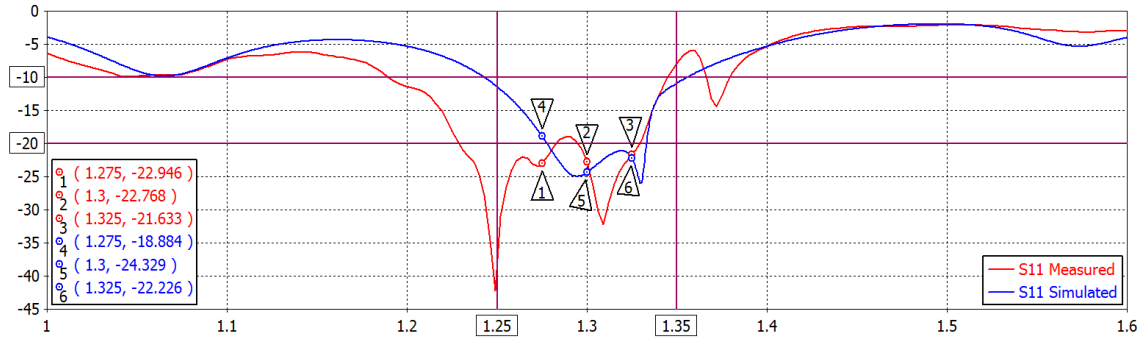

Figure 5.10: Simulated (Blue) versus measured (Red) S_{11} magnitude [dB] results for the re-optimised antenna with the phase centre of the feed at the focal point of the antenna. While the two curves do not perfectly align, the measured result shows that the waveguide has a wider bandwidth than expected with the reflection coefficient being roughly -19 dB or greater across the entire band of interest.

Figure 5.10 shows that while the measured antenna performs similar to the simulated one, the correlation between the two is not as distinct as with previous results. The measured result shows a much wider usable bandwidth and generally higher performance than the simulated results across the band of interest. The ripples in the measured results can be attributed to the environment with reflections off the roof being the main culprit.

Figure 5.11 shows a comparison between the CST simulated S_{21} port-to-port isolation after re-optimisation and the measured S_{21} port-to-port isolation of the reconstructed optimised feed.

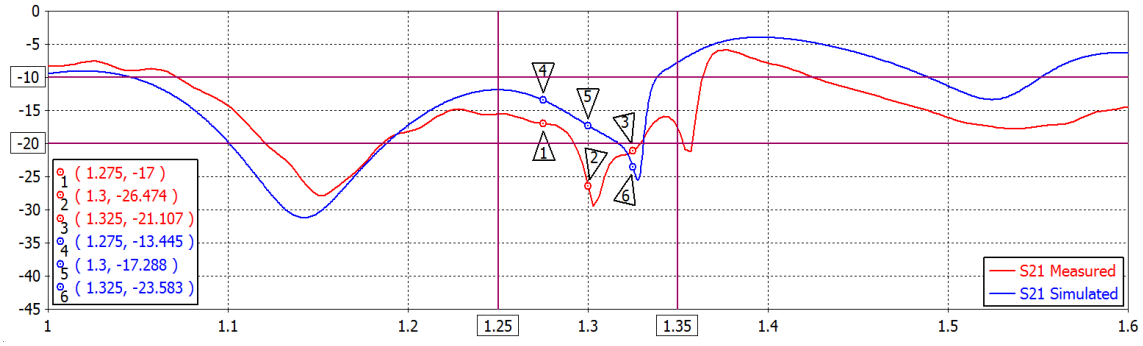

Figure 5.11: Simulated (Blue) versus measured (Red) S_{21} port-to-port isolation magnitude [dB] results for the re-optimised antenna with the phase centre of the feed at the focal point of the antenna. The measured results appear to show a higher port-to-port isolation than the simulated results, with the port-to-port isolation being greater than -17 dB across the entire band of interest.

Similar to the result found in Figure 5.10, the measured response does not completely line up with the simulated response although, much like the S_{11} result, the S_{21} result conforms to roughly the same shape across large parts of the measured bandwidth. As

with the S_{11} measurements, the ripple across the curve can be attributed to environmental factors such as reflections off the roof.

Figure 5.12 shows a comparison between the simulated and measured S_{22} parameter for the antenna with the re-optimised feed.

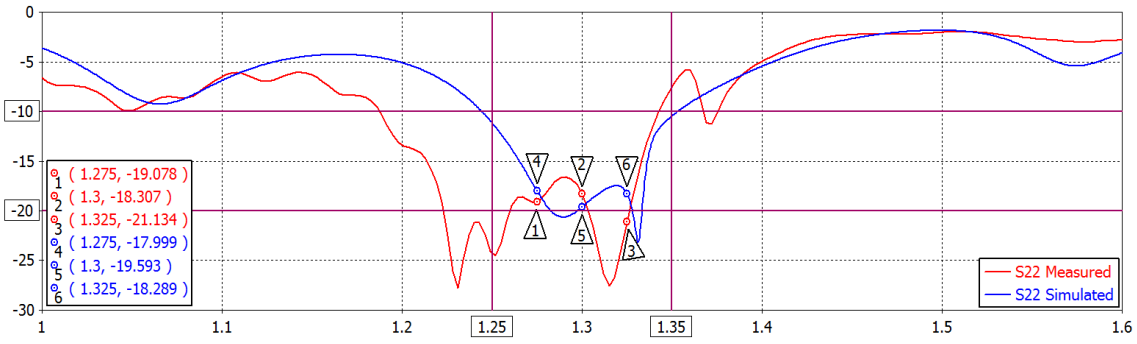

Figure 5.12: Simulated (Blue) versus measured (Red) S_{22} magnitude [dB] results for the re-optimised antenna with the phase centre of the feed at the focal point of the antenna. The measured S_{22} results show a decrease in performance over the measured S_{11} results, however, the reflection coefficient remains greater than -15 dB across the entire band of interest.

Figure 5.12 illustrates a continuation of the results shown by Figures 5.10 and 5.11 in that the measured feed has considerably wider bandwidth than the simulated feed, while the overall performance across the band of interest is well above what is required. The difference in the measured and the simulated results is partly due to manufacturing tolerances as all dimensions were only within ± 0.5 mm accuracy of the optimised simulated dimensions. If the feed were to be made with the exact same dimensions as the optimised diameters, it is expected that the measured results would be much closer aligned to the simulated ones.

5.2.4 Summary

Figure 5.13 summarises the measured S-parameter performance of the optimised antenna feed when it is attached to the antenna with its phase centre at the focal point.

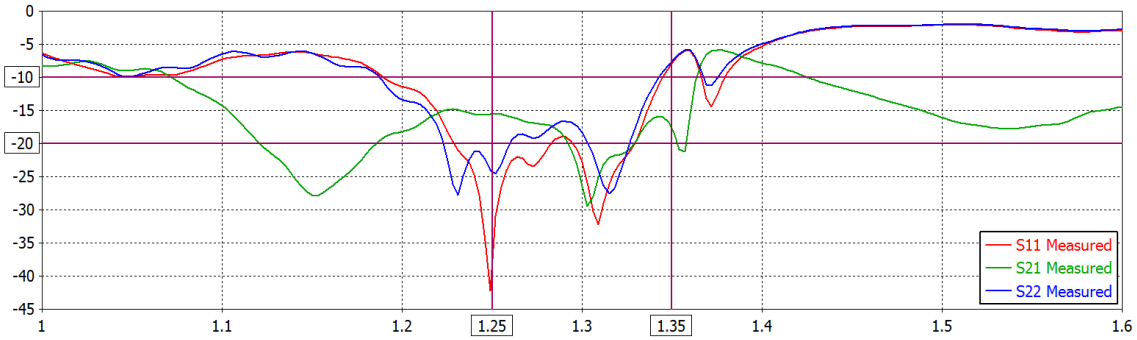

Figure 5.13: Measured S_{11}, S_{21} and S_{22} magnitudes [dB] showing the re-optimised feed results. Combining the results from all S-parameter measurements shows that while the measurements between each probe differ due to manufacturing tolerances, the waveguide feed and antenna system perform as expected with all measurements remaining greater than -15 dB across the entire band of interest.

Figures 5.10, 5.11, 5.12 and 5.13 have shown that while the measured results are slightly different from the simulated results, the re-optimisation achieved the goal of improving the antenna feed performance over the initial results, with both S_{11}, S_{21} and S_{22} being greater than -15 dB across the entire band of interest. It is believed that the differences between simulated and measured results are due to manufacturing tolerances as well as inaccurate modelling of the surface of the antenna where the feed support protrudes.

Improving the manufacturing tolerances would improve the correlation between simulated and measured results, however as the measured results in Figure 5.13 show, the feed performance meets all the requirements and should ensure that the antenna system performs as designed.

5.3 Beam Pattern Measurements

Once the antenna feed measurements had been completed and the feed shown to perform efficiently, the far field radiation pattern measurements were done. The measurement process, including the site choice and location is described while the results of the measurements are discussed in detail throughout the remainder of this chapter.

5.3.1 Choosing a Site

UCT does not posses an anechoic chamber and a suitable site had to be found for antenna testing. The first step to choosing the correct site was to determine the far-field distance of the antenna. The far-field distance would be the minimum allowable

distance between the Tx and Rx antennas when measuring the far-field antenna radiation pattern. The far-field distance for the antenna can be calculated, resulting in a far-field distance of:

$$R_{ff} = \frac{2 \times D^2}{\lambda_0} = \frac{2 \times (1350)^2}{230} = 15.8 \text{ m} \tag{5.1}$$

A minimum separation distance of 15.8 m between the two antennas is required. It was found that the distance between the two adjacent Menzies and Snape buildings at UCT is approximately 20 m, which puts it well within the far-field region of the antenna. Figures 5.14 and 5.15 illustrate the building layout.

Figure 5.14: Google maps overhead image of UCT showing the position of the Menzies and Snape buildings as well as the distance between the two measurement sites being ≈ 20 m.

This site has been found to be a good place to take antenna measurements as it provides an open environment with very little reflective surfaces surrounding the antenna under test (AUT). The close up images are shown in Figure 5.15.

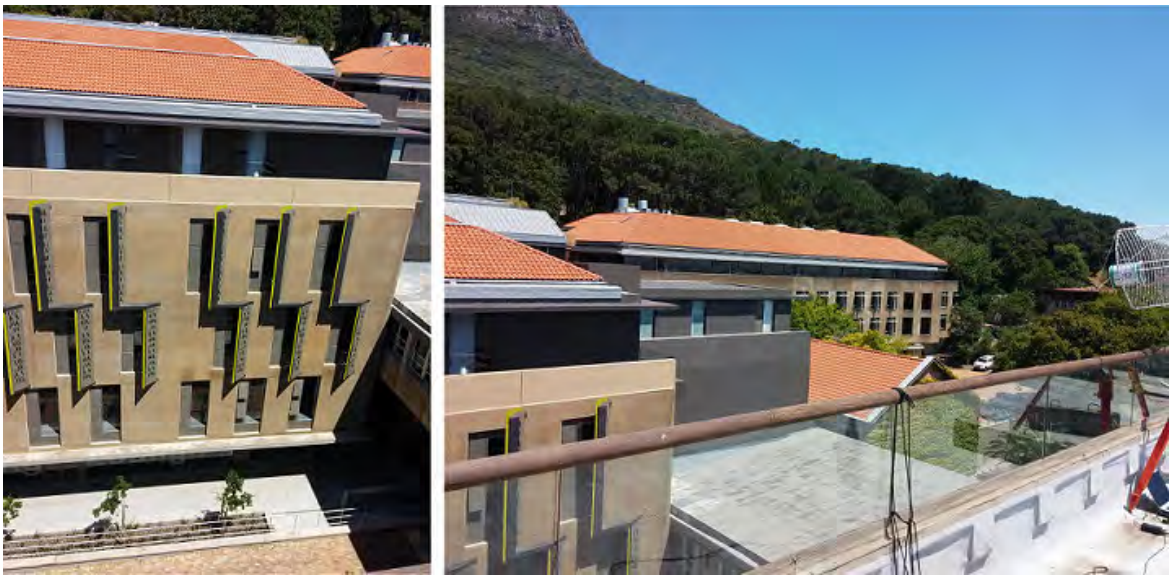

Figure 5.15: (Left) Photograph showing the height of the two buildings with the large, reflection free dip between them. (Right) Photo showing the relatively reflection free zone between Snape (far side) and Menzies (near side) buildings.

Figure 5.16 illustrates the basic geometry between the two buildings.

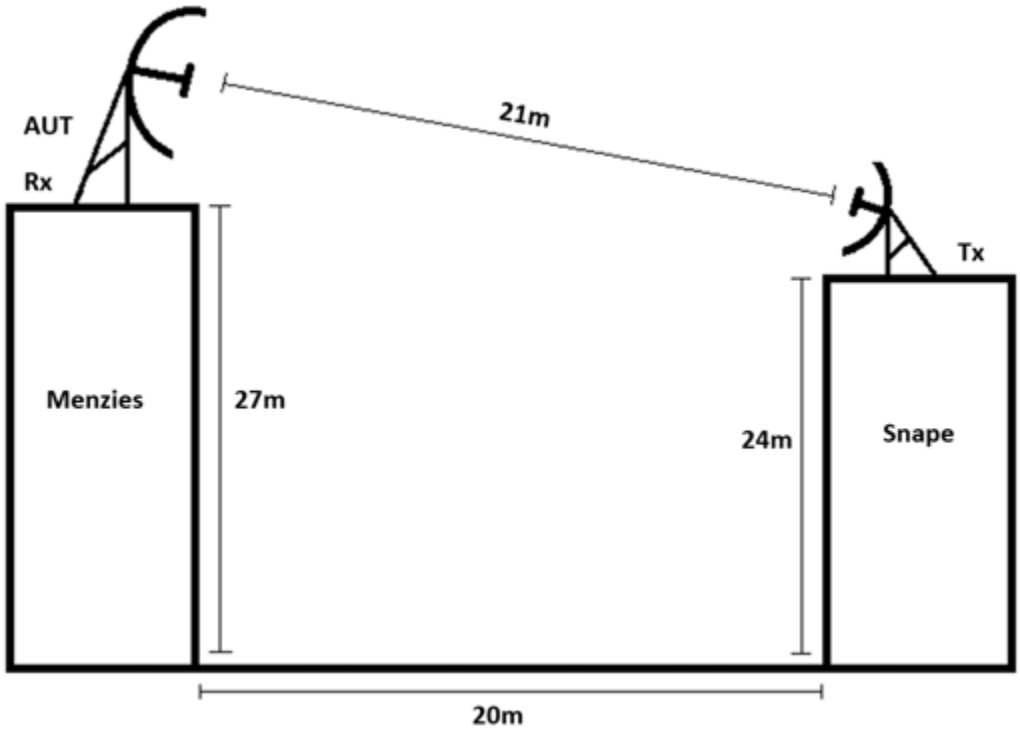

Figure 5.16: Basic antenna test range geometry showing the distance between the transmit and receive antennas to be more than 20 m and therefore satisfying the far-field requirement of 15.8 m.

It has therefore been decided that the rooftops of the Snape and Menzies buildings at UCT would be ideal for the far-field radiation pattern testing of the antenna.

5.3.2 Equipment Used

The tests were conducted on the rooftops of the Snape and Menzies buildings at UCT as shown in Figure 5.15. To perform the far-field radiation pattern tests, the following equipment was used:

- 1x ThinkRF WSA5000 100 kHz to 18 GHz Spectrum Analyser (SA)[§]
- 1x Rohde & Schwartz SMF 100A Signal Generator (SG)
- 1x Transmitting antenna (Open ended L-Band waveguide antenna)
- 1x 50Ω DC-18 GHz MCL Anne-50+ termination for the unconnected waveguide port
- 1x Tripod with rotating head incremented in 1° increments
- 1x Laptop with proprietary software

The transmit antenna was placed on the balcony of the Snape building where it was excited with a 1.3 GHz, 30 dBm continuous wave signal by the signal generator. The ThinkRF SA was set up as a receiver and attached to the receive antenna on the tripod on the roof of Menzies as shown in Figure 5.16. The unconnected feed port was terminated using a 50 Ω termination. The receive antenna (the AUT) was positioned over the edge of the Menzies rooftop balcony such that it pointed directly at the transmitting antenna and the received power was at a maximum. It was then rotated 360 degrees in 1° increments.

[§]The SA has a SFDR of 100 dBc with a RTBW of 0.1 MHz and 70 dBc with a RTBW of 10 MHz

Figure 5.17: Measured antenna mounted to tripod on the Menzies building roof, pointing to the transmit antenna situated on the Snape building roof. The antenna is mounted to a base that allows 360 degrees of rotation in 1˚increments.

Using proprietary software that has been written specifically for these measurements, the ThinkRF SA could be used to capture the magnitude of the signal being received by the antenna. The antenna that is being rotated is the antenna that is being measured, regardless of whether it is transmitting or receiving [12].

As the AUT was rotated through the full 360° rotation, the received data was stored in .csv format after which the results were plotted and analysed using MATLAB.

A $\pm 0.5°$ error margin is introduced as a result of the rotating pedestal accuracy while the measured power levels are relative and therefore any negative effects due to cable losses are mitigated.

5.3.3 Antenna Measurements

The azimuth and elevation radiation patterns of the antenna were measured in each plane of polarisation the results of which are summarised in Table 5.2.

Table 5.2: Summary of measured prototype antenna results.

Measured Parameters	**Horizontal Polarisation**	**Vertical Polarisation**
Azimuth HPBW	12.4°	13.9°
Elevation HPBW	20.0°	19.6°
Azimuth SLL	17.4 dB	16.4 dB
Elevation SLL	15.7 dB	15.8 dB

The results of these tests are shown in the figures and are compared to the simulated results found in Section 4.2.4.

Horizontally Polarised Azimuth Radiation Pattern

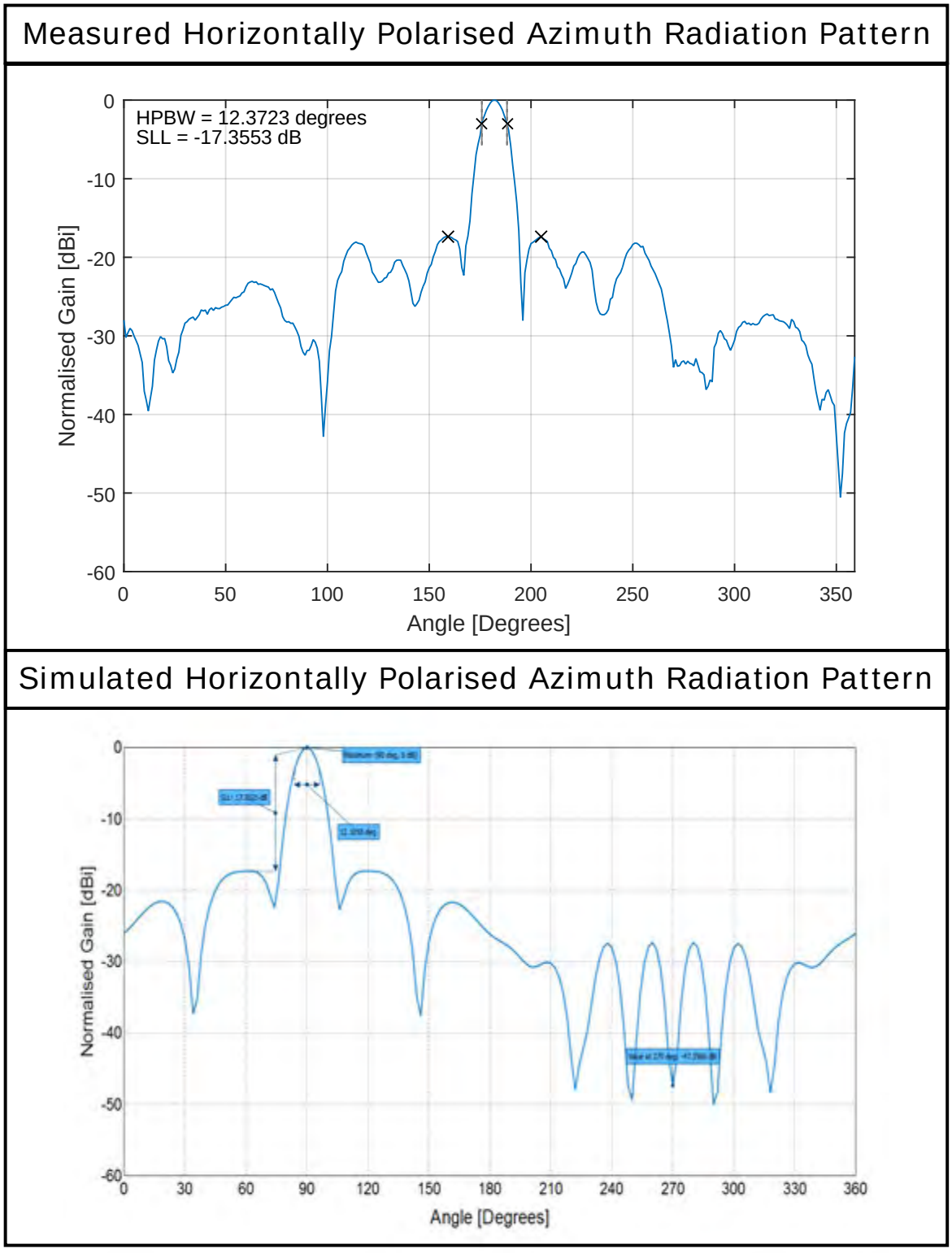

Figure 5.18: Horizontally polarised azimuth cartesian plot for the manufactured prototype antenna. (Top) Measured result. (Bottom) FEKO simulated result. The measured HPBW is shown to be within 0.5° of the simulated result while the measured SLL is found to be within 0.1 dB of the simulated result.

From Figure 5.18 it can be seen that the measured and simulated azimuth radiation pattern for the horizontally polarised prototype antenna show the same characteristics. The HPBW of the measured antenna (12.4°) is slightly wider than the FEKO simulated HPBW (12.1°) however, this is well within the margin of error of ±0.5°. The side lobe levels are also well within the margin for error with the difference between simulated and measured results being ±0.1 dB.

Figure 5.19 illustrates the antenna beam pattern as a polar diagram.

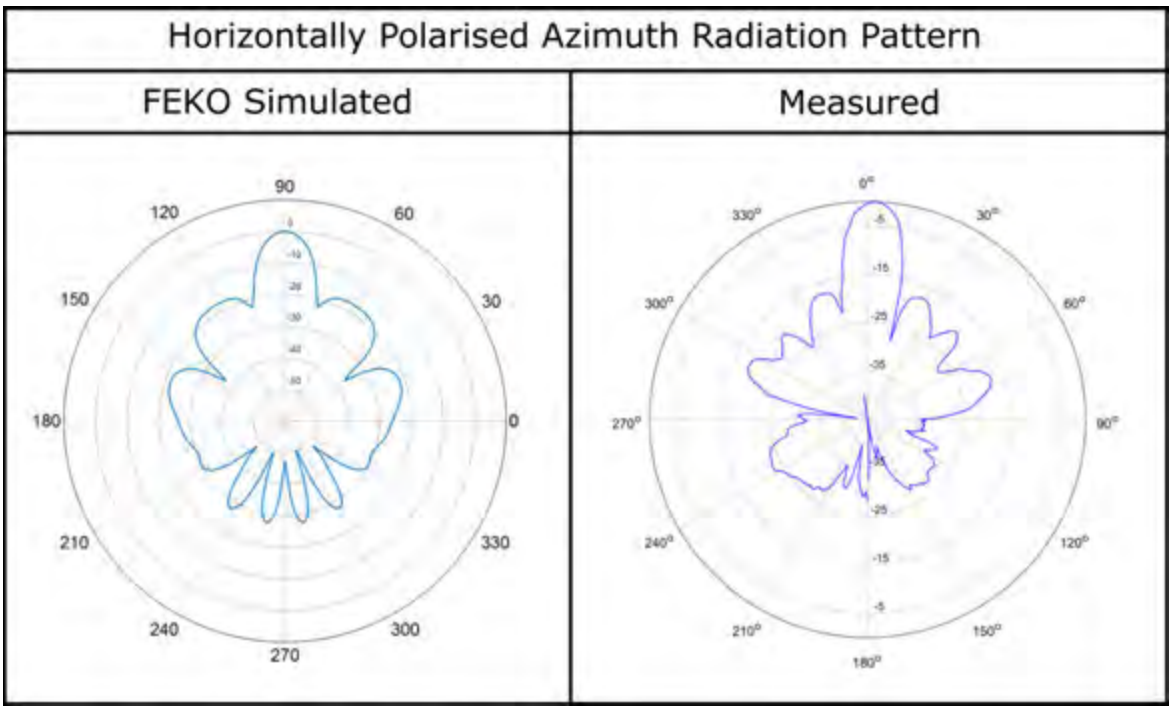

Figure 5.19: Horizontally polarised azimuth polar plot for the manufactured prototype antenna. (Left) FEKO simulated result. (Right) Measured result. The measured polar plot matches the simulated result across the main beam before deviating slightly towards the back-lobes.

It can be seen from Figure 5.19 that the measured beam pattern aligns with the simulated beam pattern for the main lobe before deviating slightly for the back and side lobes.

One source of error is due to the antenna rotating slightly off-axis. This was unavoidable due to the mounting mechanism used. Another possible source of error can be attributed to environmental factors such as buildings to the far left and right of the test environment.

Horizontally Polarised Elevation Radiation Pattern

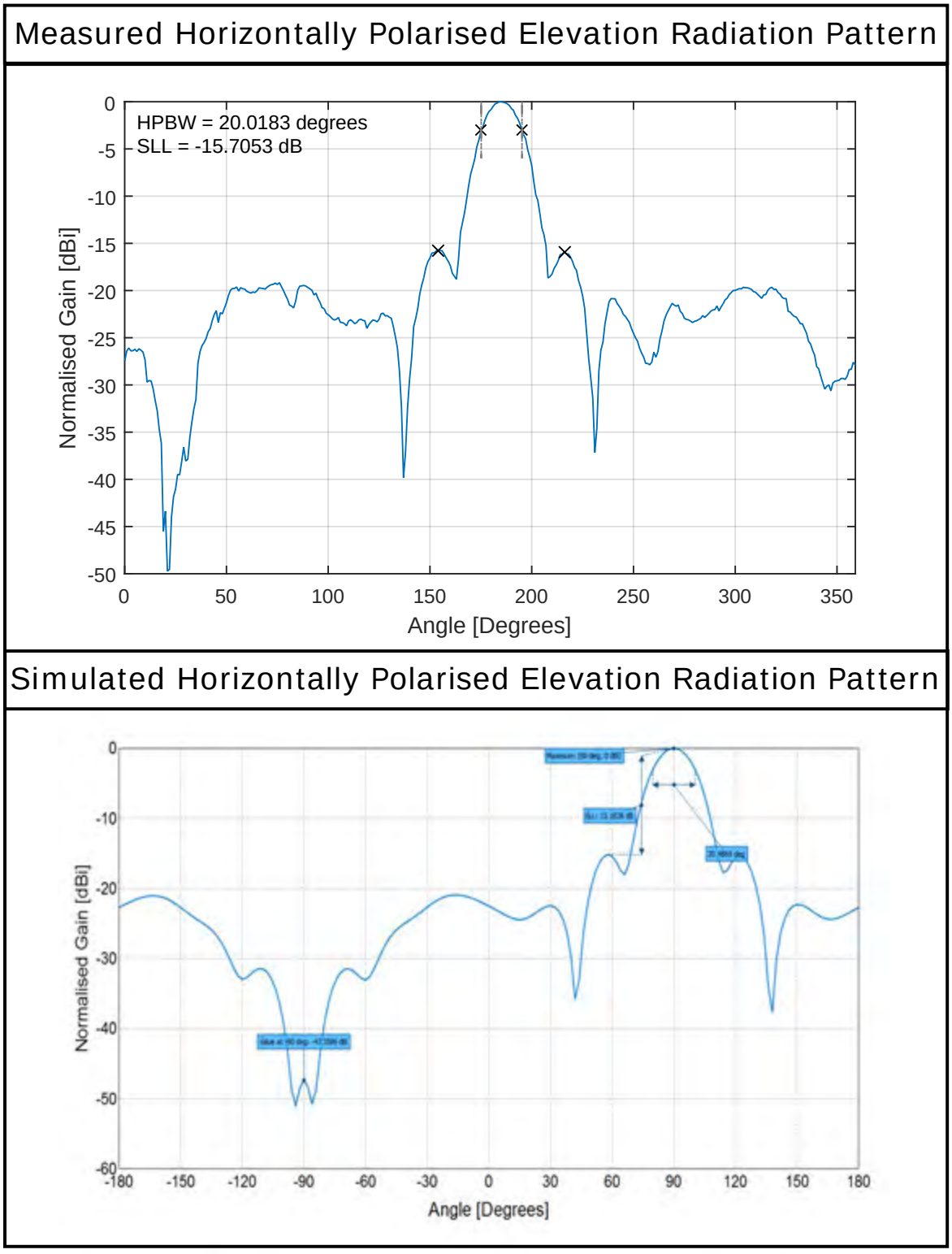

Figure 5.20: Horizontally polarised elevation cartesian plot for the manufactured prototype antenna. (Top) Measured result. (Bottom) FEKO simulated result. The measured main beam HPBW is shown to be within 0.5˚ of the simulated results. The SLL of the measured result is found to be within 0.5 dB of the simulated result.

Figure 5.20 illustrates the similarities between the measured and simulated elevation radiation pattern for the horizontally polarised prototype antenna. It can be seen that the HPBW of the measured antenna (20.0°) is slightly narrower than the FEKO simulated HPBW (20.5°) however this is within the margin of error of ±0.5°. The side lobe levels are also well within the margin for error with the difference between simulated and measured results being ±0.5 dB.

Figure 5.21 illustrates the antenna beam pattern as a polar diagram.

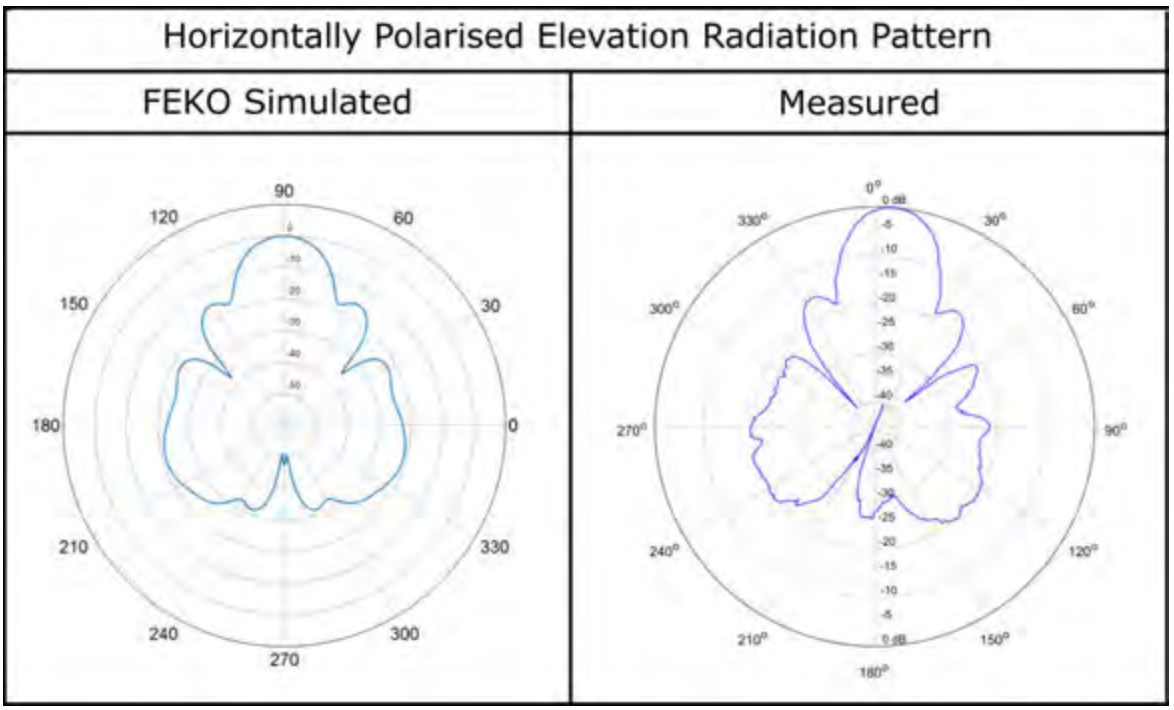

Figure 5.21: Horizontally polarised elevation polar plot for the manufactured prototype antenna. (Left) FEKO simulated result. (Right) Measured result. The polar diagram of the measured result shows an almost exact match to the simulated result. The apparent squinting of the measured polar plot is due to the plotting technique used.

Figure 5.21 shows the correlation between the measured and simulated beam patterns. It can be seen that the measured beam pattern aligns almost exactly with the FEKO simulated beam pattern.

Vertically Polarised Azimuth Radiation Pattern

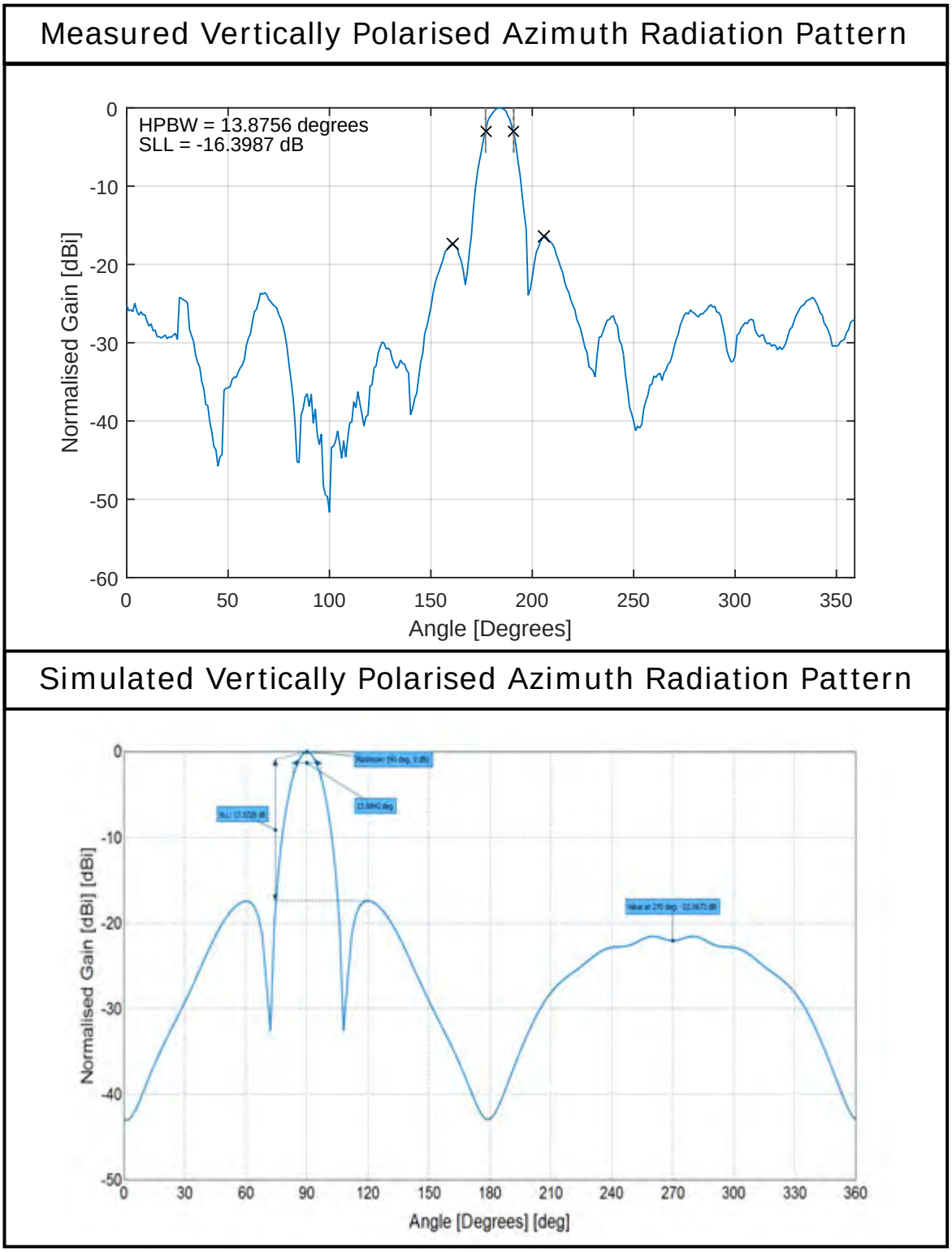

Figure 5.22: Vertically polarised azimuth cartesian plot for the manufactured antenna prototype. (Top) Measured result. (Bottom) FEKO simulated result. The measured HPBW is shown to be the same as the simulated HPBW of 13.9°. The SLL of the measured result is found to be ≈1 dB higher than the simulated result of -17.4 dB.

Figure 5.22 shows a comparison between the measured and simulated azimuth radiation pattern for the vertically polarised prototype antenna. It can be seen that the HPBW of the measured antenna (13.9°) is exactly the same as the FEKO simulated HPBW (13.9°). The side lobe levels are also well within the margin for error with the difference between simulated and measured results being ±1 dB.

The full beam pattern can be seen in Figure 5.23 where the simulated and measured beam patterns are plotted as polar diagrams.

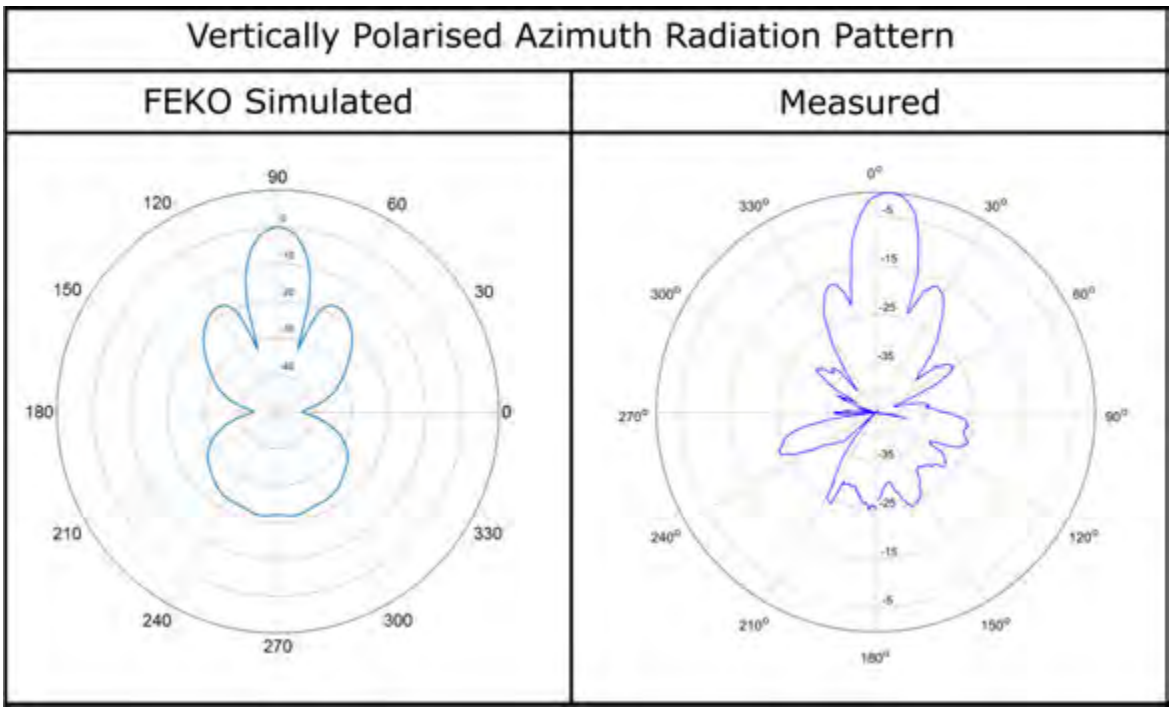

Figure 5.23: Vertically polarised azimuth polar plot for the manufactured prototype antenna. (Left) FEKO simulated result. (Right) Measured result. The measured polar diagram aligns with the simulated polar diagram, showing all major features in the same angular position with approximately the same magnitudes.

The polar plots shown in Figure 5.23 indicate that the measured result is very similar to the FEKO simulated one. It can be seen that the main beam and side lobes exhibit the same characteristics with a null found approximately 90 degrees either side of the main beam.

The distortion seen on the measured antenna can be attributed to environmental factors such as buildings to the far left and right of the test environment.

Vertically Polarised Elevation Radiation Pattern

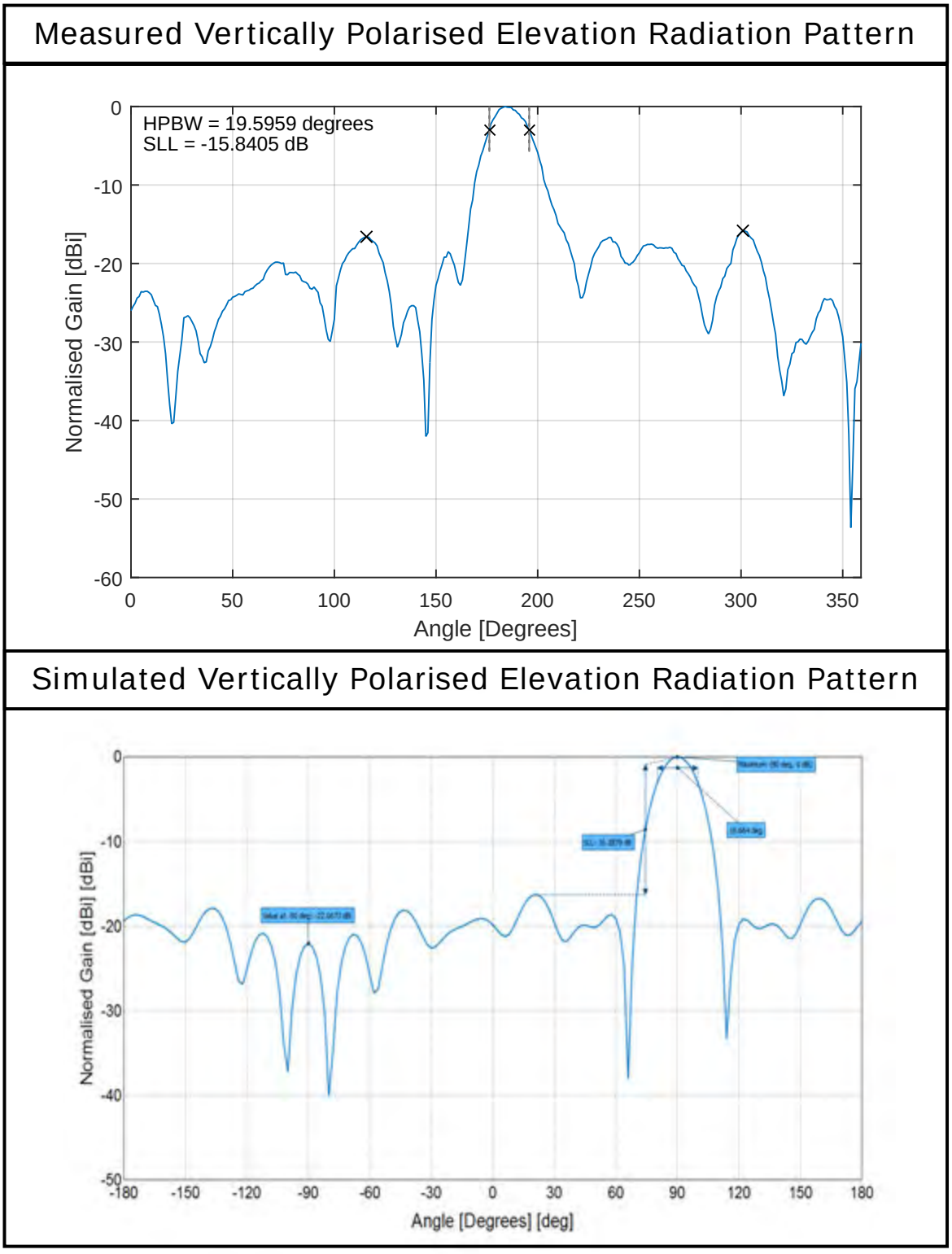

Figure 5.24: Vertically polarised elevation cartesian plot for the manufactured prototype antenna. (Top) Measured result. (Bottom) FEKO simulated result. The main beam HPBW of the measured result is within 0.1˚ of the simulated result while the measured SLL is found to be within 0.5 dB of the simulated result.

Figure 5.24 illustrates the comparison between the measured and simulated elevation radiation pattern for the vertically polarised prototype antenna. It can be seen that the HPBW of the measured antenna (19.6°) is slightly narrower than the FEKO simulated HPBW (19.7°) which is well within the error margin of ±0.5°. The side lobe levels are also well within the margin for error with the difference between simulated and measured results being ±0.5 dB.

The full beam pattern can be seen in Figure 5.25 where the simulated and measured beam patterns are plotted as polar diagrams.

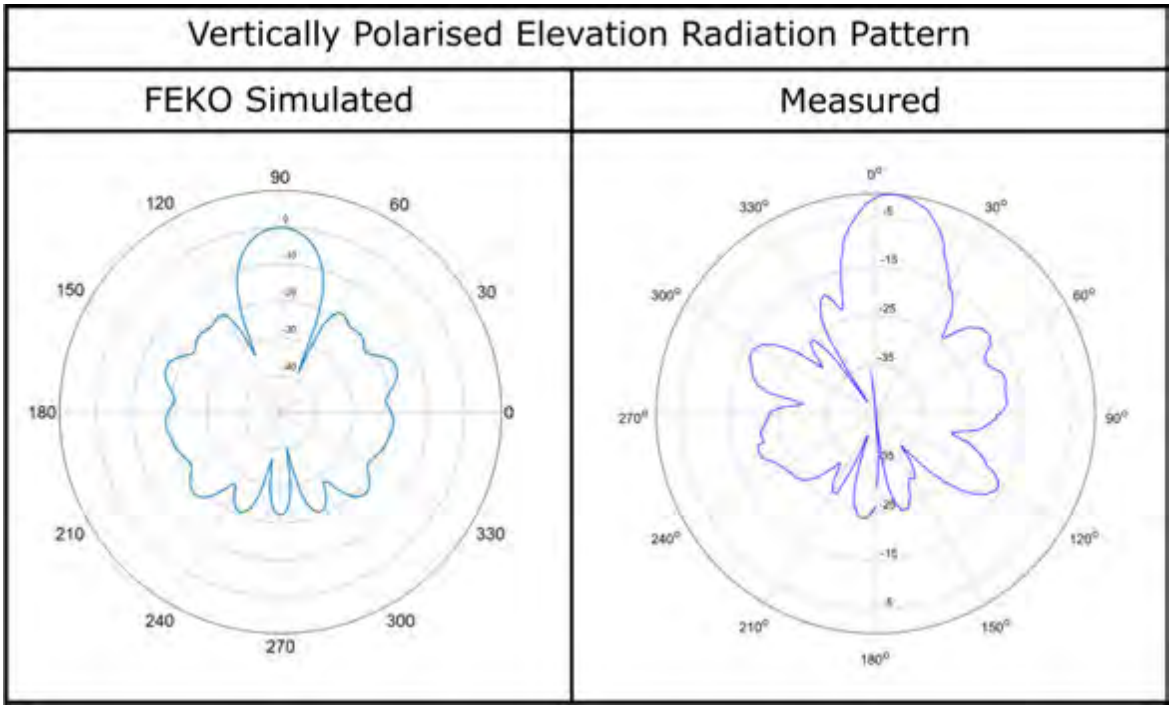

Figure 5.25: Vertically polarised elevation polar plot for the manufactured prototype antenna. (Left) FEKO simulated result. (Right) Measured result. The measured polar diagram exhibits similar features to the simulated result for the main beam however, the polar plots seem to diverge slightly along the back-lobes.

The polar plots shown in Figure 5.25 show that the measured result deviates slightly from the FEKO simulated when looking at the side lobes. It can be seen that the measured side lobes exhibit some form of deformation not seen in the simulations. The deformation seen on the measured antenna can be attributed to environmental factors such as buildings to the far left and right of the test environment. A complete side-by-side summary of the measured radiation pattern results can be found in Appendix G.4.

Gain Calculations

UCT does not have a standard gain horn that is required to do accurate gain measurements of the antenna. Due to the lack of a standard gain horn, the gain calculations are therefore estimated using the approximated directivity of the antenna using the aperture area [12].

The HPBW in both the azimuth and elevation plane was found to be:

$\theta = 13.9^{\circ}$
$\varphi = 19.6^{\circ}$

$$D_0 = \frac{41,253}{\theta_{deg}\varphi_{deg}} = \frac{41,253}{13.9 \times 19.6} = 151.42 \tag{5.2}$$

Where the radiation efficiency, η =0.96

$$G_{\text{dBi}} = 10\log_{10}(0.96 \times 151.42) = 21.6 \text{ dBi} \tag{5.3}$$

To compare this to the calculated theoretical gain using the measured aperture area, the aperture area is measured as:

$$A = 600 \times 1350 = 810000 \text{ mm}^2 \tag{5.4}$$

It is important to note that the aperture of the dish is not rectangular and this will result in a lowered aperture efficiency because the actual size is less. Small dish antennas have an aperture efficiency between 45 and 50%, while the radiation efficiency was shown to be above 96% across the entire band of interest in Section 5.2 [4][12][17].

The gain of the antenna is therefore:

$$G = \eta_{rad} \times \eta_{ap}\frac{4\pi A}{\lambda^2} = 0.96 \times 0.5 \times \frac{4\pi \times 810000}{230^2} = 19.7 \text{ dBi} \tag{5.5}$$

Comparing the two gain calculations, it is shown that they are fairly close and the differences between the two can be attributed to the assumed efficiencies of the antenna. As expected, both calculations correspond to the 19.85 dBi gain that is found when the antenna is simulated.

5.4 Summary

This Chapter has given a description of the testing process that has been used to characterise the overall performance of the antenna. The equipment used has been described in detail as well as the specific measurements taken. The S-parameters have been fully measured, including the return loss (S_{11} and S_{22}) as well as the cross-polarisation isolation between each probe (S_{21}). The azimuth and elevation radiation patterns in both planes of polarisation have been measured.

The results of these measurements have been analysed using MATLAB and compared to the simulated results found in both FEKO and CST. All sources of error and uncertainties within the measurements, including system losses, have been accounted for and elaborated upon in detail.

Due to various manufacturing difficulties, the shape and size of the antenna could not be built exactly as the simulated version and as a result, small inconsistencies between the simulated and measured results are to be expected. With this in mind, the simulated results have shown a close comparison to the measured results. A summary of the measured antenna results can be found in Figures G.5, G.6 and G.7 in Appendix G.4. Table 5.3 summarises the results found in both the FEKO and CST simulations as well as the measured results.

Table 5.3: Comparison of results between FEKO simulations, CST simulations and prototype antenna measurements.

	Horizontal Polarisation			**Vertical Polarisation**		
	FEKO	**CST**	**Measured**	**FEKO**	**CST**	**Measured**
Az HPBW	12.1°	12.2°	12.4°	13.9°	14.2°	13.9°
El HPBW	20.5°	20.4°	20.0°	19.7°	19.5°	19.6°
Az SLL	-17.3 dB	-17.0 dB	-17.4 dB	-17.4 dB	-17.2 dB	-16.4 dB
El SLL	-15.2 dB	-15.2 dB	-15.7 dB	-16.3 dB	-16.9 dB	-15.8 dB

Table 5.3 confirms what can be seen in Figures 5.18 to 5.25, that the measured results closely match the simulated results from both FEKO and CST[¶]. From this, it is concluded that while the azimuth beamwidth in each plane of polarisation is greater than the required 10°, the prototype antenna performs as designed and simulated.

The S-parameter simulations have been found to be accurate and reliable for all test cases. Deviations between the simulated and measured S-parameters have been found when the feed is attached to the focal point of the dish antenna. These deviations can

[¶]For the CST simulated plots, see Appendix G.1

be attributed inconsistent mesh shape and “flatness” as well as the feed placement and spacing inaccuracies due to the manufacturing process.

From the results of the measurements, it has been shown that manufacturing tolerances are critical to the performance of the antenna. However, with this in mind, it can be seen that the simulations are accurate and with proper manufacturing facilities, the optimised design can be manufactured and will perform as designed and simulated.

Chapter 6

Conclusions and Recommendations

6.1 Conclusions

The objectives of this dissertation have been to design and implement an L-Band antenna that would meet the user requirements as given in Section 1.2. While not all these specifications have been met due to manufacturing difficulties, it has been shown that when manufactured, the antenna performs as designed as the measured results match the simulated results. Table 6.3 summarises the built antenna prototype specifications and characteristics. The complete graphical summary of the antenna performance can be found in Figures G.5, G.6 and G.7 in Appendix G.4.

From the results of the simulations and measurements, the following conclusions have been drawn.

Using an open ended waveguide as a feed for the dish antenna has been found to be most efficient for the antennas designed in this dissertation. As all the dish antennas designed in this dissertation are considered electrically small dish antennas (less than $10\lambda_0$ in diameter), the effect of feed blockage on antenna performance is significant. It is required that the feed be as small as possible to obtain satisfactory performance. The effect of reflections back into the feed on small, deep dish antennas is significant and decreases as the dish becomes flatter. Using a circular waveguide feed over a square waveguide feed improves port-to-port isolation considerably (up to 8 dB) when dual polarised. Using a circular waveguide feed also provides a more even aperture illumination when compared to a square feed. Using N-Type connectors as launchers for the coaxial-to-waveguide transitions allow for high power handling, therefore ensuring the power specification be met by the design.

The effect on the beam pattern of the antenna due to the feed support structure has

been simulated and it was found that on small dish antennas, the effect of the support feed is significant. It has been shown through Figure D.1 in Appendix D that using a conducting feed support causes significant beam squinting. This has been solved using a single non-conducting support from the centre of the dish. It has also been found that supporting the feed using nylon ties helps to maintain the overall dish shape as well as ensure proper feed support.

It has been shown that a full dish antenna, as designed in Section 4.2.2, would provide the best performance, however, it is too large to be used as intended on a single tripod. The CAD drawings of the full dish antenna can be found in Appendix H. The radiation patterns of the antenna in both azimuth and elevation planes for both planes of polarisation (horizontal and vertical) have been simulated and the antenna dimensions optimised using FEKO. Table 6.1 below summarises the results of the simulated optimal design.

Table 6.1: Simulated antenna performance characteristics for the FEKO optimised full dish antenna.

Parameter	**FEKO Optimised**
Diameter	1500 mm
Depth	284.1 mm
Focal Point	495 mm
f/D ratio	0.33
Inner Waveguide Radius	87.5 mm
Inner Waveguide Length	230 mm
Probe Length	56.9 mm
Probe Backshort	133.3 mm
Feed Phase Centre	+25.8 mm
Parabolic Equation	$y = (5.05 \times 10^{-4})x^2$
HPBW (Az)	H-Pol - 10.04° V-Pol - 10.06°
HPBW (El)	H-Pol - 10.06° V-Pol - 10.04°
SLL (V-Pol)	Azimuth - 23.12 dB Elevation - 21.61 dB
SLL (H-Pol)	Azimuth - 21.61 dB Elevation - 23.12 dB
F/B ratio	25.4 dB

To reduce the size of the antenna, a truncated dish antenna has been designed and simulated. It has been found that the truncated dish antenna would be fully capable of

meeting all the requirements as set in Section 1.2. Table 6.2 summarises the simulated performance of the truncated dish antenna.

Table 6.2: Simulated antenna performance characteristics for the FEKO optimised truncated dish antenna.

Parameter	**FEKO Optimised**
Diameter	1440 mm
Height	744 mm
Depth	290.3 mm
Focal Point	446 mm
f/D ratio	0.31
Inner Waveguide Radius	87.5 mm
Inner Waveguide Length	230 mm
Probe Length	56.9 mm
Probe Backshort	80.4 mm
Feed Phase Centre	+25.8 mm
Parabolic Equation	$y = (5.56 \times 10^{-4})x^2$
HPBW (Az)	H-Pol - 10.7° V-Pol - 10.0°
HPBW (El)	H-Pol - 16.4° V-Pol - 16.6°
SLL (Az)	H-Pol - 20.3 dB V-Pol - 16.9 dB
SLL (El)	H-Pol - 15.1 dB V-Pol - 15.0 dB
F/B ratio	H-Pol - 24.7 dB V-Pol - 30.7 dB

Due to the manufacturing limitations in this project, it was decided that the prototype antenna would be built by modifying a bought pre-fabricated antenna. The CAD drawings for the optimised truncated dish antenna can be found in Appendix H. The built prototype antenna has been designed in Section 4.2.4 and the CAD drawings can be found in Appendix H. The built prototype has been designed, simulated and manufactured based off a bought pre-fabricated 2.45 GHz Wi-Fi dish antenna. The built prototype has been tested and found to agree with the simulated version. The measured results can be seen in Table 6.3.

It has been shown that the built prototype antenna has the following properties when vertically polarised:

- HPBW in the azimuth plane of 12.4°
- HPBW in the elevation plane of 20.0°
- S_{11}, S_{21} and S_{22} parameters greater than -15 dB between 1.275 GHz to 1.325 GHz

It has been shown that the built prototype antenna has the following properties when horizontally polarised:

- HPBW in the azimuth plane of 13.9°
- HPBW in the elevation plane of 19.6°
- S_{11}, S_{21} and S_{22} parameters greater than -15 dB between 1.275 GHz to 1.325 GHz

It has been found that the measured parameters closely align with the simulated parameters, with the small deviations being attributed to manufacturing tolerances as well as environmental factors caused by the lack of a reflection free testing facility such as an anechoic chamber. A summary of the antenna beam pattern measurements can be found in Appendix G.4. The built prototype antenna has shown that the simulations are accurate and can be used as a very accurate indicator as to the performance of any antenna design found within this dissertation.

Due to the requirement for a dual polarised antenna, the feed to the antenna had to remain symmetrical. This means that the HPBW of the feed remains the same in both azimuth and elevation planes. The result of this is that there is a large amount of spillover in the elevation plane, leading to increased back and side lobe levels. The meshing structure used performs as intended. It has however, been found to deform slightly when the antenna is moved around and had to be attended to before every test to ensure that the parabolic curvature of the surface remained accurate.

Table 6.3: Built prototype antenna parameters and characteristics.

Measured Parameter	**Value**
Frequency	1.3 GHz
Bandwidth	<100 MHz
Polarisation	Dual (H and V)
Diameter	1350 mm
Height	600 mm
Depth	370 mm
Focal Point	307.85 mm
f/D ratio	0.23
Inner Waveguide Radius	87.5 mm
Inner Waveguide Length	230 mm
Probe Length	56.9 mm
Probe Backshort	121.2 mm
Feed Phase Centre	+25.8 mm
Parabolic Equation	$y = (8.16 \times 10^{-4})x^2$
F/B ratio	28 dB
Gain	19.65 dBi
Weight	9 kg
HPBW (Az)	H-Pol - 13.9° V-Pol - 12.4°
HPBW (El)	H-Pol - 19.6° V-Pol - 20.0°
SLL (Az)	H-Pol - 17.4 dB V-Pol - 16.4 dB
SLL (El)	H-Pol - 15.7 dB V-Pol - 15.8 dB

6.2 Recommendations and Future Work

The following recommendations are made from the results and conclusions found throughout this dissertation.

The use of open ended circular waveguides as antenna feeds allows for improved probe-to-probe isolation. However, manufacturing a circular waveguide can be extremely difficult. As a result, a pipe or a tin can should be used. To improve waveguide performance, a thicker walled waveguide (3 mm) is required as this will allow better shape retention while making it easier to fix the probe to the waveguide. Probe placement is of critical importance and it is therefore recommended that placing of the probes be done as accurately as possible with the use of a lathe.

To improve antenna measurements, all new measurements, including the characterisation of any new antenna, needs to be done in an anechoic chamber to ensure accurate and precise results. A full, continuous, 3D spherical plot can be done which will allow direct comparisons between the simulated 3D radiation patterns and the measured ones to be made. It is critical to ensure that the Tx and Rx antennas are perfectly aligned and that the axis of rotation is perfectly centred. Accurate gain measurements using a standard gain horn are required to fully characterise the antenna. This should be done inside an anechoic chamber as it will result in the most accurate results.

To reduce the effects of the feed support arm(s), the use of non conducting material is of utmost importance. The feed supports work best when made from wood, fibre glass or a combination of both. A stiff, fine mesh should be used as this will give the structure rigidity and ensure that no surface deformation occurs. This is a critical aspect of the manufacturing process as any deviation from the parabolic shape will result in a reduction in performance.

One option for the manufacture of the final dish antenna is to use a block of styrofoam to cut the parabolic shape from, creating a solid former that can be used to lay fibreglass sheets onto. The fibreglass can then be removed when dry and holes can be cut to reduce wind resistance. A mesh structure can then be added to the fibreglass skeletal structure to form the parabolic reflective surface.

Manufacturing of the optimised dish design would require a workshop capable of producing a high quality parabolic surface. While the surface itself can be made using a fine meshed structure, the skeletal frame needs to be manufactured with tight tolerances to ensure optimal performance.

Bibliography

[1] S. Paine, "Design and Implementation of Dual Polarised L-Band Antenna with 10 Degree Azimuth Beamwidth," University of Cape Town, Cape Town, Tech. Rep., 2014.

[2] S. R. Doughty, "Development and performance evaluation of a multistatic radar system," Ph.D. dissertation, University College London, 2008.

[3] M. Inggs, H. Griffiths, F. Fioranelli, M. Ritchie, and K. Woodbridge, "Multistatic radar: System requirements and experimental validation," in *Radar Conference (Radar), 2014 International*, Oct 2014, pp. 1–6.

[4] W. L. Stutzman and G. A. Thiele, *Antenna Theory and Design*, 3rd ed. New York: John Wiley & Sons, Inc., 2013.

[5] "RT/Duroid 5870/5880 High Frequency Laminates," Rogers corporation, accessed: April 28, 2016. [Online]. Available: http://www.rogerscorp.com/documents/606/acm/RT-duroid-5870-5880-Data-Sheet.aspx

[6] J. Carr, "Practical Antenna Handbook," pp. 19–48, November 15, 2011.

[7] G. McDonald, "Stacking Yagi Antennas," 2009, accessed: April 28, 2016. [Online]. Available: http://www.ifwtech.co.uk/g3sek/stacking/stacking2.htm

[8] R. A. Formato, "Improving Bandwidth of Yagi-Uda Arrays," *Wireless Engineering and Technology*, vol. 3, no. 1, pp. 18–24, 2012.

[9] Naval Air Systems Command, "Electronic Warfare and Radar Systems Engineering Handbook," no. April 1997, p. 299, 1999.

[10] J. Lawson, "Yagi Antenna Basics," 2016. [Online]. Available: http://www.hamuniverse.com/yagibasics.html

[11] Nikolova, "Class Lecture, Topic: "Horn Antenna Design and Synthesis"," 2014, accessed: April 28, 2016. [Online]. Available: http://www.ece.mcmaster.ca/faculty/nikolova/antenna_dload/current_lectures/L18_Horns.pdf

[12] C. A. Balanis, *Antenna Theory: Analysis and Design*, 3rd ed. New York: John Wiley & Sons, Inc., 2011.

[13] P. Wade, "Parabolic Dish Feeds," 1998, accessed: April 28, 2016. [Online]. Available: http://www.w1ghz.org/antbook/chap11.pdf

[14] M. Fazaelifar, "Design, Fabrication and Test of Parabolic Cylinder Reflector and Horn for Increasing the Gain of Vlasov Antenna," pp. 191–203, 2008.

[15] J. P. Wakbl, "Simulation and Measurement of the Effects of Reflections from a Prime Focus Dish back into a Circularly Polarized Feed," *High Frequency Electronics Summit Technical Media, LLC*, accessed: April 28, 2016. [Online]. Available: http://www.highfrequencyelectronics.com/Aug10/HFE0810_Pawlan_2.pdf

[16] W. Paul Wade, "Offset-Fed Parabolic Dish Antennas," vol. 2, 1998. [Online]. Available: http://www.w1ghz.org/antbook/contents.htm

[17] ——, "Parabolic Dish Focus , Zoom , and Tilt," vol. 2, no. 1, 2009.

[18] P. J. Bevelacqua, "Antenna Theory," 2014, accessed: April 28, 2016. [Online]. Available: http://www.antenna-theory.com/

[19] P. Hazdra and R. Galuscak, "Loop Feed With Enhanced Performance," vol. 1, no. 1, pp. 1–19, 2009.

[20] P. Krunal, "Designing optimized cassegrain with balanced feed," *International Journal of Computer Applications (IJCA)*, vol. 4, pp. 26–34, jan 2011.

[21] B. Downing, "Microwave Components and Antennas," EEE5121Z lecture notes, Department of Electrical Engineering, University of Cape Town, South Africa, 2014.

[22] N. Dick Comly, "Parabolic Antennas and Their Feeds," accessed April 28, 2016. [Online]. Available: http://www.packratvhf.com/Article_9/Dish_Not.pdf

[23] Altier, "FEKO," 2015, accessed: 2016-01-18. [Online]. Available: https://www.feko.info/product-detail/overview-of-feko

[24] CST Studio, "CST Studio Suite 2015," 2015, accessed: April 28, 2016. [Online]. Available: https://www.cst.com/Content/Articles/article909/CST-STUDIO-SUITE-2015.pdf

[25] Gregory Charvat, Jonathan Williams, Alan Fenn, Steve Kogon, and Jeffrey Herd, "Build a small radar system capable of sensing range, doppler, and synthetic aperture radar imaging," (Massachusetts Institute of Technology: MIT), accessed: June 13, 2015. [Online]. Available: http://ocw.mit.edu

[26] G. L. Charvat, "MIT IAP 2011 Laptop Based Radar: Block Diagram, Schematics, Bill of Material , and Fabrication Instructions," *Presented at the 2011 MIT Independent Activities Period (IAP)*, pp. 1–51, 2012.

[27] P. Wade, "Understanding Circular Waveguide - Experimentally," 2001, accessed: November 27, 2015. [Online]. Available: http://www.w1ghz.org/QEX/circular_wg.pdf

[28] F. Gustrau, "RF and Microwave Engineering," Wiley-Interscience, March, 2005.

[29] T. G. et. al., "Linear to radial polarization conversion in the thz domain using a passive system," *Opt. Express*, vol. 16, no. 23, pp. 18 895–18 909, Nov 2008, accessed April 28, 2016. [Online]. Available: http://www.opticsexpress.org/abstract.cfm?URI=oe-16-23-18895

[30] *N / Composite N / N 18 GHz series*, Radiall, 2010, rev. 1. [Online]. Available: http://www.radiall.com/media/files/N%20D1C004XEe.pdf

[31] N. C. Karmakar and S. K. Padhi, "Coaxial lines and waveguides," in *Encyclopedia of RF and Microwave Engineering*. John Wiley & Sons, Inc., 2005.

[32] K W. Whites, "TEM, TE, and TM Modes for Waveguides," pp. 1–10, 2012, accessed April 28, 2016. [Online]. Available: http://whites.sdsmt.edu/classes/ee481/notes/481Lecture10.pdf

Appendix A

Waveguide Theory

As mentioned in Section 3.1.4, the feed of an antenna plays a vital role in the overall performance of the antenna. There are many different ways in which an antenna can be fed. However, as was found in a previous investigation [1], using a waveguide feed is most appropriate for this type of system. For a waveguide to act as a transmission line for an EM wave, the following conditions, known as Maxwells boundary conditions, need to be met [31]:

- "A tangential electric field must vanish at the boundary of a perfect electric conductor."
- "Any magnetic field that is normal to a perfectly conducting boundary must also vanish at the boundary."

Waveguide Modes

Most practical waveguide structures rely on single-mode operation and can therefore be characterised based on their mode of operation.

Waveguide modes are defined as certain field patterns that can propagate down a waveguide independently. There are four main classifications of waveguide modes, these include:

- Transverse Electromagnetic (TEM)
- Transverse Electric (TE)
- Transverse Magnetic (TM)
- Hybrid Modes

A TEM mode is defined as having both electric and magnetic fields that are perpendicular to each other and transverse to the direction of propagation of the wave. TE modes are defined as having only electric fields that are transverse to the direction of propagation while TM modes are defined as having only a magnetic field that is transverse to the direction of propagation. Each mode can therefore be described mathematically as [21]:

- TEM modes: $E_z = 0,\ H_z = 0$
- TE modes: $E_z = 0,\ H_z \neq 0$
- TM modes: $E_z \neq 0,\ H_z = 0$
- Hybrid modes: $E_z \neq 0,\ H_z \neq 0$

The TEM mode is the dominant mode in coaxial cables and stripline transmission lines. This is due to the fact that a conventional electric and magnetic field can be supported as the wave travels down the transmission line. This is not the case in metallic waveguides whereby the dominant mode is TE or TM [12][32]. Figure A.1 illustrates the satisfying of boundary conditions by different modes within a circular waveguide.

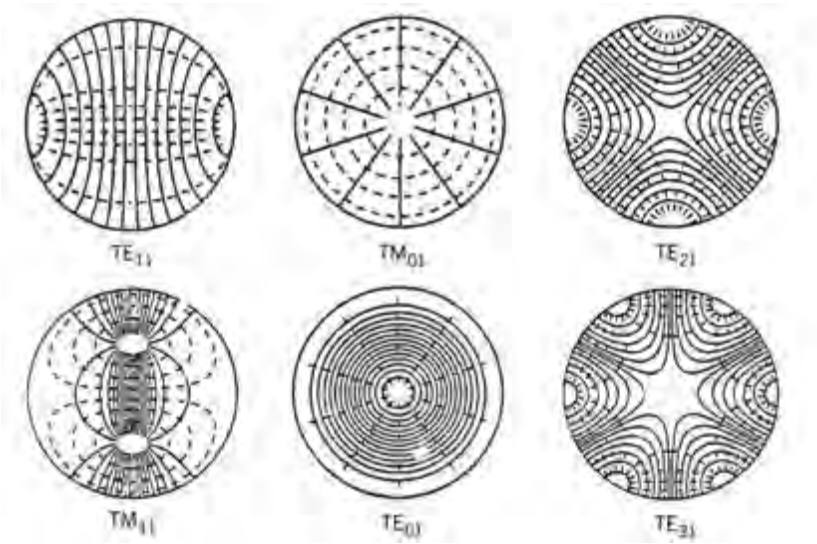

Figure A.1: Fundamental modes found in a circular waveguide where the solid lines represent the E-field and the dashed lines represent the H-field. From left to right, with the fundamental mode being the TE_{11} mode and the next high order mode being the TE_{21} mode and so forth [29].

Dominant Mode of Propagation

Waveguides are frequency dependant devices that are designed with both a lower and upper cut-off operating frequency in mind. The dominant mode of propagation is the mode that experiences the least attenuation while also having a lower cut-off frequency than the other modes. What this means is that higher order modes are suppressed at the lower end of the waveguide bandwidth (usually at the design frequency), therefore allowing only propagation of the fundamental or dominant mode. Higher order modes can however, propagate at higher frequencies where their attenuation becomes insignificant when compared to the dominant mode. Higher order modes are undesirable and are generally avoided by placing upper frequency limits on the specification of a waveguide [21][28][29].

The fundamental mode or dominant mode of operation for a rectangular waveguide is TE_{10}, TEM for a coaxial structure where there is an inner and outer conductor and TE_{11} for a circular waveguide. Hybrid or Quasi-TEM modes are generally seen in microstrip, slotline or coplanar transmission lines. This is due to the variation in dielectric constants between the upper and lower bounds of the inner and outer conducting surfaces.

Figure A.2 illustrates fundamental mode of operation that exists in rectangular, coaxial and circular waveguide structures.

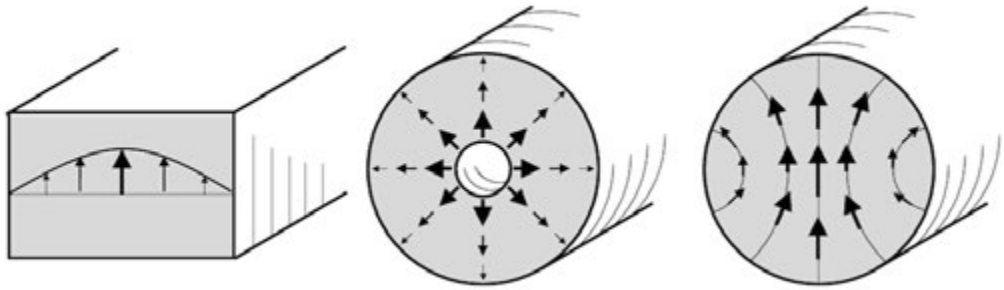

Figure A.2: Fundamental modes in different transmission line structures where the arrows represent the relative strength of the electric field distribuiton within the structure: (Left) Rectangular waveguide; (Centre) Coaxial cable; (Right) Circular waveguide [1].

Metallic waveguides come in many different shapes and sizes with the most common being rectangular and circular.

Rectangular and circular waveguides are similar in that they are both constructed as single, enclosed conductors and both support TE and TM modes of operation. Each mode has a cut-off frequency, below which the EM energy is drastically attenuated and no wave (in that mode) can propagate down the transmission line [29].

Dual Polarising a Waveguide

One of the major advantages to using circular waveguides as opposed to rectangular waveguides is when dual polarisation is required. There are many ways in which a waveguide can be dual polarised. The simplest method is to simply insert two probes orthogonally to each other. This way, one of the probes allows for vertical polarisation while the other allows for horizontal polarisation. Figure A.3 shows the basic geometry of the probes [1].

Figure A.3 illustrates the placement of orthogonal probes in both a rectangular and circular waveguide.

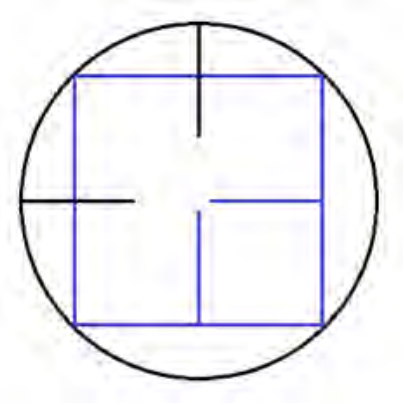

Figure A.3: Dual polarised waveguide. The blue lines represent the square waveguide and probes while the black lines represent the same probes in an equivalent circular waveguide [1].

It can be seen from Figure A.3 that the probes in the circular waveguide are further spaced than those in the equivalent square waveguide. This is an important aspect to consider as the isolation between probes plays a major role in antenna performance.

The co- and cross-polarisation isolation requirements depend heavily on system specifications. Ideally there will be no cross-polarisation components and the port-to-port isolation would be infinite, however this in reality, does not exist. Achieving a port-to-port isolation better than 15 dB is generally appropriate for most practical requirements [1][12][15].

Theoretically, the isolation between the probes should be infinite as they are perpendicular to each other and therefore do not interact. In practice however, there are fringing fields on the end of the probes which result in interactions between the probes. Another issue is that in real systems, achieving perfectly perpendicular probes is difficult. Provided no fringing fields, being even 1 degree out results in a maximum isolation of $\cos(1) = 38$ dB [1].

One way of reducing the effect of the fringing fields is by separating the probes by half a wavelength. This is done such that the one pin is positioned in a null of the radiating pin. Figure A.4 shows an example of such an offset.

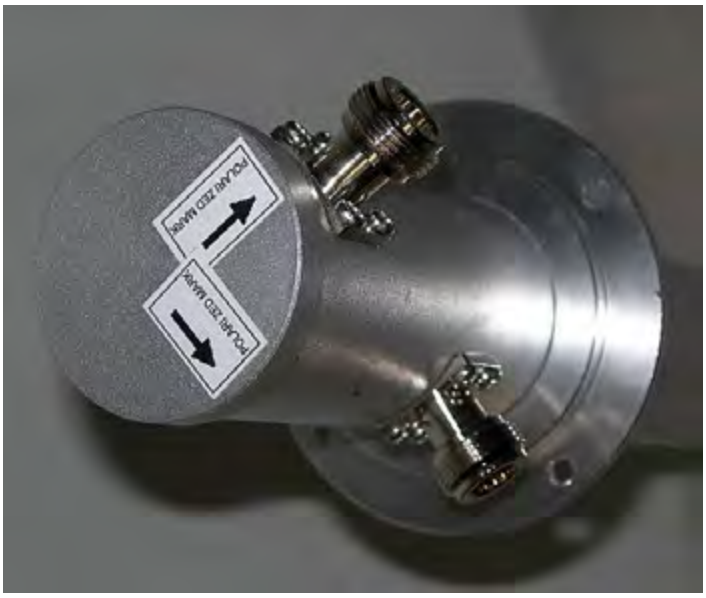

Figure A.4: Dual polarised circular waveguide with half wavelength seperation between the probes for improved polarisation isolation [1].

The downside to this is that it elongates the waveguide and is therefore not suitable for compact or low frequency designs. Other methods include the use tuning screws, these are discussed in more detail in Section 4.

Phase Velocity, Group Velocity and Waveguide Wavelength

The phase velocity of a wave is defined as "the velocity of the resultant intersecting point of the two propagating transverse EM waves." [21] Which is defined mathematically as:

$$V_p = \frac{C}{\cos(\alpha)} = \frac{C\lambda_g}{\lambda_0} \tag{A.1}$$

where,

V_p – Phase Velocity
C – Speed of Light in a Vacuum
α – Phase Angle
λ_g – Waveguide Wavelength
λ_0 – Free-space Wavelength

The waveguide wavelength, λ_g, for a rectangular waveguide, is given by:

$$\lambda_g = \frac{\lambda_0}{\sqrt{1 - (\frac{\lambda_0}{2a})^2}} \tag{A.2}$$

Where 'a' is the inner width of the waveguide as shown in Figure A.5.

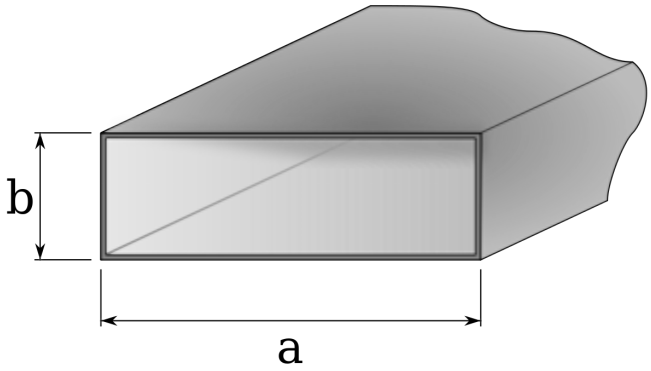

Figure A.5: Inner dimensions of a rectangular waveguide [31].

The waveguide wavelength for a circular waveguide is slightly different from that of a rectangular waveguide and is given by:

$$\lambda_g = \frac{\lambda_0}{\sqrt{1 - (\frac{\lambda_0}{1.705D})^2}} \tag{A.3}$$

Where 'D' is the inner waveguide diameter.

It can therefore be seen from (A.1), (A.2) and (A.3) that the phase velocity, V_p, is greater than the speed of light. This phenomenon holds true only because no energy is transferred and the velocity at which energy is propagated down a waveguide is given by the group velocity, V_g [21].

The group velocity, V_g, of a wave is given by:

$$V_g = \frac{C\lambda_0}{\lambda_g} \tag{A.4}$$

By comparing equations A.1 and A.4, it can be seen that a waves phase and group velocity can be related by:

$$V_p = \frac{C^2}{V_g} \tag{A.5}$$

Equation (A.2) indicates that in order for a wave to propagate down a waveguide, the following conditions need to be satisfied:

- When $\lambda_0 < 2a$, then λ_g is real and positive
- When $\lambda_0 = 2a$, then λ_g tends to infinity while $\lambda_0 = \lambda_c$
- When $\lambda_0 > 2a$, then λ_g is imaginary

These conditions show that a wave will only propagate down a rectangular waveguide when $\lambda_0 < 2a$. A similar set of conditions can be drawn up for circular waveguides and is explored in more detain in Section 4 [21].

Appendix B

Designs Considered

The following results are from a report titled: "Design and Implementation of a Dual Polarised L-Band Antenna with 10 Degree Azimuth Beamwidth" [1].

B.1 Patch Array Antenna

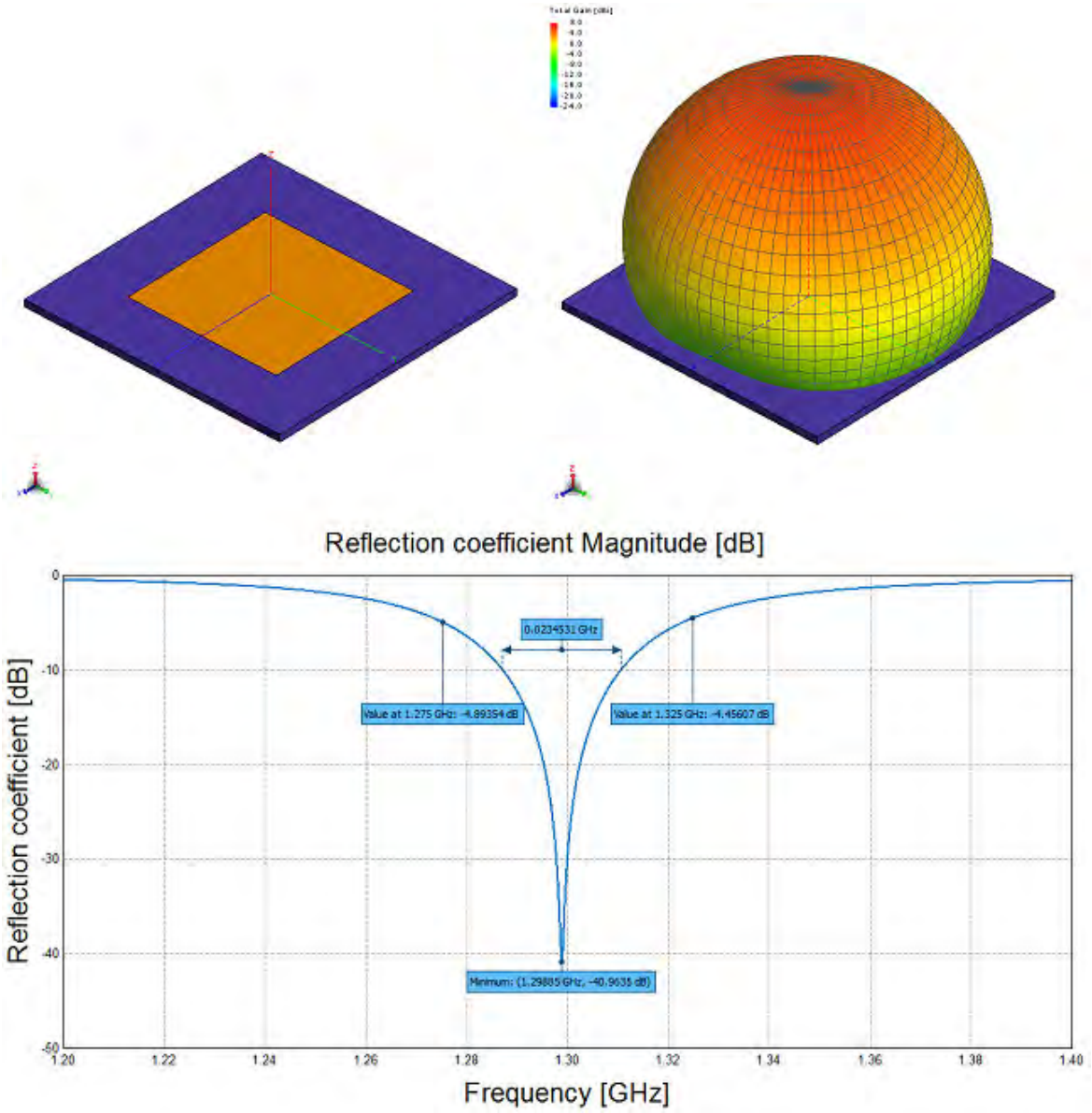

Figure B.1: Single patch antenna on RT/Duroid 5880 substrate. (Top left) 3D render of patch and substrate. (Top right) 3D far-field plot of single patch. (Bottom) Simulated S_{11} parameter for single patch [1].

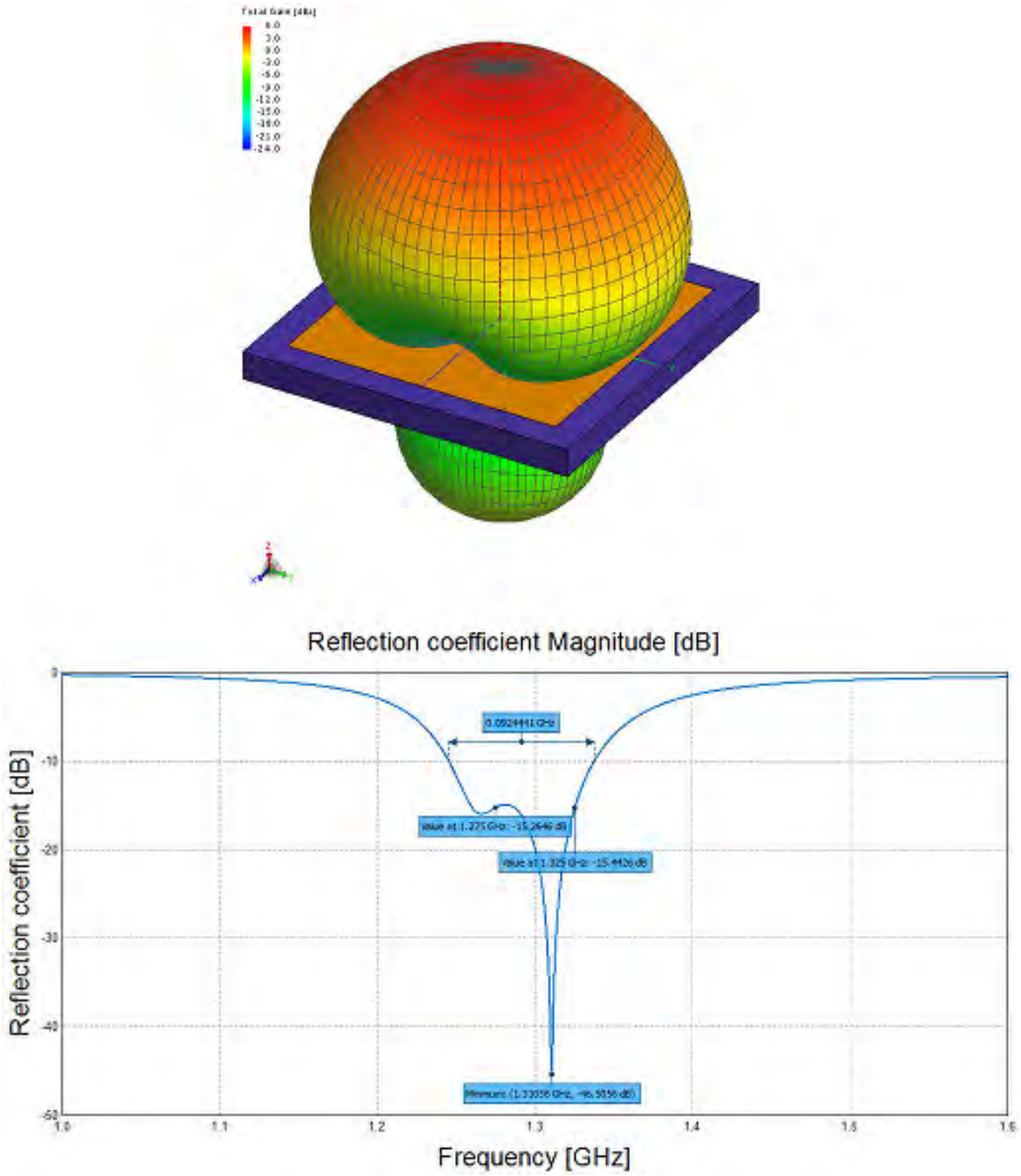

Figure B.2: Single patch antenna with air substrate in the form of expanded polystyrene (EPS). (Top) 3D far-field plot. (Bottom) Simulated S_{11} parameter for single patch [1].

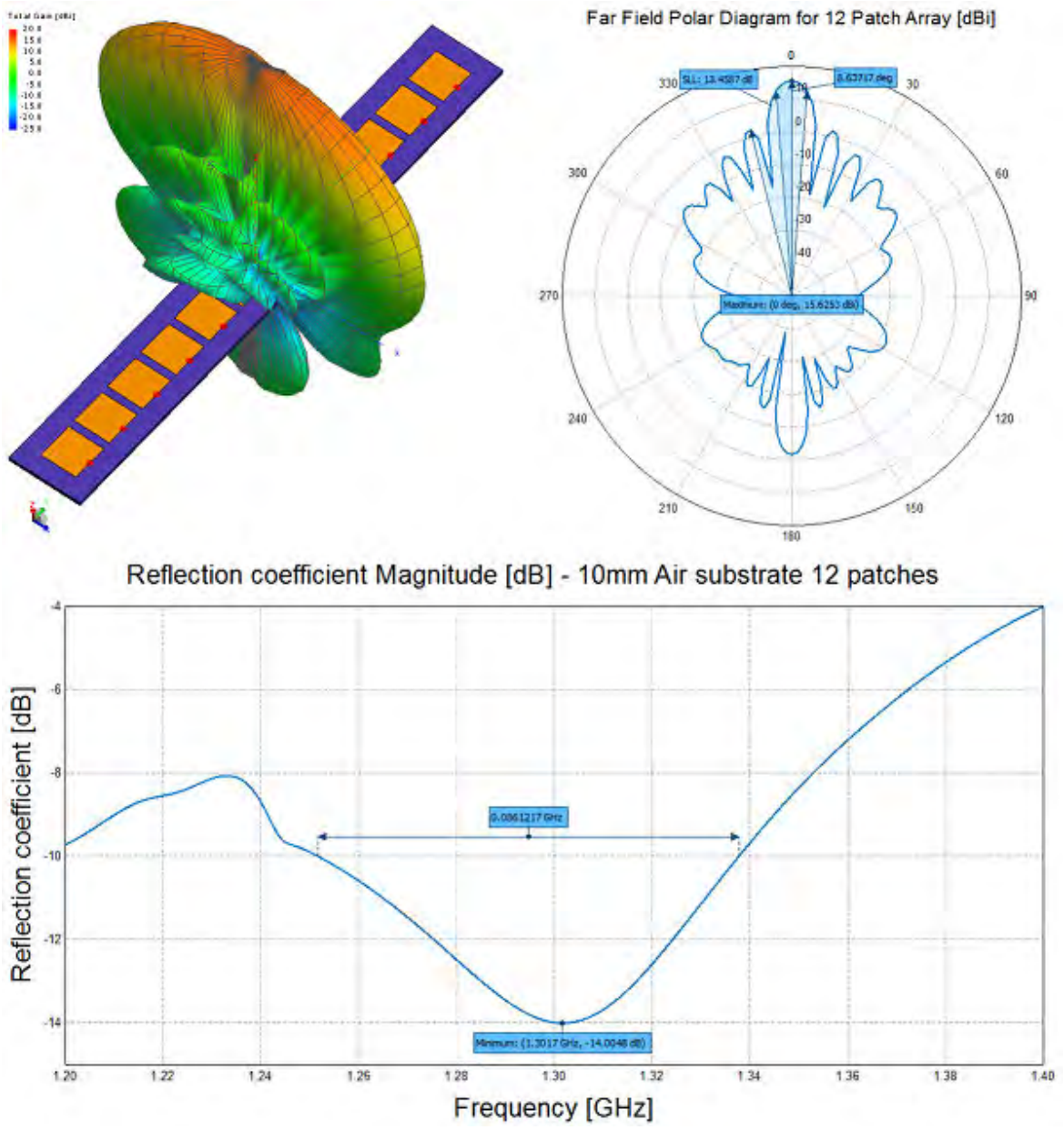

Figure B.3: 12 element patch antenna array. (Top left) 3D far-field plot. (Top right) Simulated azimuth polar diagram for the array. (Bottom) Simulated S_{11} parameter [1].

B.2 Sectoral Horn Antenna

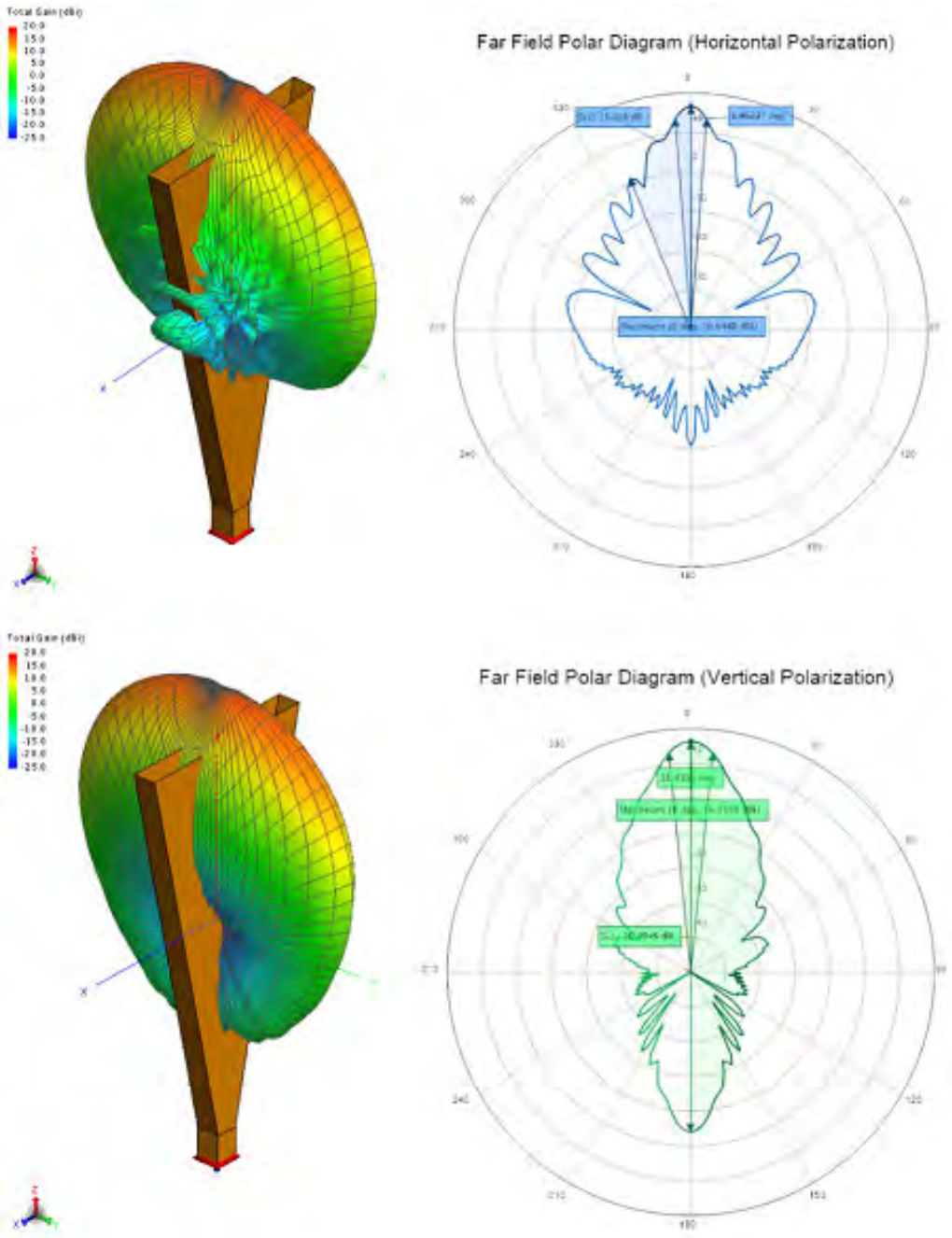

Figure B.4: Sectoral horn antenna simulations. (Top) Horizontally polarised 3D far-field plot and azimuth plane polar plot. (Bottom) Vertically polarised 3D far-field plot and azimuth plane polar plot [1].

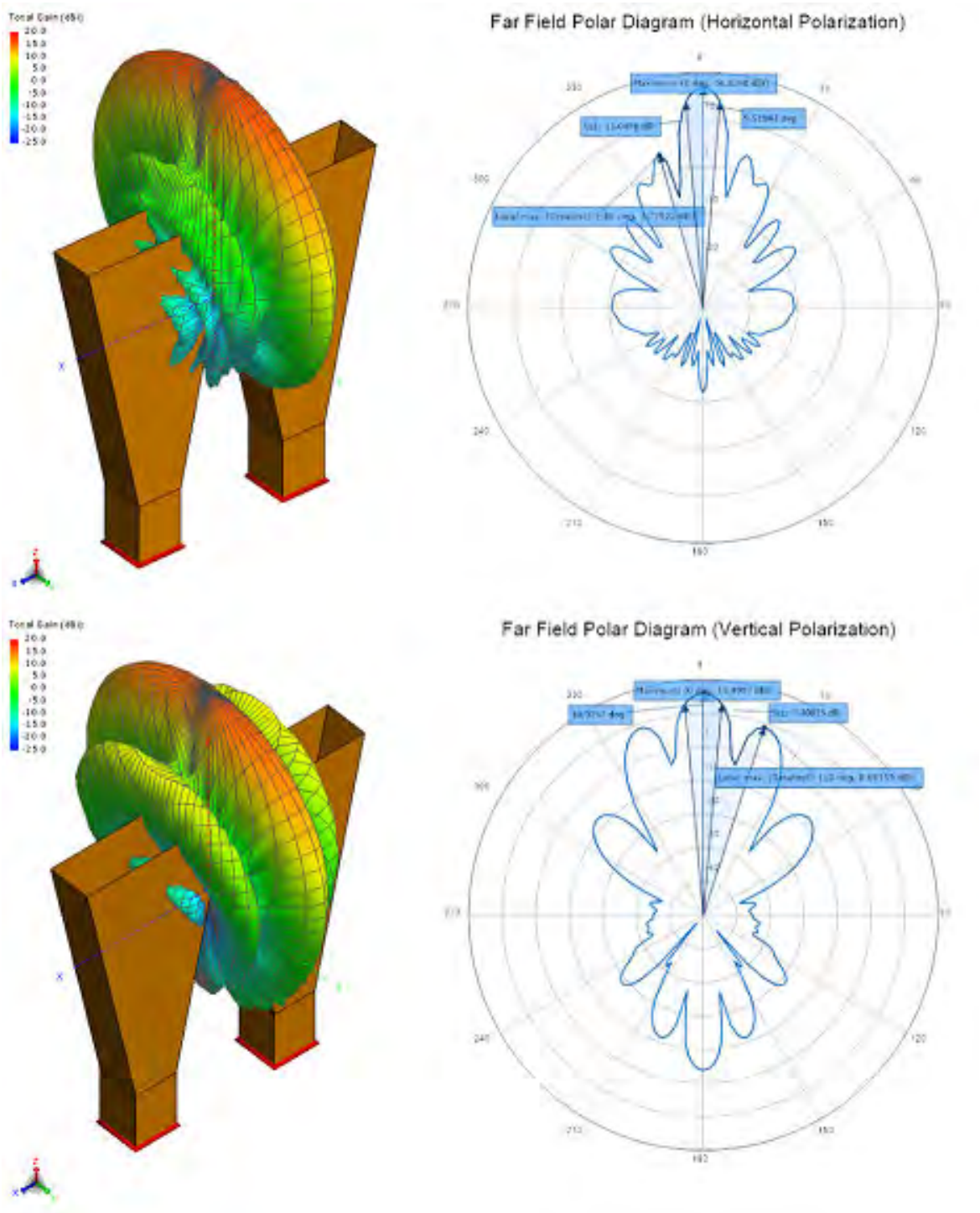

Figure B.5: Simulation of a sectoral horn antenna array. (Top) Horizontally polarised 3D far-field plot and azimuth plane polar plot. (Bottom) Vertically polarised 3D far-field plot and azimuth plane polar plot [1].

B.3 Pillbox Antenna

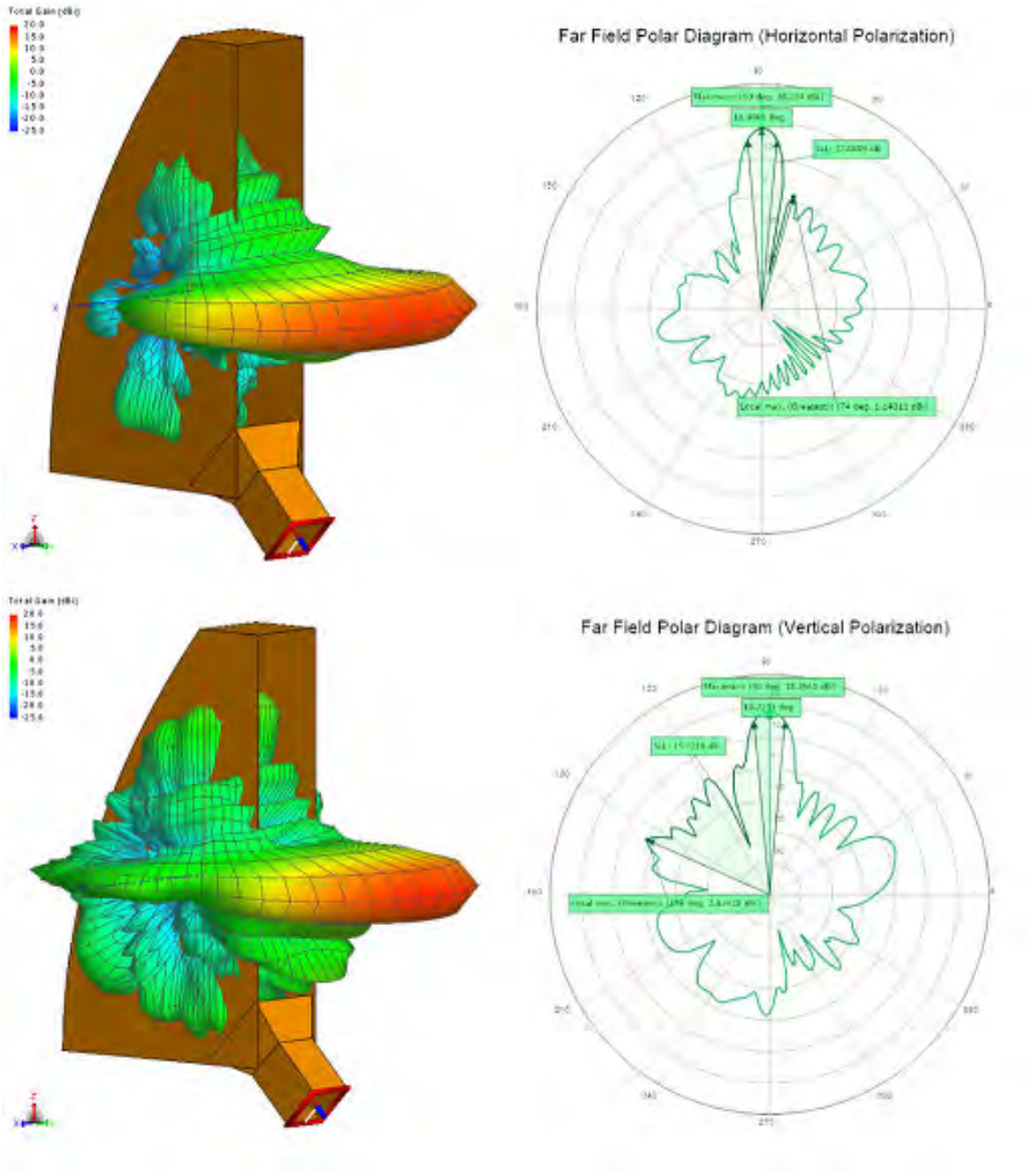

Figure B.6: Simulated pillbox antenna performance. (Top) Horizontally polarised 3D far-field plot and azimuth plane polar plot. (Bottom) Vertically polarised 3D far-field plot and azimuth plane polar plot [1].

Appendix C

Prime Focus Dish Efficiency

Figure C.1 illustrates the effect of feed blockage on efficiency of a dish antenna.

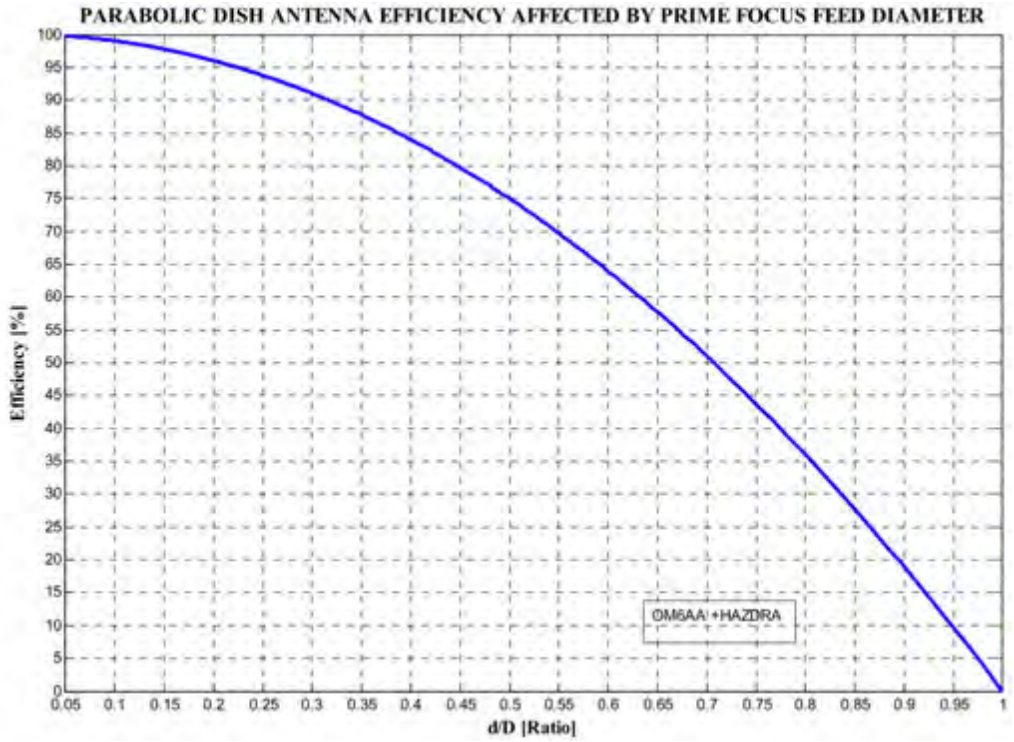

Figure C.1: Effect of feed blockage on efficiency for a uniformly illuminated parabolic dish antenna [19].

Appendix D

Beam Squinting

Figure D.1 shows the effect on the main beam when a metallic support arm is used. Figure D.2 shows the same simulation as seen in Figure D.1 however, with the use of a wooden feed arm as opposed to an aluminium one.

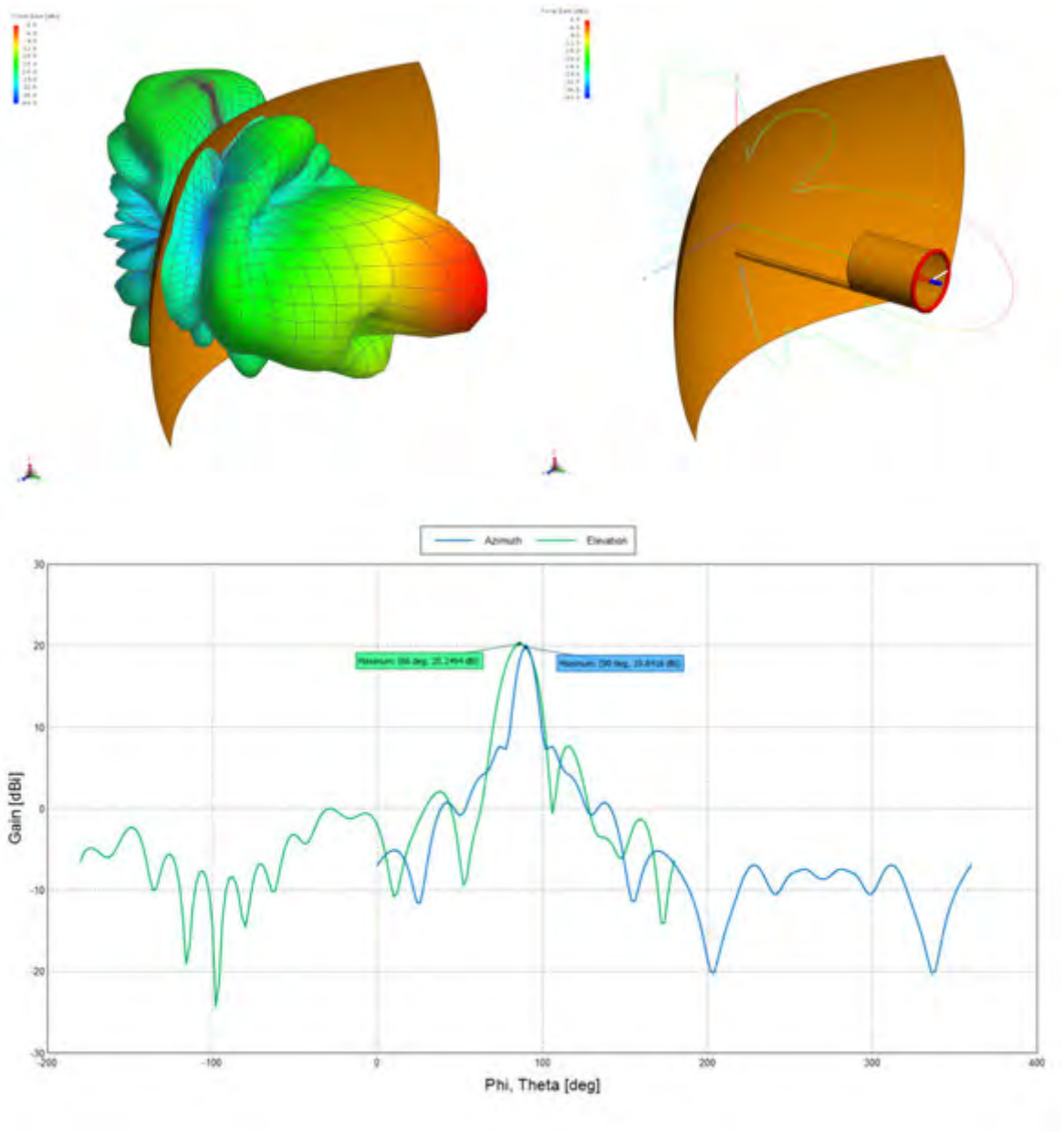

Figure D.1: Simulated antenna showing beam pattern squinting. (Top Left) 3D radiation plot showing deformation of the overall beam pattern. (Top Right) Elevation radiation pattern showing squinted elevation beam pattern in relation to antenna structure. (Bottom) Cartesian plot showing the boresight difference between the azimuth and elevation maximum points.

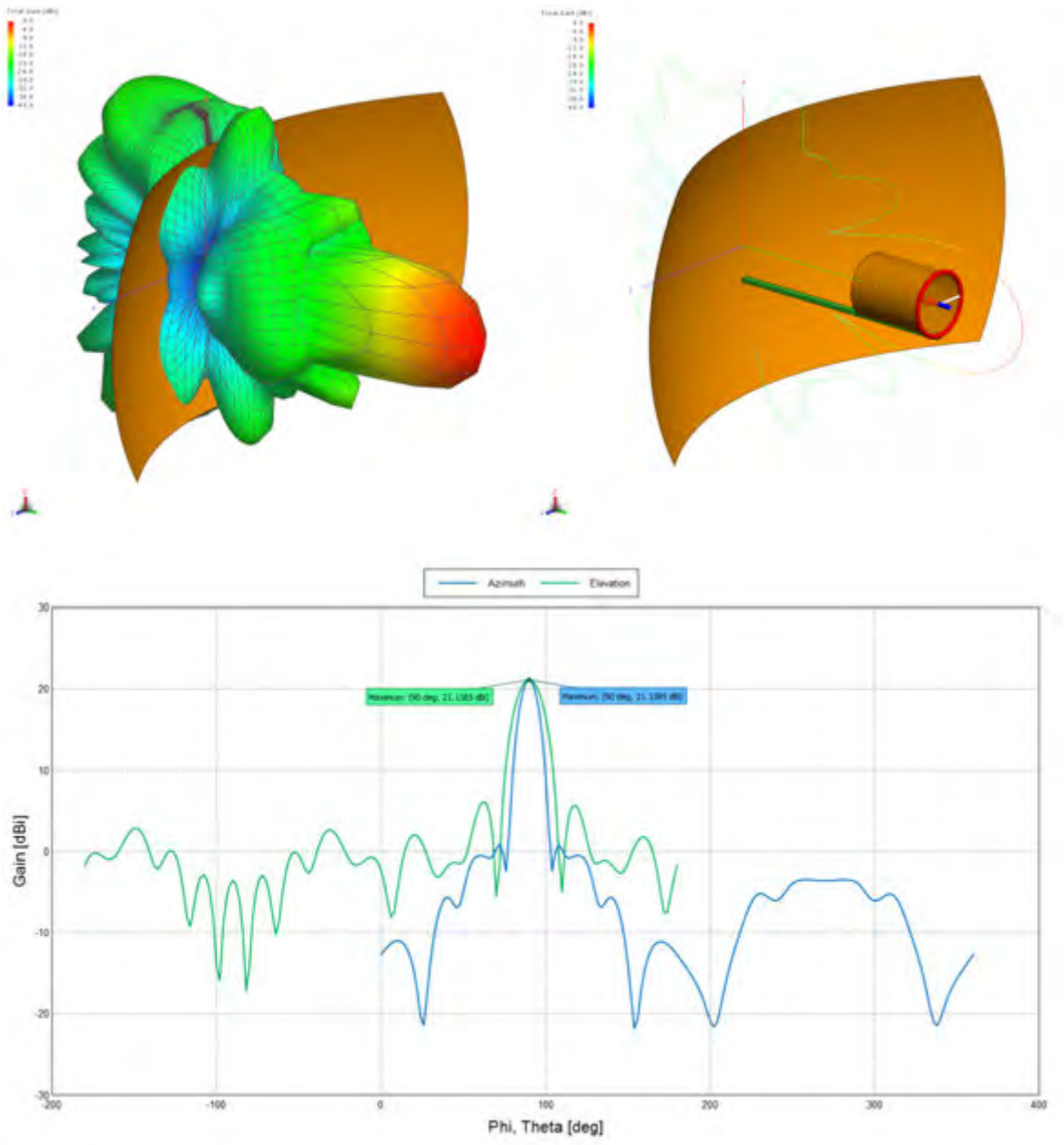

Figure D.2: Simulated antenna showing beam pattern with no squinting. (Top Left) 3D radiation plot showing no deformation of the overall beam pattern. (Top Right) Elevation radiation pattern showing elevation beam pattern in relation to antenna structure. (Bottom) Cartesian plot showing the both azimuth and elevation patterns on boresight.

Appendix E

Simulated Designs

E.1 Full Dish Simulations

Figures E.1 and E.2 show the FEKO optimised 3D render, the polar plot as well as the cartesian plot of the full dish antenna simulation results respectively.

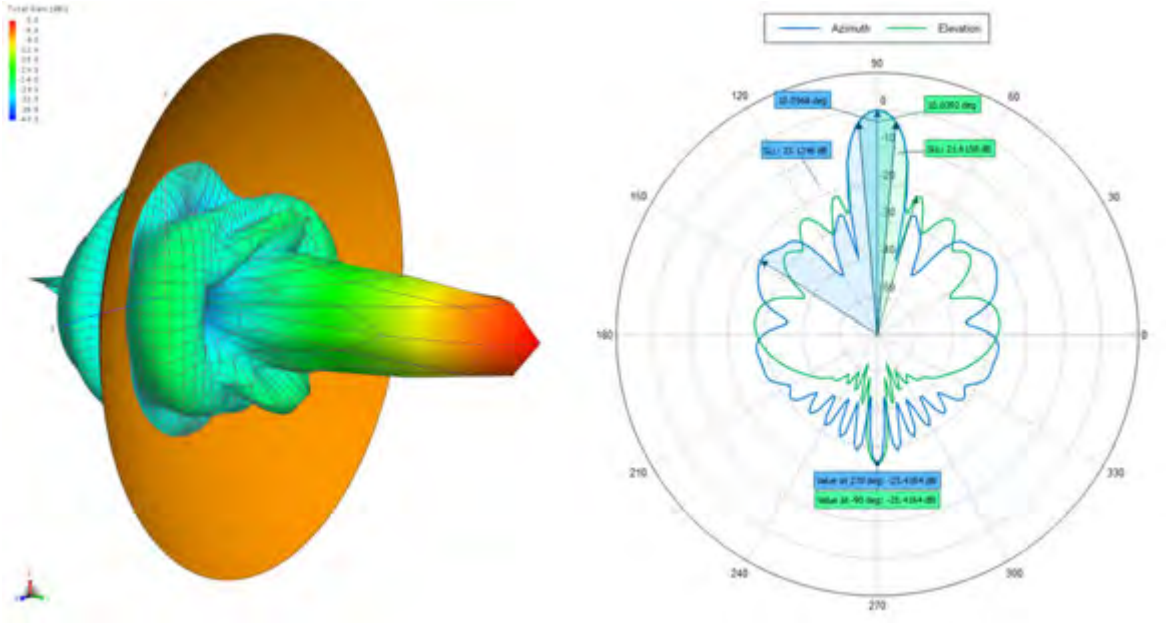

Figure E.1: (Left)3D render of full dish antenna optimised in FEKO. (Right) Simulated polar plot of FEKO optimised full dish antenna showing both azimuth and elevation beam patterns.

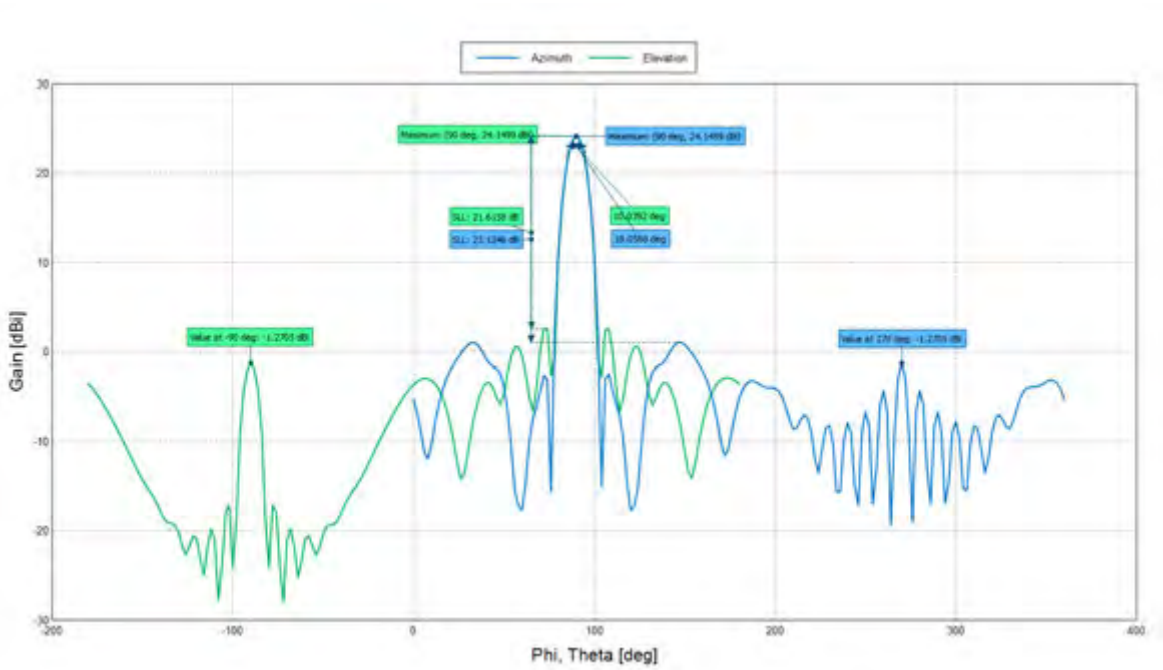

Figure E.2: Simulated cartesian plot of FEKO optimised full dish antenna showing both azimuth and elevation beam patterns.

E.2 Truncated Dish Simulations

Calculated Antenna Simulation Results

Figures E.3 and E.4 show the FEKO simulated 3D render, the polar plot as well as the cartesian plot of the truncated dish simulation results respectively using the calculated parameters.

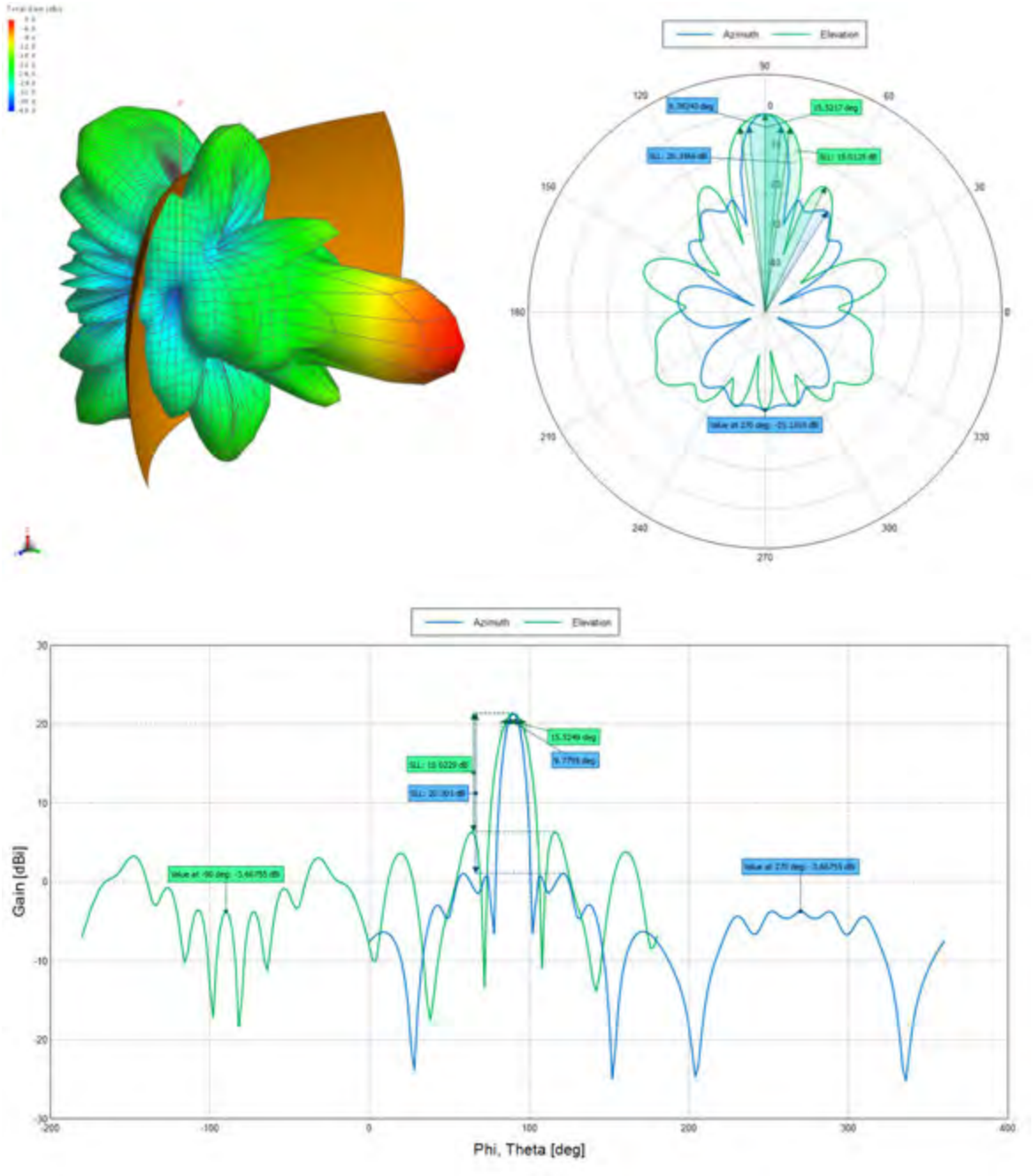

Figure E.3: Horizontally polarised FEKO simulated result for the dish antenna as calculated in Section 4.2.3. (Top left) 3D FEKO render of far-field radiation pattern. (Top right) FEKO simulated polar plot of the azimuth and elevation radiation pattern. (Bottom) Azimuth and elevation cartesian radiation pattern.

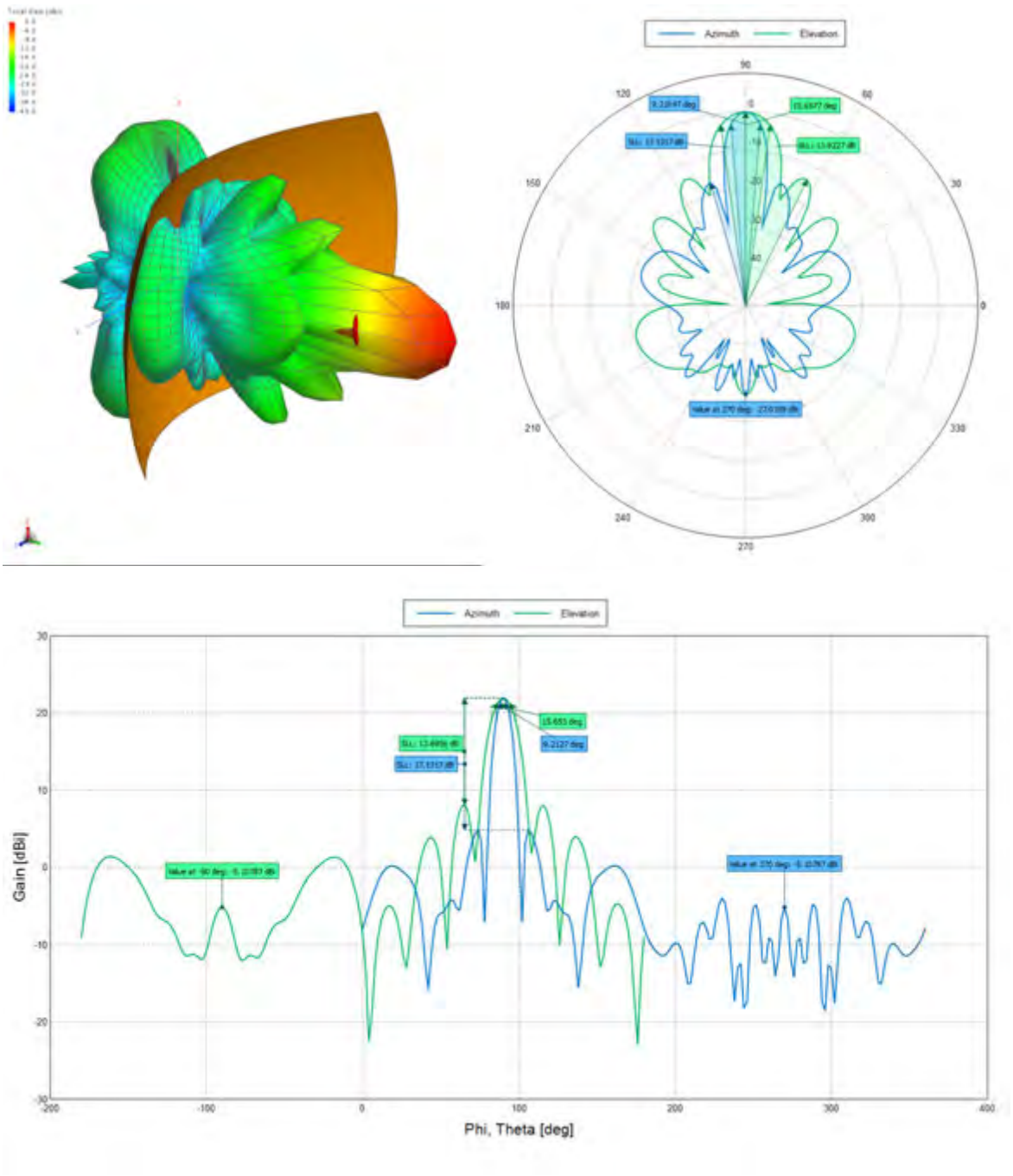

Figure E.4: Vertically polarised FEKO simulated result for the dish antenna as calculated in Section 4.2.3. (Top left) 3D FEKO render of far-field radiation pattern. (Top right) FEKO simulated polar plot of the azimuth and elevation radiation pattern. (Bottom) Azimuth and elevation cartesian radiation pattern.

FEKO Optimised Simulation Results

Figures E.5 and E.6 show the FEKO optimised 3D render, the polar plot as well as the cartesian plot of the truncated dish simulation results respectively.

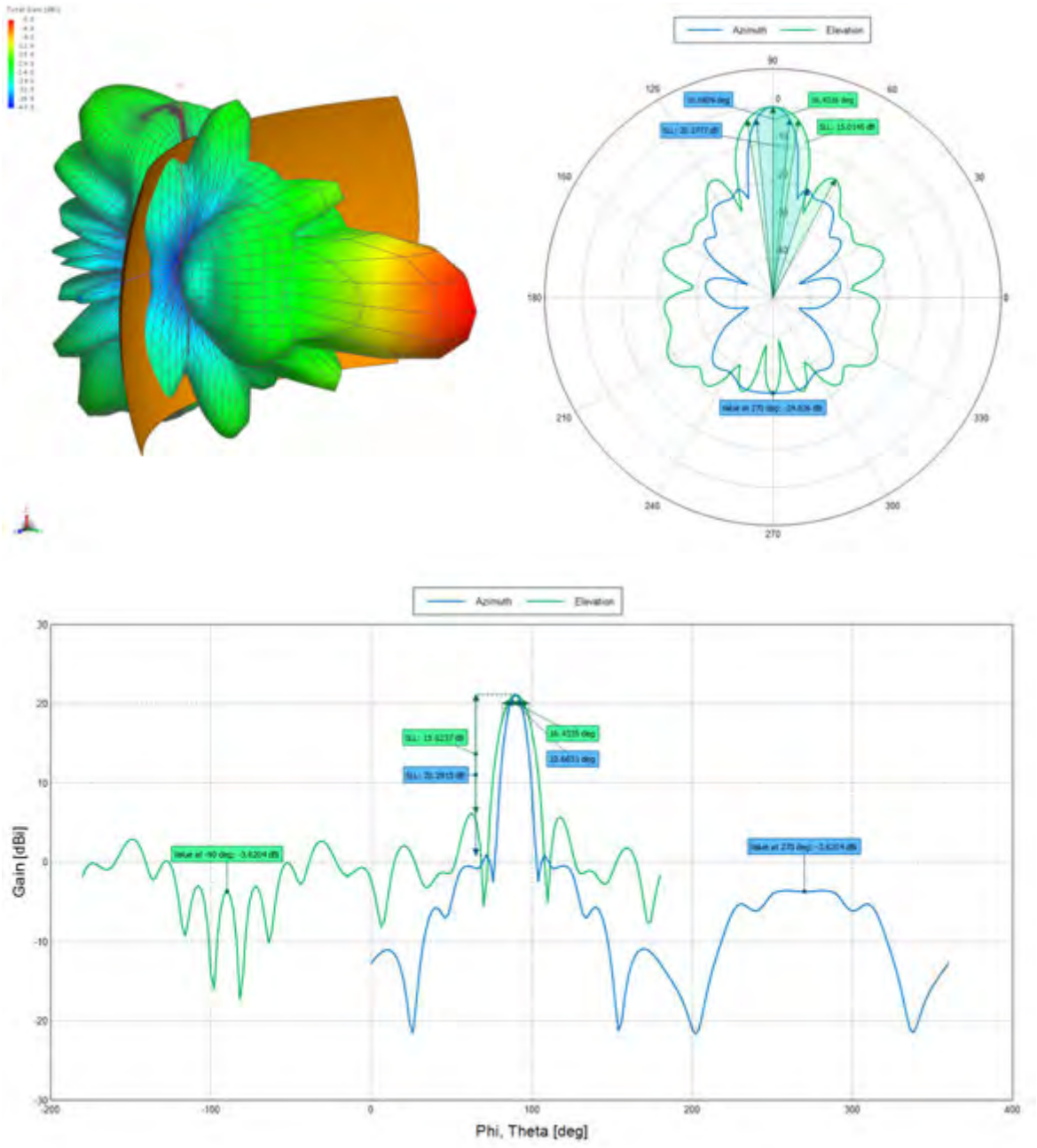

Figure E.5: Horizontally polarised FEKO simulated result for the FEKO optimised truncated dish antenna. (Top left) 3D FEKO render of far-field radiation pattern. (Top right) FEKO simulated polar plot of the azimuth and elevation radiation pattern. (Bottom) Azimuth and elevation cartesian radiation pattern.

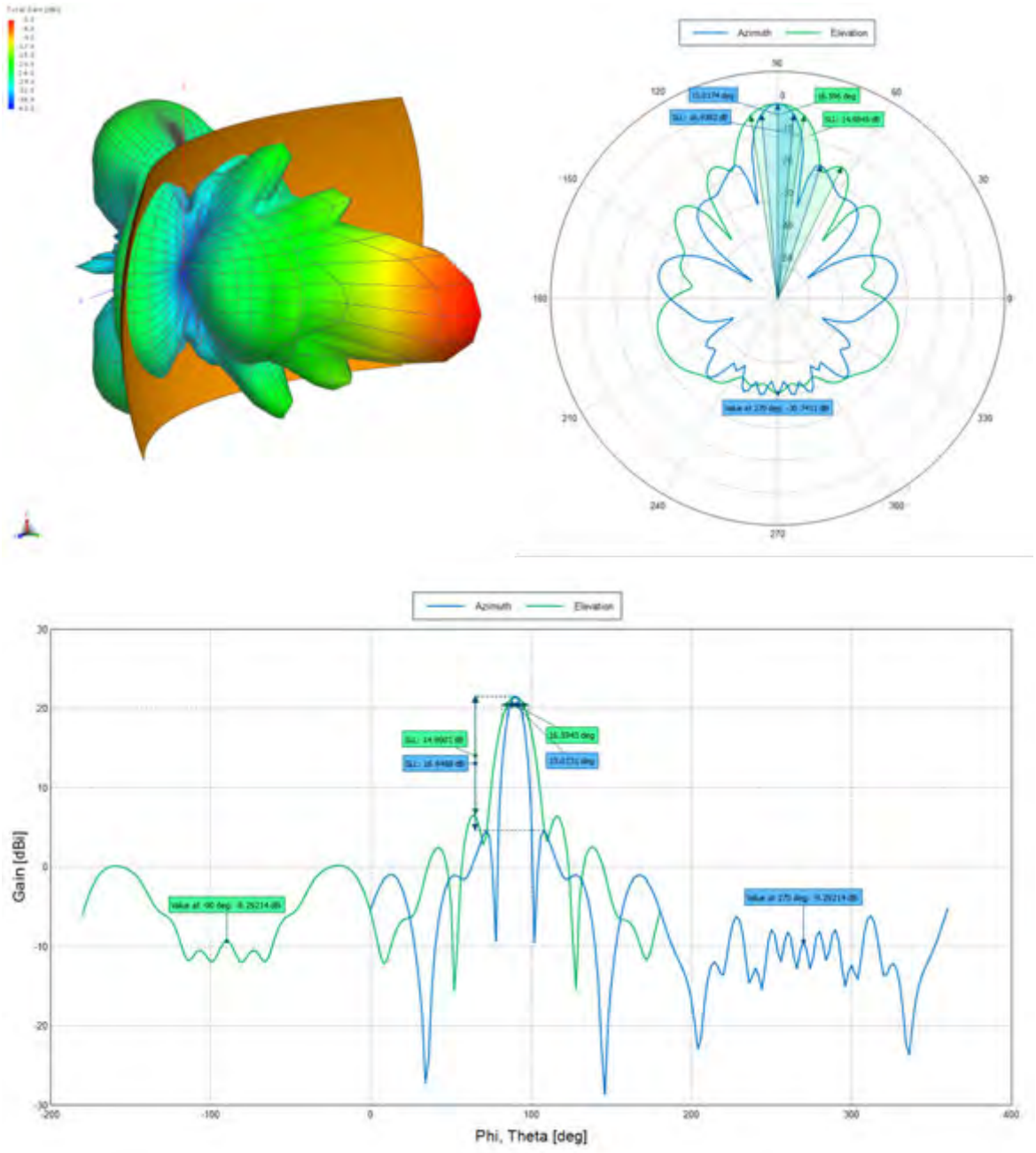

Figure E.6: Vertically polarised FEKO simulated result for the FEKO optimised truncated dish antenna. (Top left) 3D FEKO render of far-field radiation pattern. (Top right) FEKO simulated polar plot of the azimuth and elevation radiation pattern. (Bottom) Azimuth and elevation cartesian radiation pattern.

Appendix F

Bought Antenna Measurements

Figure F.1 shows the results of the rooftop measurements for the bought pre-fabricated 2.45 GHz antenna.

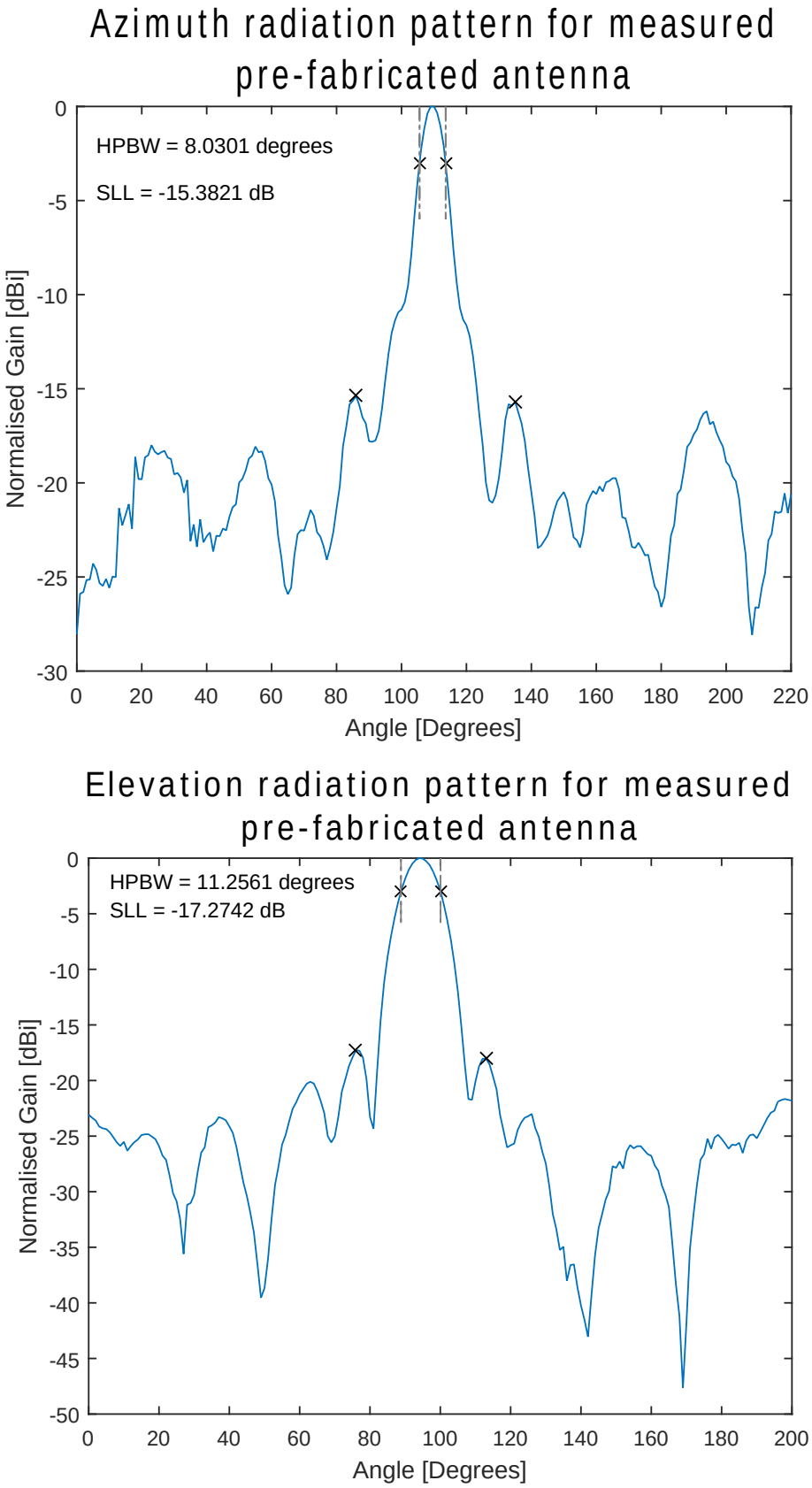

Figure F.1: Measured results for 2.45GHz pre-fabricated antenna. (Top) Azimuth radiation pattern. (Bottom) Elevation radiation pattern.

Appendix G

Built Antenna Results

G.1 Built Antenna Simulations

Figures G.1, G.2 ,G.3 and G.4 illustrate the CST simulated antenna as designed in Section 4.2.4.

G.2 Horizontal Polarisation

Azimuth Plane

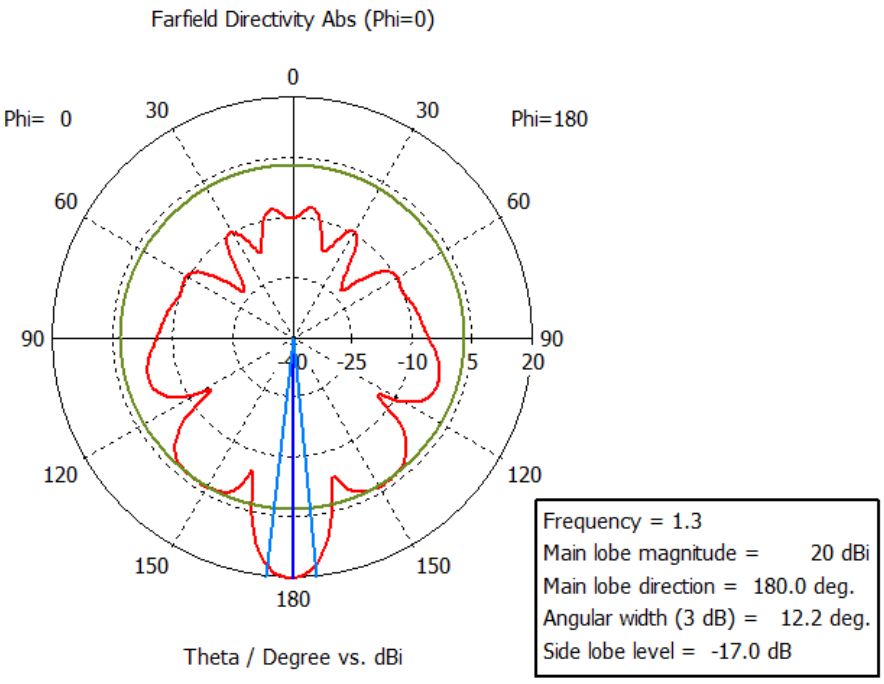

Figure G.1: Horizontally polarsed CST azimuth simulation.

Elevation Plane

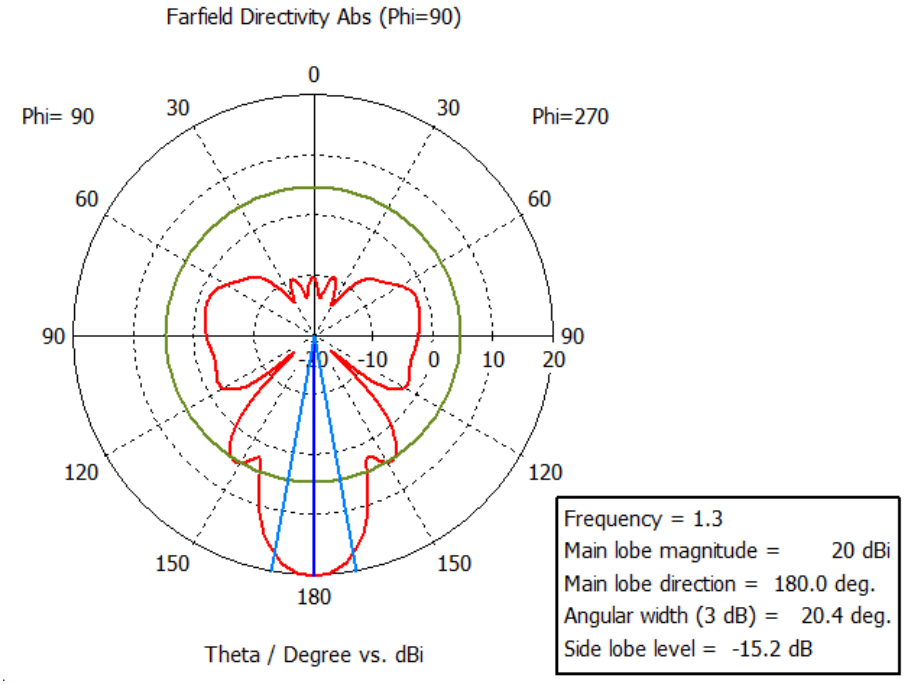

Figure G.2: Horizontally polarised CST elevation simulation.

G.3 Vertical Polarisation

Azimuth Plane

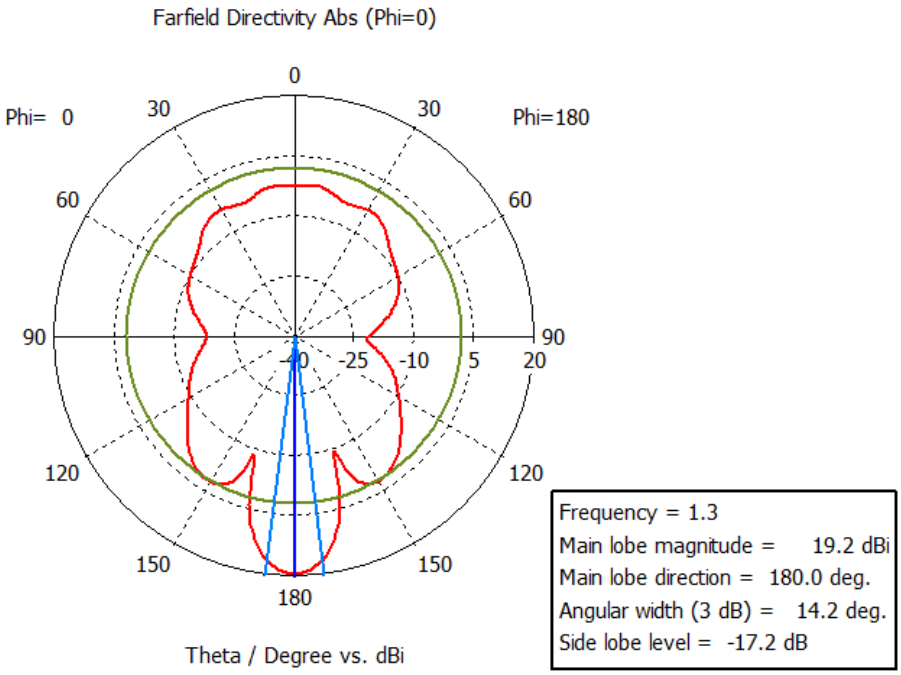

Figure G.3: Vertically polarised CST azimuth simulation.

Elevation Plane

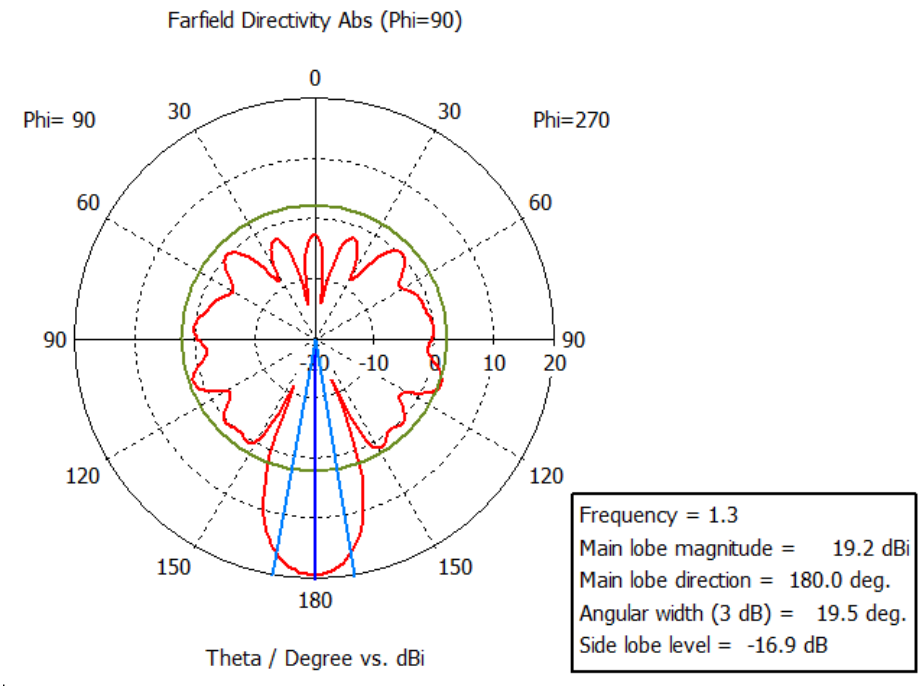

Figure G.4: Vertically polarised CST elevation simulation.

G.4 Built Antenna Measurements

The figures illustrate the summarised antenna measurements as described in Section 4.2.4. Figure G.5 illustrates the measured azimuth and elevation cartesian plots for each plane of polarisation.

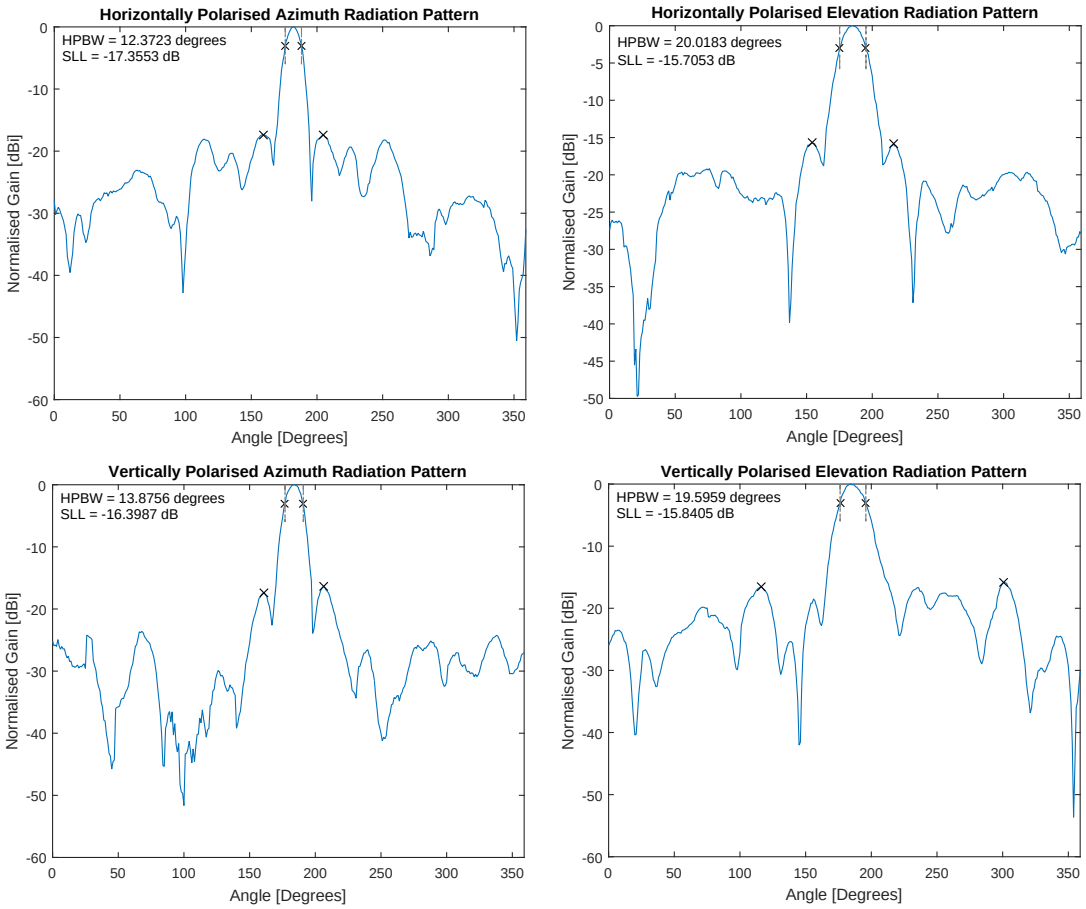

Figure G.5: Combined cartesian plots for the measured antenna. (Top left) Horizontally polarised azimuth radiation pattern. (Top right) Horizontally polarised elevation radiation pattern. (Bottom left) Vertically polarised azimuth radiation pattern. (Bottom right) Vertically polarised elevation radiation pattern.

Figures G.6 and G.7 illustrate the measured and simulated azimuth and elevation polar plots for each plane of polarisation. The slight offset from the 0° is due to the plotting style and not an indication of squinting.

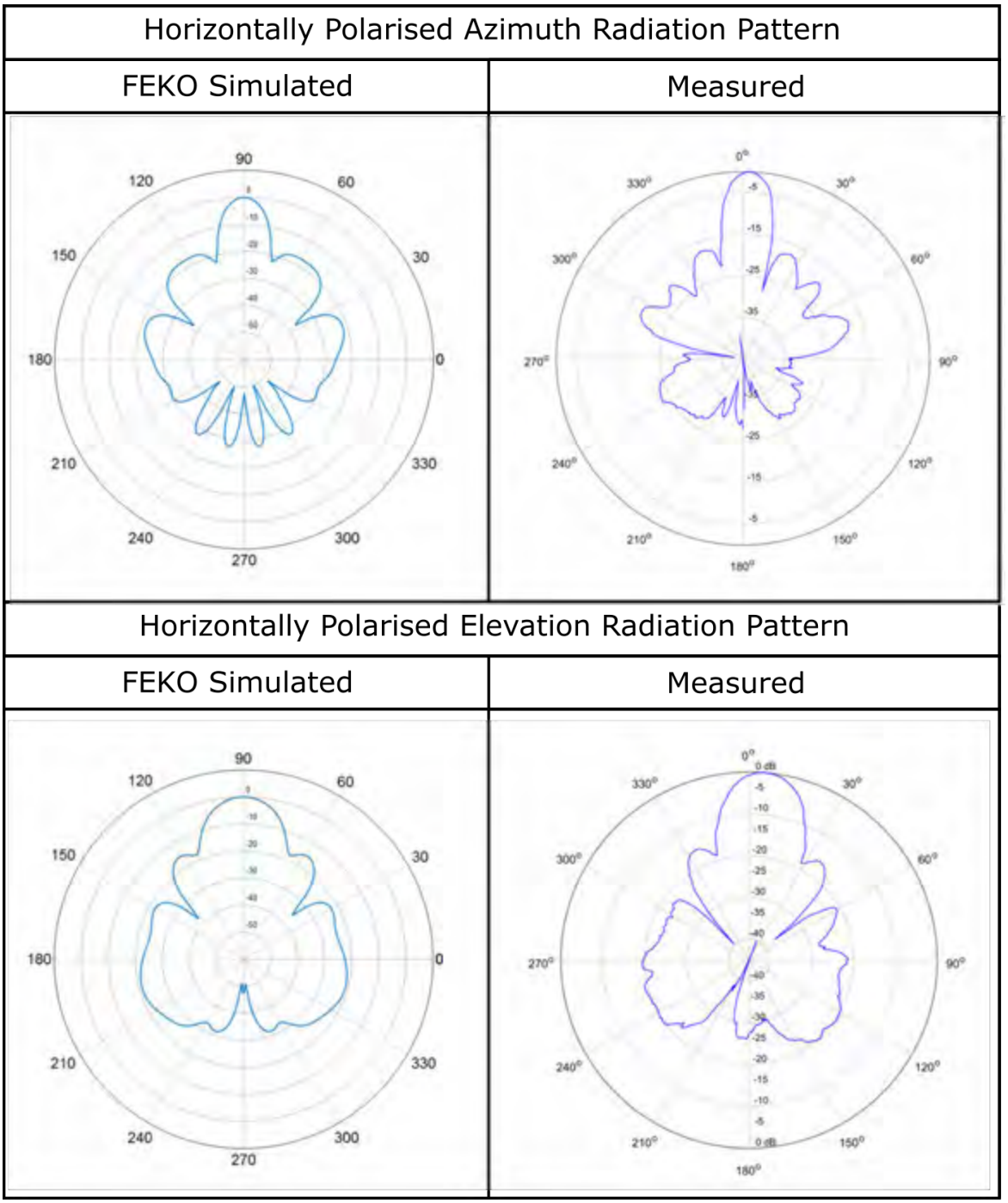

Figure G.6: Horizontally polarised azimuth and elevation measured and simulated polar plots. (Top) Azimuth plane. (Bottom) Elevation plane.

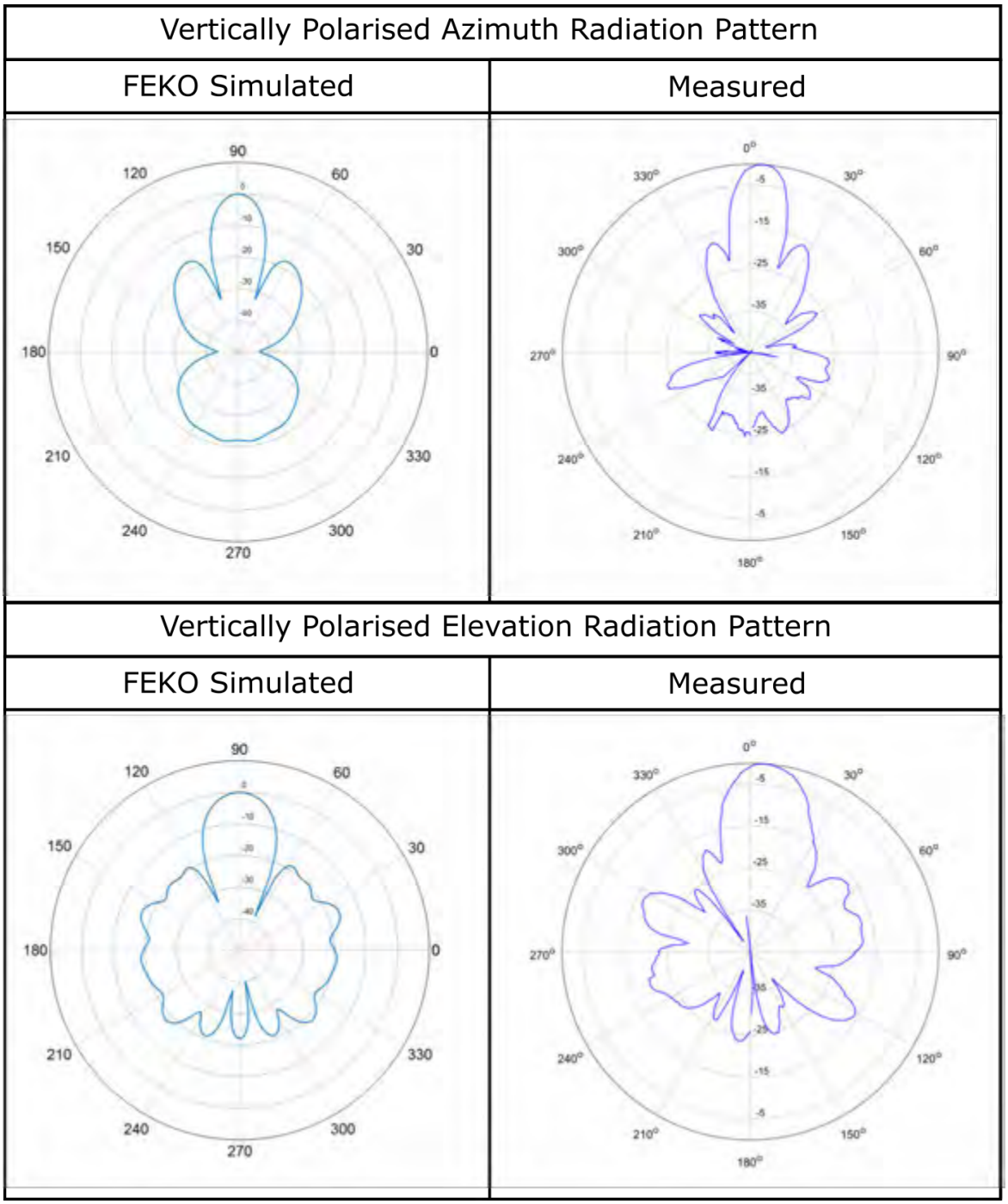

Figure G.7: Vertically polarised azimuth and elevation measured and simulated polar plots. (Top) Azimuth plane. (Bottom) Elevation plane.

Appendix H

Antenna CAD Designs

H.1 Full Dish Antenna

Table H.1 summarises the antenna dimensions.

Table H.1: FEKO optimised full dish antenna dimensions.

Parameter	**Value**
Diameter	1500 mm
Focal Point	495 mm
f/D ratio	0.33
Inner Waveguide Radius	87.5 mm
Inner Waveguide Length	230 mm
Probe Length	56.9 mm
Probe Backshort	121.2 mm
Feed Phase Centre	+25.8 mm
Parabolic Equation	$y = (5.05 \times 10^{-4})x^2$

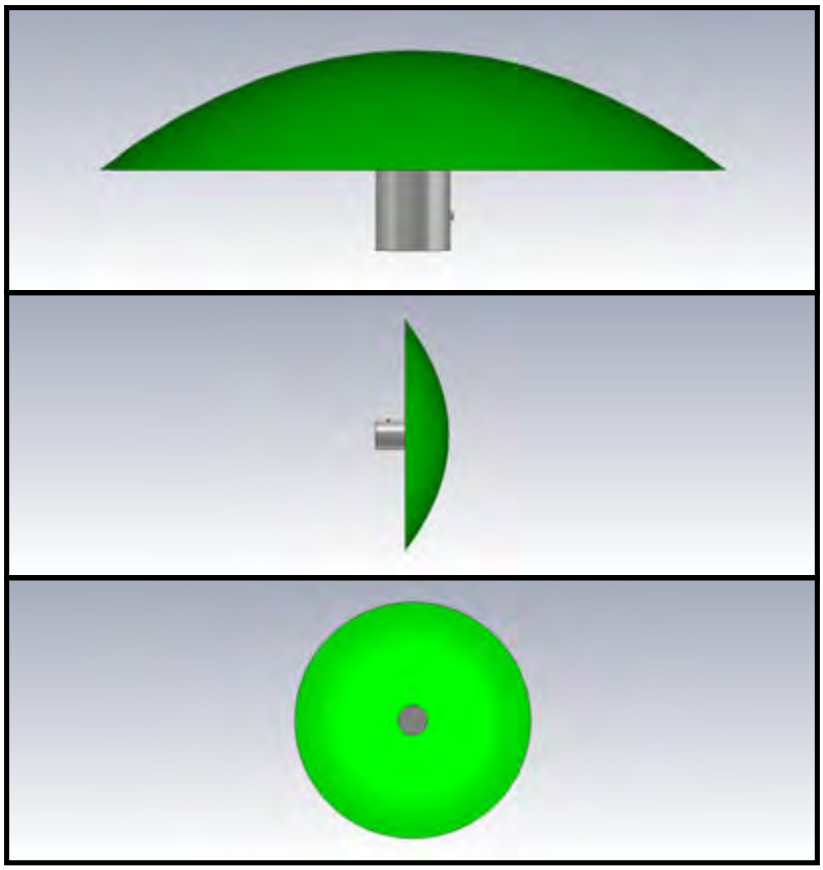

Figure H.1: Full dish antenna CAD design. (Top) Top view. (Middle) Side view. (Bottom) Front View.

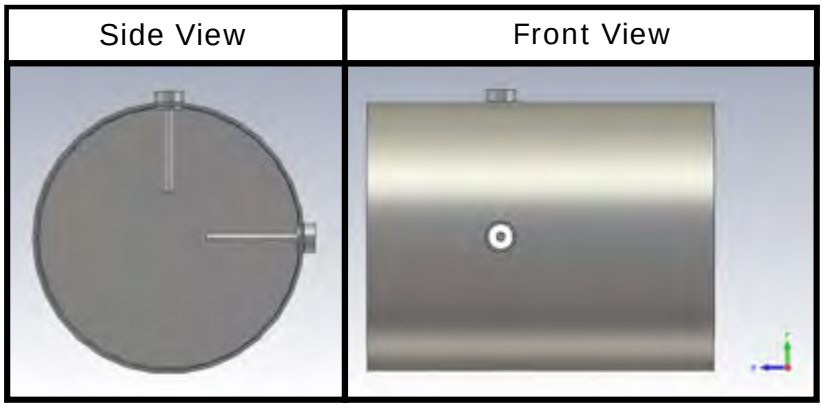

Figure H.2: Built waveguide CAD design. (Left) Front view. (Right) Side view.

H.2 Optimised Cut Dish Antenna

Table H.2 summarises the antenna dimensions.

Table H.2: FEKO optimised truncated dish antenna dimensions.

Parameter	**Value**
Diameter	1440 mm
Height	744 mm
Depth	290.3 mm
Focal Point	446 mm
f/D ratio	0.31
Inner Waveguide Radius	87.5 mm
Inner Waveguide Length	230 mm
Probe Length	56.9 mm
Probe Backshort	80.4 mm
Feed Phase Centre	+25.8 mm
Parabolic Equation	$y = (5.56 \times 10^{-4})x^2$

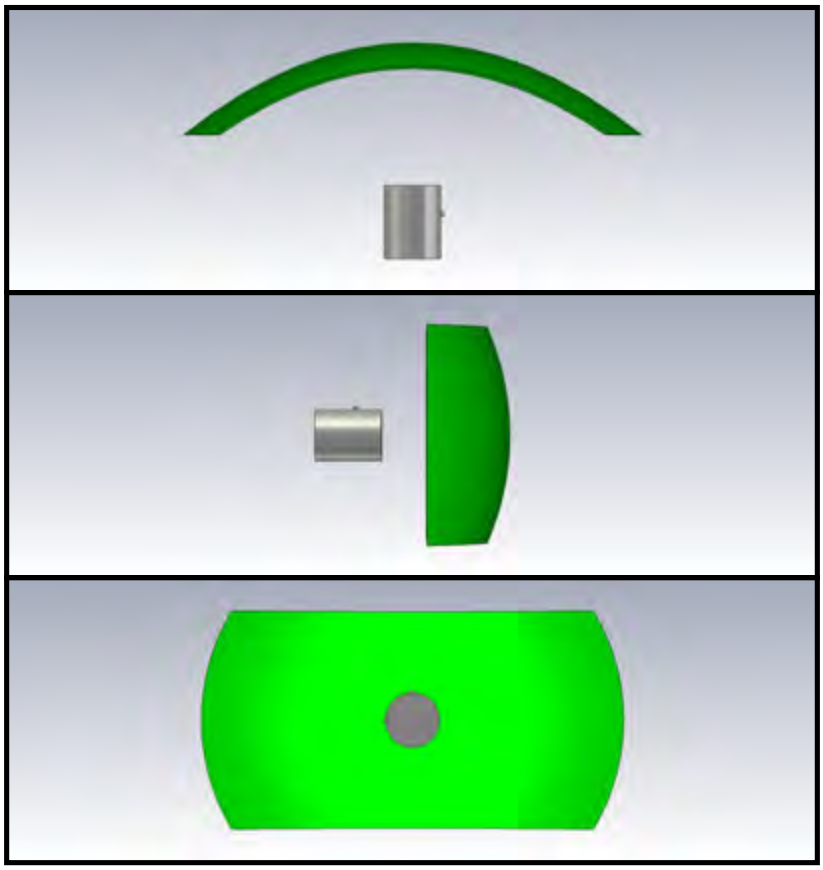

Figure H.3: Optimised truncated dish antenna CAD design. (Top) Top view. (Middle) Side view. (Bottom) Front View.

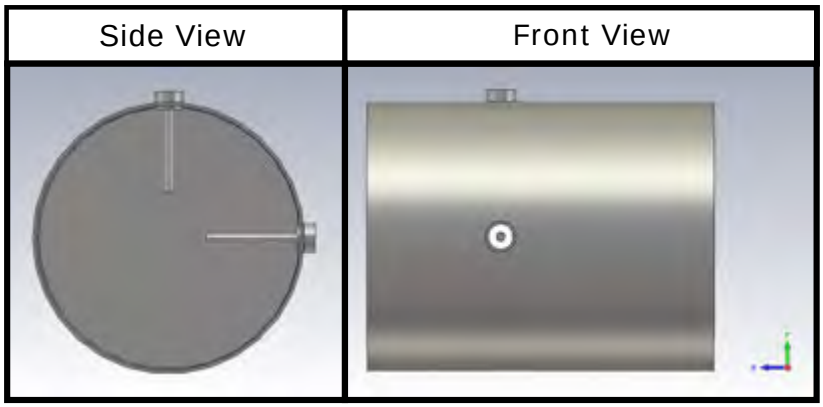

Figure H.4: Built waveguide CAD design. (Left) Front view. (Right) Side view.

H.3 Built Prototype Antenna

Table H.3 summarises the antenna dimensions.

Table H.3: Built prototype antenna dimensions.

Parameter	**Value**
Diameter	1350 mm
Height	600 mm
Depth	370 mm
Focal Point	307.85 mm
f/D ratio	0.23
Inner Waveguide Radius	87.5 mm
Inner Waveguide Length	230 mm
Probe Length	56.9 mm
Probe Backshort	133.3 mm
Feed Phase Centre	+25.8 mm
Parabolic Equation	$y = (8.16 \times 10^{-4})x^2$

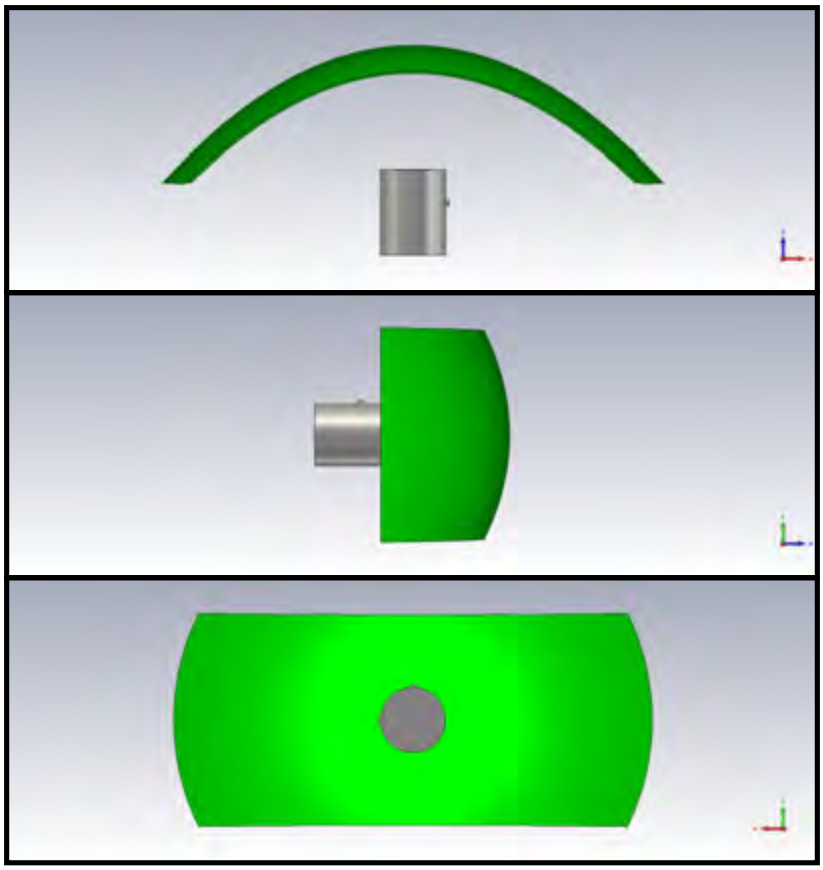

Figure H.5: Built antenna CAD design. (Top) Top view. (Middle) Side view. (Bottom) Front View.

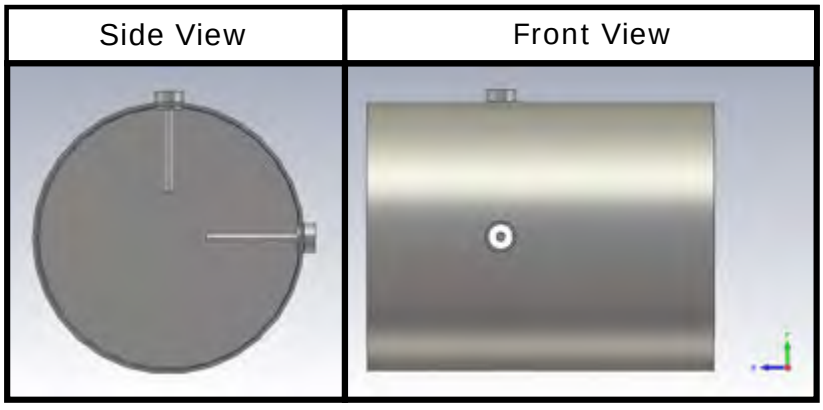

Figure H.6: Built waveguide CAD design. (Left) Front view. (Right) Side view.

Appendix I

Built Dish Pictures

Figures I.1, I.6 to are taken of the final Manufactured antenna prototype as designed in Section 4.2.4.

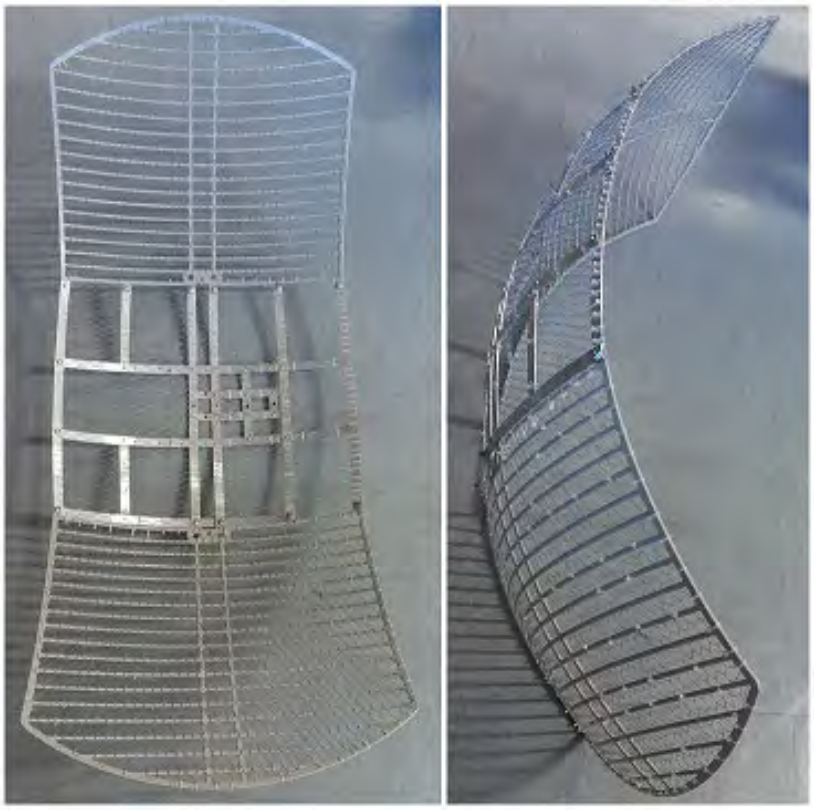

Figure I.1: Manufactured antenna (Left) Front view, (Right) Side view.

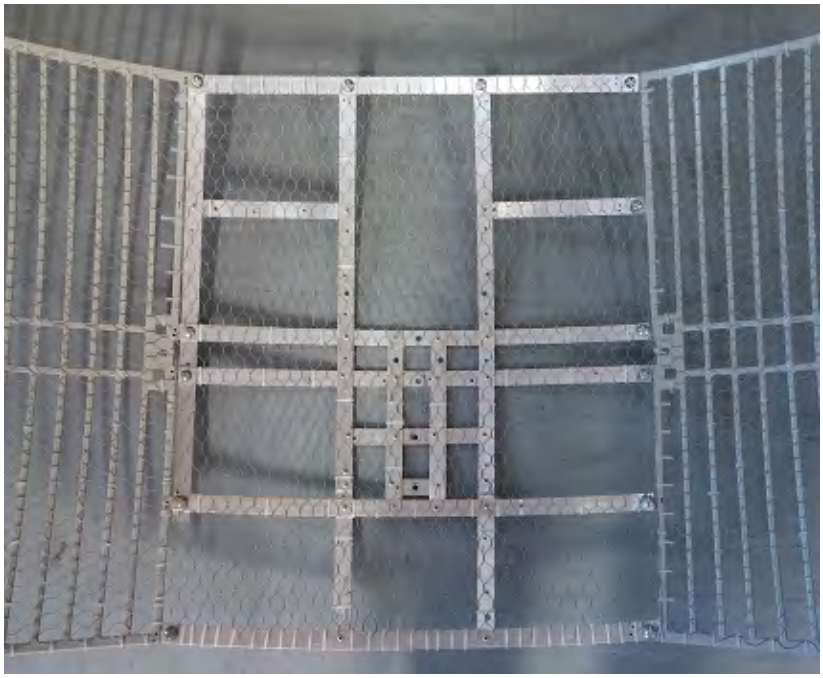

Figure I.2: Manufactured antenna front view showing mesh.

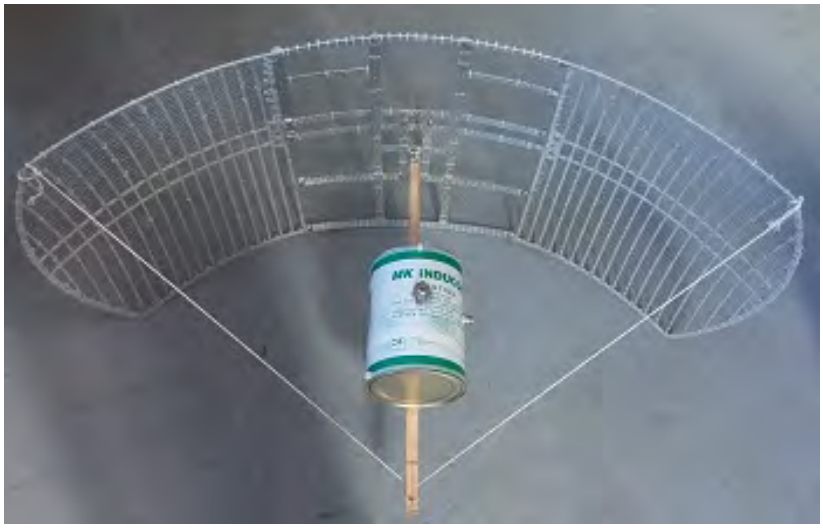

Figure I.3: Manufactured antenna top view with feed.

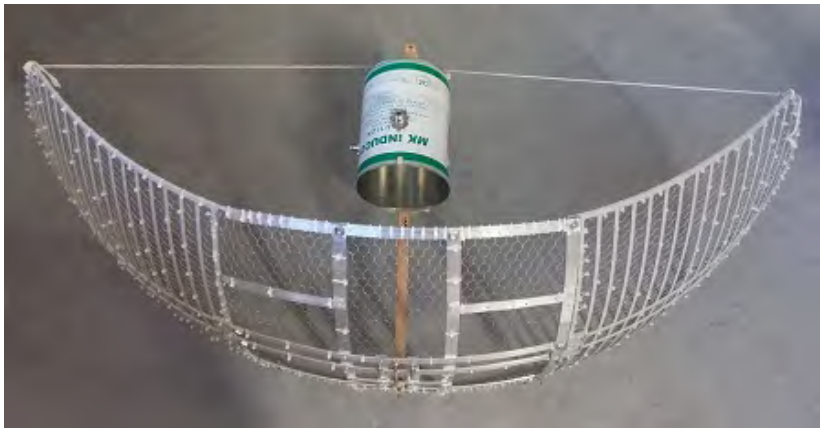

Figure I.4: Manufactured antenna complete top view.

Figure I.5: Manufactured antenna back view.

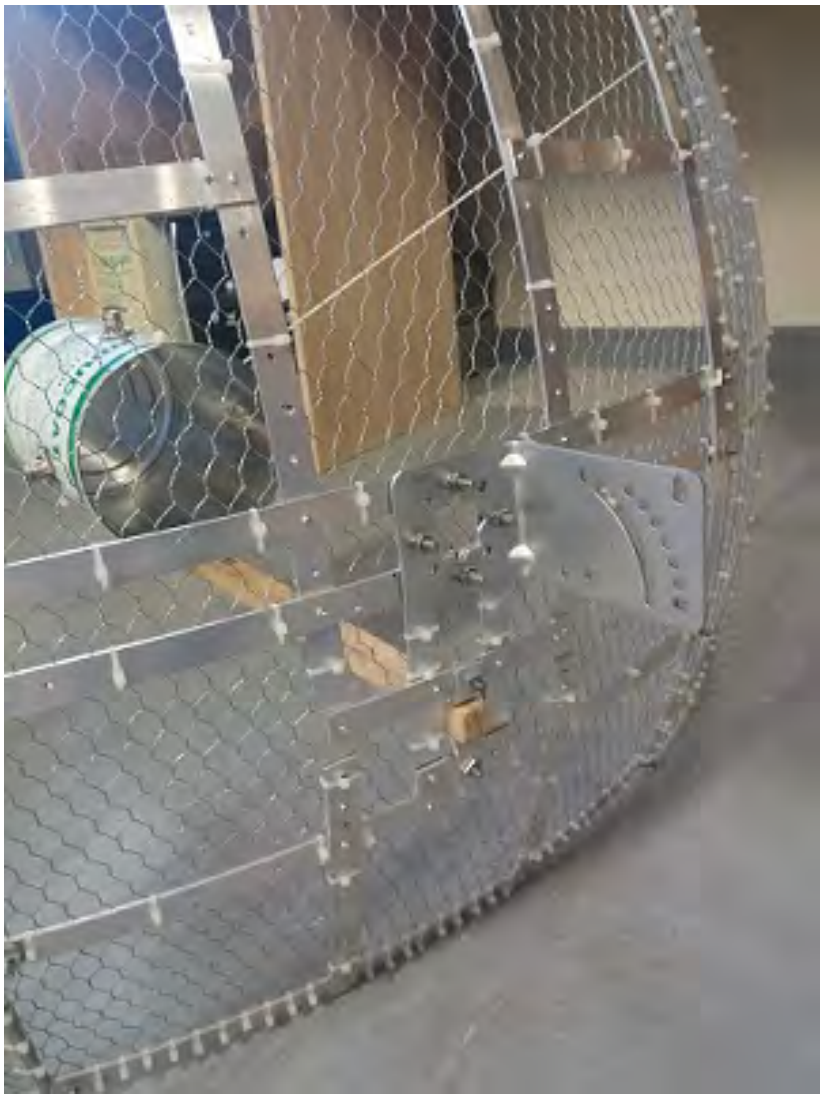

Figure I.6: Manufactured antenna mounting bracket.

Appendix J

Ethics Form

EBE Faculty: Assessment of Ethics in Research Projects (Rev2)

Any person planning to undertake research in the Faculty of Engineering and the Built Environment at the University of Cape Town is required to complete this form before collecting or analysing data. When completed it should be submitted to the supervisor (where applicable) and from there to the Head of Department. If any of the questions below have been answered YES, and the applicant is NOT a fourth year student, the Head should forward this form for approval by the Faculty EIR committee: submit to Ms Zulpha Geyer (Zulpha.Geyer@uct.ac.za; Chem Eng Building, Ph 021 650 4791).
NB: A copy of this signed form must be included with the thesis/dissertation/report when it is submitted for examination

This form must only be completed once the most recent revision EBE EiR Handbook has been read.

Name of Principal Researcher/Student: **Stephen Paine** Department: **EBE**

Preferred email address of the applicant: **PNXSTE002@myuct.ac.za**

If a Student: Degree: **MSc** Supervisor: **Prof. Daniel O'Hagan**

If a Research Contract indicate source of funding/sponsorship: **CSIR Ledger**

Research Project Title: **Design and Implementation of a Dual Polarised L-Band Parabolic Dish Antenna for NeXtRAD**

Overview of ethics issues in your research project:

Question 1: Is there a possibility that your research could cause harm to a third party (i.e. a person not involved in your project)?		NO
Question 2: Is your research making use of human subjects as sources of data? If your answer is YES, please complete Addendum 2.		NO
Question 3: Does your research involve the participation of or provision of services to communities? If your answer is YES, please complete Addendum 3.		NO
Question 4: If your research is sponsored, is there any potential for conflicts of interest? If your answer is YES, please complete Addendum 4.		NO

If you have answered YES to any of the above questions, please append a copy of your research proposal, as well as any interview schedules or questionnaires (Addendum 1) and please complete further addenda as appropriate. Ensure that you refer to the EiR Handbook to assist you in completing the documentation requirements for this form.

I hereby undertake to carry out my research in such a way that

- there is no apparent legal objection to the nature or the method of research; and
- the research will not compromise staff or students or the other responsibilities of the University;
- the stated objective will be achieved, and the findings will have a high degree of validity;
- limitations and alternative interpretations will be considered;
- the findings could be subject to peer review and publicly available; and
- I will comply with the conventions of copyright and avoid any practice that would constitute plagiarism.

Signed by:

	Full name and signature	Date
Principal Researcher/Student:	Stephen Paine	14 Feb. 16

This application is approved by:

Supervisor (if applicable):		14 Feb. 16
HOD (or delegated nominee): *Final authority for all assessments with NO to all questions and for all undergraduate research.*	Edward Boje	14 Feb. 16
Chair : Faculty EIR Committee For applicants other than undergraduate students who have answered YES to any of the above questions.		

ADDENDUM 1:
Please append a copy of the research proposal here, as well as any interview schedules or questionnaires:

To whom it may concern,

My final year undergraduate project was based on the design and implementation of a dual polarized L-Band antenna with 10 degree azimuth beamwidth for the NeXtRAD system. It is my intention to continue with the development of a novel antenna design for the UCT NeXtRAD system. The full details of the research will be decided with the UCT radar group members, and in particular with Prof. O'Hagan.

Yours sincerely,
Stephen Paine
PNXSTE002

ADDENDUM 2: To be completed if you answered YES to Question 2:

It is assumed that you have read the UCT Code for Research involving Human Subjects (available at http://web.uct.ac.za/depts/educate/download/uctcodeforresearchinvolvinghumansubjects.pdf) in order to be able to answer the questions in this addendum.

2.1 Does the research discriminate against participation by individuals, or differentiate between participants, on the grounds of gender, race or ethnic group, age range, religion, income, handicap, illness or any similar classification?		NO
2.2 Does the research require the participation of socially or physically vulnerable people (children, aged, disabled, etc) or legally restricted groups?		NO
2.3 Will you not be able to secure the informed consent of all participants in the research? (In the case of children, will you not be able to obtain the consent of their guardians or parents?)		NO
2.4 Will any confidential data be collected or will identifiable records of individuals be kept?		NO
2.5 In reporting on this research is there any possibility that you will not be able to keep the identities of the individuals involved anonymous?		NO
2.6 Are there any foreseeable risks of physical, psychological or social harm to participants that might occur in the course of the research?		NO
2.7 Does the research include making payments or giving gifts to any participants?		NO

If you have answered YES to any of these questions, please describe below how you plan to address these issues:

ADDENDUM 4: To be completed if you answered YES to Question 4

4.1 Is there any existing or potential conflict of interest between a research sponsor, academic supervisor, other researchers or participants?		NO
4.2 Will information that reveals the identity of participants be supplied to a research sponsor, other than with the permission of the individuals?		NO
4.3 Does the proposed research potentially conflict with the research of any other individual or group within the University?		NO

If you have answered YES to any of these questions, please describe below how you plan to address these issues: